



On the influence of self-heat on temperature measurements in VSL's water calorimeter

Erik Paardekam
Delft, June 2016

Development of a new measurement setup and method for the determination of the self-heat correction factor for the NTC thermistors in VSL's primary standard for absorbed-dose-to-water measurements.

A thesis submitted in partial fulfilment of the requirements for the degree of BEng Applied Physics at The Hague University

Supervisors:

Mr. L.A. de Prez (VSL)
Mr. J.L. van Yperen (THUAS)
Mr. N.L. van der Houwen (THUAS)

VSL

Thijsseweg 11
2629 JA Delft
Postbus 654
2600 AR Delft
Nederland

T +31 15 269 15 00

F +31 15 261 29 71

E info@vsl.nl

I www.vsl.nl

This work has been carried out by:	Erik Paardekam
On request of:	VSL
For the applicant:	Leon de Prez

Summary

The thermally-sensitive resistors (*thermistors*) used in VSL's water calorimeter to detect the radiation-induced temperature change in water are affected by self-heat. The measurement current used to determine their resistance causes their temperature to increase above that of their environment. The self-heat of the thermistors must be corrected for when performing water calorimetry to isolate the temperature change that is caused by the radiation.

In this study, the relationship between the self-heat temperature and the power dissipated by the thermistors is investigated. A measurement method and setup are designed to measure the thermistor's temperature as a function of dissipated power in an automated fashion. The data is analyzed using two methods. The first is based on a linear fit of the data from the measurement setup, resulting in a self-heat temperature that is proportional to the dissipated power. The other method is based on a 2nd order polynomial fit of the same data, where non-linear influences which are assumed to be caused by convection are taken into account. Analysis of the data leads to the determination of a self-heat correction factor k_{sh} , which is used to isolate the change in water temperature during water calorimetry.

The lead resistances of the measurement setup are incorporated in the calculations to increase the accuracy of the results. The new measurement setup and automated data acquisition program are successfully validated. With the new setup, the self-heat correction factor is determined for two thermistors. k_{sh} is determined to be 1.00638 ± 0.00018 ($k = 1$) for thermistor VSL13T025 and 1.01016 ± 0.00018 ($k = 1$) for thermistor VSL13T033. With the automated method, the standard relative uncertainty of k_{sh} is reduced to 0.018% while also requiring minimal human input, making it well-suited for on-site measurements of the self-heat correction factor.

Table of contents

LIST OF FIGURES	6
LIST OF TABLES	7
1 INTRODUCTION	8
1.1 WATER CALORIMETRY	8
1.2 NTC THERMISTORS	11
1.3 THERMISTOR SELF-HEAT	12
1.4 AGILENT 3458A DIGITAL MULTIMETER	13
1.5 EVALUATION OF MEASUREMENT UNCERTAINTIES	15
2 MATERIALS AND METHODS	16
2.1 MEASUREMENT METHOD	16
2.2 EQUIPMENT	18
2.2.1 <i>Equipment interfacing box</i>	20
2.2.2 <i>Keithley 7001 Switch system</i>	21
2.2.3 <i>Custom measurement program</i>	21
2.3 MEASUREMENT OF LEAD AND INTERNAL RESISTANCES	23
2.3.1 <i>Measurement of thermistor lead resistances</i>	26
2.4 VALIDATION OF MEASUREMENT METHOD AND SETUP	27
2.4.1 <i>Method validation experiments</i>	27
2.4.2 <i>Measurement of thermistor settling time</i>	27
2.4.3 <i>Validation of automated data acquisition</i>	28
2.5 SELF-HEAT PARAMETER MEASUREMENTS	28
3 RESULTS	29
3.1 LEAD RESISTANCE MEASUREMENT RESULTS	29
3.1.1 <i>Parallel resistor lead resistances, r_p</i>	29
3.1.2 <i>Thermistor lead resistances, r</i>	30
3.1.3 <i>Determination of total lead resistance in parallel resistor and thermistor circuits</i>	30
3.2 RESULTS FROM VALIDATION OF MEASUREMENT METHOD AND SETUP	31
3.2.1 <i>Validation of setup and method using internal resistor</i>	31
3.2.2 <i>Validation of setup and method with proxy thermistor</i>	32
3.2.3 <i>Validation of setup and method with proxy thermistor and extension leads</i>	32
3.2.4 <i>Settling time determination</i>	33
3.2.5 <i>Validation of automated data acquisition program</i>	34
3.3 RESULTS FROM SELF-HEAT PARAMETER MEASUREMENTS	37
4 ANALYSIS OF UNCERTAINTIES IN THE RESULTS	41
4.1 UNCERTAINTY OF THERMISTOR RESISTANCE	41
4.2 UNCERTAINTY OF LINEAR SELF-HEAT PARAMETER $C_{SH,1}$	43
4.3 UNCERTAINTY ANALYSIS OF 2 ND ORDER SELF-HEAT PARAMETER $C_{SH,2}$ AND NON-LINEARITY PARAMETER B	45
4.4 OVERVIEW OF UNCERTAINTY CONTRIBUTIONS TO SELF-HEAT CORRECTION FACTOR	47
5 DISCUSSION	49
5.1 RECOMMENDATIONS	50
6 CONCLUSION	51
7 REFERENCES	52

On the self-heat effects of thermistors

8	APPENDICES	53
8.1	TECHNICAL DRAWINGS OF EQUIPMENT INTERFACE BOX.....	54
8.2	KEITHLEY 7001 SWITCH SYSTEM CHANNEL ASSIGNMENTS	56
8.3	DATA FROM LEAD AND INTERNAL RESISTANCE MEASUREMENTS.....	57
8.4	DATA FROM VALIDATION PROCEDURES.....	59
8.5	UNCERTAINTY BUDGETS	61
8.5.1	<i>Uncertainty budget for lead resistance experiment</i>	<i>61</i>
8.5.2	<i>Uncertainty budget for lead resistances compensation</i>	<i>61</i>
8.5.3	<i>Uncertainty budget for validation experiments with substitute thermistor</i>	<i>62</i>
8.5.4	<i>Uncertainty budget for thermistor temperature</i>	<i>63</i>
8.5.5	<i>Uncertainty analysis of self-heat correction factor k_{sh}</i>	<i>64</i>
8.6	EXTRAPOLATION OF 34420A DMM UNCERTAINTY OVER TIME	65
8.7	ORIGINAL PROJECT DESCRIPTION	66
8.8	CALIBRATION CERTIFICATES OF DIGITAL MULTIMETERS.....	70
8.9	PICTURE OF 19" RACK CONTAINING MEASUREMENT INSTRUMENTS.....	74

List of figures

Figure 1: Cross-section of VSL's water calorimeter with zoomed-in schematic of the radiation entrance window (taken from de Prez et al. 2016). 9

Figure 2: Qualitative example of thermistor and water temperatures during an absorbed dose measurement. The red line is the thermistor's self-heat temperature ΔT_{sh} , the blue line the water's temperature T_w and the black line is the thermistor's temperature T (taken from de Prez et al. 2016). 10

Figure 3: DMM measurement sequence with OCOMP and AZERO enabled (taken from Hamoen 2013). 14

Figure 4: Qualitative representation of influence of OCOMP setting on thermistor self-heat over time (taken from Mostert 2014). 14

Figure 5: General schematic of the measurement principle. 16

Figure 6: Detailed schematic of internal resistances and equipment interfacing, as developed and constructed for this study. The x's show points P_1 and P_2 from Figure 5 for each resistor. Certain parts of the schematic are examined in more detail in the figures listed above. 19

Figure 7: Connection between circuit 1 and circuit 2 for current measurements (see also Figure 6). 20

Figure 8: Schematic of current measurement through thermistor using 2nd DMM. 21

Figure 9: User interface of the self-heat parameter measurement program. 22

Figure 10: Path measured during 2-wire resistance measurement of single resistor. 23

Figure 11: Schematic of switch system internal resistance measurement on a channel's HI side. 24

Figure 12: Schematic of path resistance measurement inside interface box. 25

Figure 13: Path from DMM to thermistor and back (solid line). 26

Figure 14: Single circuit configuration with thermistor proxy tor in 4-wire mode and resistor 1 in 2-wire mode. 27

Figure 15: Thermistor resistance over time after enabling DMM measurement current. 33

Figure 16: Resistance change of thermistor over one minute intervals after DMM measurement current is enabled. 34

Figure 17: Thermistor temperature over time for the manual measurement series. 35

Figure 18: Temperature drift from $t = 10$ minutes with linear fit of the data points. 35

Figure 19: Normalized thermistor temperatures against power dissipated with drift compensation applied. Each point has error bars corresponding to their standard uncertainty, though they are less noticeable for some points. ... 36

Figure 20: Comparison of data from manual and automated measurement series. 37

Figure 21: Normalized thermistor temperature at various levels of power dissipation, with error bars indicating the standard uncertainty for each point. 38

Figure 22: Example using normalized temperature of VSL13T025 with linear and polynomial fits of the data. 38

Figure 23: Fit residuals for VSL13T025 for both fit methods applied to the data. 39

Figure 24: Qualitative illustration of minimum and maximum slopes within which all possible values of $C_{sh, 1}$ are found. 44

Figure 25: Schematic of equipment interface box circuit board with used connections and connector pins. 54

Figure 26: Schematic of connections made inside equipment interfacing box. 55

Figure 27: 34420A DMM's measurement uncertainty based on manufacturer's specifications, with extrapolation over the time period since last calibration. 65

Figure 28: Calibration certificate for DMM 1. 70

Figure 29: Calibration results for DMM 1. 71

Figure 30: Calibration certificate for DMM 2. 72

Figure 31: Calibration results for DMM 2. 73

Figure 32: 19" rack containing: switch system (top, left), Keithley 2001 DMM (top, right) and two Agilent 3458A opt 002 DMMs (center and bottom). In the background, the rear panel of the equipment interface box is also seen. 74

List of tables

Table 1: Comparison of results from two experiments to determine the total lead resistance of the circuit.	30
Table 2: Total lead resistance of each channel for both circuits.	31
Table 3: Validation experiment results with $R_p = 1 \text{ k}\Omega$	32
Table 4: Validation experiment with thermistor proxy results, with $R_p = 1 \text{ k}\Omega$	32
Table 5: Validation experiment using extension leads and thermistor proxy, with $R_p = 1 \text{ k}\Omega$	33
Table 6: Results and standard uncertainties from self-heat experiments with settling time = 600 s.	39
Table 7: Uncertainty components of measured resistance R_m and parallel resistance R_p	41
Table 8: Uncertainty components of lead resistances in parallel resistor (r_p) and thermistor (r) circuits.	42
Table 9: Sensitivity coefficients for calculated thermistor resistance from equation [23].	42
Table 10: Uncertainty budget for thermistor resistance calculated with equation [23].	42
Table 11: Example uncertainty budget for current passing through thermistor with $R_p = 5 \text{ k}\Omega$	43
Table 12: Example uncertainty budget for power dissipated by thermistor with $R_p = 5 \text{ k}\Omega$	43
Table 13: Example uncertainty budget for self-heat of thermistor VSL13T025 with $R_p = 5 \text{ k}\Omega$	44
Table 14: Uncertainty budget for self-heat parameter (1 st order) based on data from fifty measurement series.	45
Table 15: Combined standard uncertainty of 2 nd order self-heat parameter.	46
Table 16: Type B uncertainties for non-linearity parameter B	46
Table 17: Combined standard uncertainty of non-linearity parameter B	46
Table 18: Uncertainty contributions to calculated thermistor resistance with $R_p = 5 \text{ k}\Omega$	47
Table 19: Uncertainty contributions to thermistor self-heat with $R_p = 5 \text{ k}\Omega$	47
Table 20: Uncertainty contributions to self-heat correction factor.	47
Table 21: Switch system channel connections for both circuits on the 2 nd multiplexer card.	56
Table 22: Difference between 2 and 4-wire resistance measurements of the resistors in the interface box.	57
Table 23: Lead and internal resistance measurement results.	57
Table 24: Thermistor extension lead resistance measurement results.	58
Table 25: Results from first validation test of measurement setup.	59
Table 26: Results from validation with resistor as thermistor proxy.	59
Table 27: Results from validation with extension cable and known resistor.	60
Table 28: Uncertainty budget for lead resistance experiment, using R1.	61
Table 29: Uncertainty budget for thermistor and parallel resistor lead resistances.	61
Table 30: Uncertainty analysis of calculated (proxy) thermistor resistance with $R_p = \sim 1 \text{ k}\Omega$	62
Table 31: Summary of standard uncertainties with given parallel resistors.	62
Table 32: Sensitivity coefficients for equation [5].	63
Table 33: Uncertainty budget for thermistor temperature measurement.	63
Table 34: Uncertainty budget for self-heat correction factor k_{sh} for thermistor VSL13T033.	64

1 Introduction

Radiation therapy is one of the primary methods for treating cancer, alongside surgery and chemotherapy (Rosenberg 2008). Targeted application of ionizing radiation is used to kill malignant cancer cells with minimal damage to the surrounding healthy tissue. With this treatment modality, it is important to avoid over-exposing patients (WHO 2012). This requires accurate knowledge of the dose of radiation to which patients are exposed. The unit for absorbed dose of ionizing radiation is the Gray (Gy), where $1 \text{ Gy} = 1 \text{ J kg}^{-1}$. Clinical dosimetry of the high-energy photon and electron beams used in radiotherapy is typically performed using ionization chambers, which are calibrated in reference to a primary standard. VSL's primary standard for the absorbed dose to water is realized using a water calorimeter (de Prez 2008; de Prez and De Pooter 2008; de Prez et al. 2016). The use of a water calorimeter for absorbed dose to water measurements in reference conditions was first proposed by the National Institute of Standards and Technology (Domen 1982). Since then, the technology has improved significantly (Domen 1994; Krauss 2006; de Prez 2008) which led to it being adopted as the primary standard for absorbed dose to water calibrations in The Netherlands. VSL's most recent water calorimeter design can be used to perform on-site calibrations due to its portability and compact form-factor. This requires that the measurement equipment used is also portable, which imposes restrictions on the instruments and measurement method that can be used.

In water calorimetry, a beam of ionizing radiation is emitted into a phantom of water. The energy of the radiation is absorbed by the water, causing its temperature to increase by $\sim 0.24 \text{ mK} \cdot \text{Gy}^{-1}$. This change in water temperature is measured using thermally-sensitive resistors (called *thermistors*), which experience a change in resistance when their temperature changes. When measuring the resistance of the thermistor, the required source current causes the thermistor's temperature to rise above that of the water by 150 mK to 200 mK due to the dissipated power; this effect is called *self-heat*. A radiation-induced temperature change in the water will affect the thermistor's self-heat, as this change in water temperature affects its resistance. Therefore, the self-heat effect must be corrected for when determining the absorbed dose based on the thermistor's temperature measurements and is done by applying a *self-heat correction factor*. This correction factor is typically between 1.005 and 1.01 and has an estimated relative standard uncertainty of 0.07 % (de Prez et al. 2016).

In this study, the following steps have been taken towards improving the measurement of thermistor self-heat:

- Design, implementation and validation of an automated measurement method and equipment setup for measuring thermistor temperature as a function of dissipated power.
- Design and testing of a printed circuit board which connects the instruments in the measurement setup.
- Determination of an uncertainty budget.

The result is a validated measurement setup and automated method for determining the self-heat correction factor in an accurate and traceable manner that can be performed in VSL's laboratory as well as on-site.

1.1 Water calorimetry

VSL's primary standard for absorbed dose to water measurements is a water calorimeter. A sealed cylindrical phantom of water is surrounded by insulating material and equipment used for cooling the water. The water inside the phantom is brought to 4 °C. At this temperature water is at its maximum density, which reduces the influence of convection due to temperature gradients in the water phantom (explained in more detail in section 1.3). VSL's current water calorimeter design emphasizes portability and a compact form-factor without compromising the accuracy of its measurements (de Prez et al. 2016). Figure 1 provides an overview of several key components of the calorimeter.

On the self-heat effects of thermistors

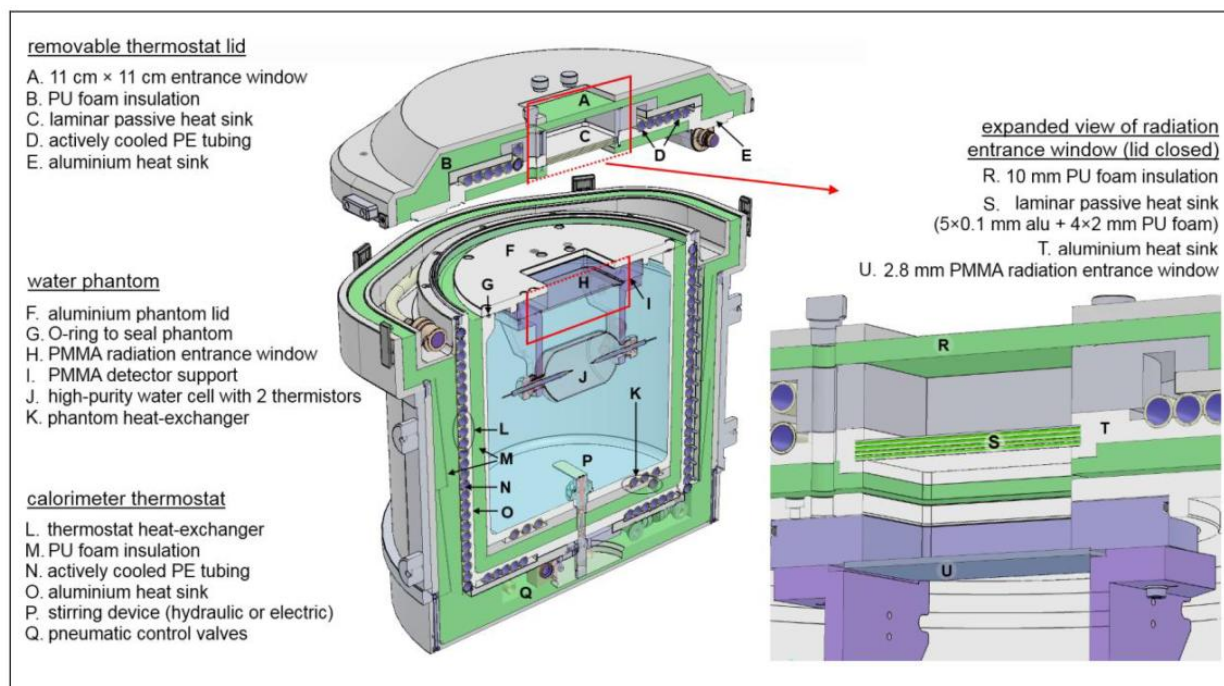


Figure 1: Cross-section of VSL's water calorimeter with zoomed-in schematic of the radiation entrance window (taken from de Prez et al. 2016).

Two negative temperature coefficient (NTC) thermistors with a nominal resistance of 10 kΩ at 4 °C are used to measure the radiation-induced temperature change in the water phantom. The thermistors are contained inside a cylindrical high-purity water cell made of glass. The cell is placed at a specific depth beneath the surface of the water calorimeter's lid; this is called the reference depth and it is one of the standardized reference conditions. The cell is filled with high-purity water obtained from a Millipore Milli-Q Integral 3 water purifier. Remaining impurities which could affect the temperature measurements are removed by saturating the water with argon gas. The thermistors are glued inside glass pipettes using an epoxy adhesive and connected to insulated, 4-wire electrical leads.

In water calorimetry, the absorbed dose to water D_w is determined based on a radiation-induced temperature increase in water (Seuntjens and Duane 2009) and is given by:

$$D_w = \Delta T_w \cdot c_{p,w} \cdot (1 - h)^{-1} \cdot \Pi k \quad [1]$$

where:

ΔT_w	Change in water temperature	[K]
$c_{p,w}$	Specific heat capacity of water at constant pressure	[J·kg ⁻¹ ·K ⁻¹]
h	Chemical heat defect	[-]
Πk	Product of correction factors	[-]

Included in Πk are factors to correct for perturbation due to the presence of non-water materials (mainly glass) and deviations from reference conditions (such as measurement depth and distance from radiation source).

On the self-heat effects of thermistors

Due to the self-heating of thermistors, there will be a difference between the water temperature T_w and the temperature T of the thermistor. The relationship between these temperatures is described by:

$$T_w = T - \Delta T_{sh} \tag{2}$$

where ΔT_{sh} in Kelvin is the self-heat temperature of the thermistor. When the temperature of the water rises, both the thermistor's temperature and self-heat change; the thermistor's temperature increases, which decreases its resistance, which in turn decreases its self-heat temperature. To provide an accurate reading of the water's temperature change ΔT_w when measuring a radiation-induced temperature change ΔT , a correction must be applied to compensate for thermistor self-heat:

$$\Delta T_w = \Delta T \cdot k_{sh} \tag{3}$$

with:

ΔT_w	Change in water temperature	[K]
ΔT	Change in thermistor temperature	[K]
k_{sh}	Self-heat correction factor	[-]

The need for this correction is illustrated in Figure 2.

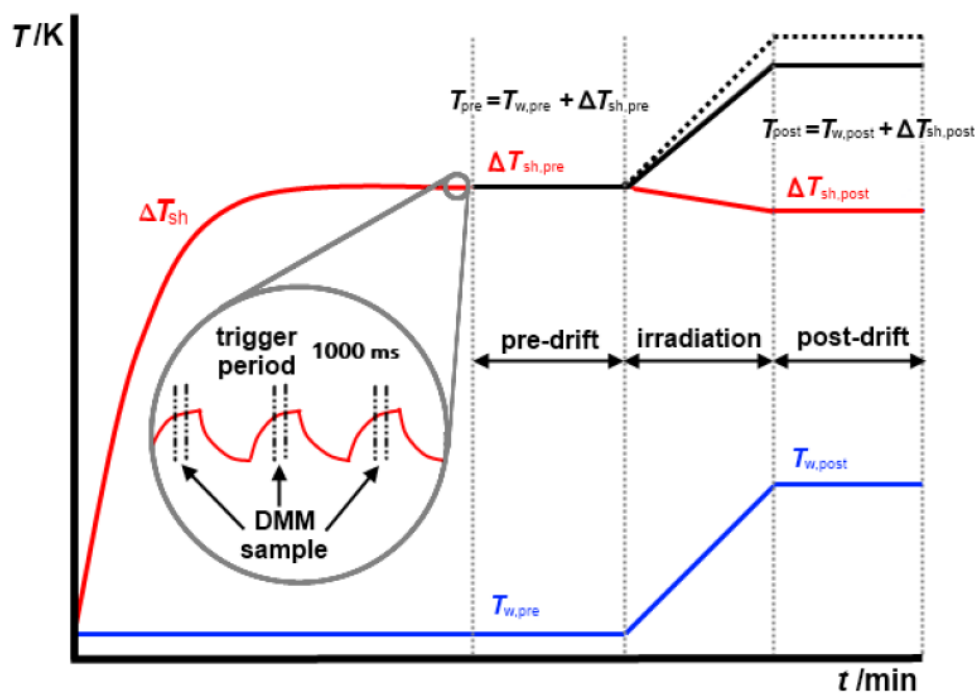


Figure 2: Qualitative example of thermistor and water temperatures during an absorbed dose measurement. The red line is the thermistor's self-heat temperature ΔT_{sh} , the blue line the water's temperature T_w and the black line is the thermistor's temperature T (taken from de Prez et al. 2016).

At $t = 0$ minutes, self-heat causes the thermistor's temperature to rise until it reaches equilibrium. Once a steady state has been reached, radiation measurements can begin. During irradiation, the thermistor's self-heat changes due to the increasing water temperature causing a decrease in resistance, which in turn decreases power dissipation. This leads to the thermistor "under-reporting" the temperature change of the water. The result of applying k_{sh} to the measured temperature change is shown by the dotted line in Figure 2, where the thermistor's temperature rise is equal to that of the water. The value of k_{sh} is typically between 1.005 and 1.01 for the thermistors in VSL's

On the self-heat effects of thermistors

Page 11 of 74

water calorimeter, depending on the magnitude of the thermistor's self-heat (further explained in section 1.3). The influence of the settings of the digital multimeter (DMM) is also highlighted, which will be explained further in section 1.4. Before deriving k_{sh} , some background information about NTC thermistors is needed.

1.2 NTC thermistors

The change in water temperature in the water calorimeter is measured using temperature-sensitive resistors, referred to as thermistors (from thermal resistor). The thermistors used in VSL's water calorimeter have a negative temperature coefficient (NTC), which means that their resistance decreases with an increase in temperature. Typically, NTC thermistors consist of a small amount of semi-conducting material pressed into a specific shape, such as a sphere. The amount of electrical current that passes through the thermistor (which, at a constant voltage, is inversely proportional to its resistance according to Ohm's law) is determined by the number of active charge carriers in the conduction band of the semi-conductor (Park and Bang 2003). When the temperature of the material increases, more charge carriers are promoted to the conduction band, allowing more current to pass through the material at the same applied voltage. An NTC thermistor's resistance can change as much as 6 % per Kelvin (Epcos 2009), making them highly suited for measuring small temperature changes. The following relationship is typically used to link a thermistor's resistance R and its temperature T :

$$R = R_0 \cdot e^{\beta \cdot \left(\frac{1}{T} - \frac{1}{T_0}\right)} \quad [4]$$

with:

R	Thermistor resistance	[Ω]
T	Thermistor temperature	[K]
T_0	Reference temperature	[K]
R_0	Thermistor resistance at reference temperature	[Ω]
β	Parameter specific to individual thermistor	[K]

Rewriting equation [4] to give the thermistor temperature in terms of the measured resistance yields:

$$T = \left(\frac{1}{T_0} + \frac{1}{\beta} \cdot \ln \left(\frac{R}{R_0} \right) \right)^{-1} \quad [5]$$

β is determined by a resistance versus temperature calibration over the temperature range of interest. Plotting the natural logarithm of R against the inverse of the temperature yields a relationship between the two parameters. β is defined as the slope of this line:

$$\beta = \frac{d(\ln R)}{d(1/T)} = -T^2 \cdot \frac{1}{R} \cdot \frac{dR}{dT} \quad [6]$$

This parameter is used to determine a thermistor coefficient α in K^{-1} , which is defined as the relative change in resistance per Kelvin:

$$\alpha = -\frac{\beta}{T^2} = \frac{1}{R} \cdot \frac{dR}{dT} \quad [7]$$

The calibration to determine β for the various thermistors at VSL is performed by VSL's Contact Thermometry department using 16 temperature points between 2 °C and 6 °C with a standard uncertainty of 2 mK. The uncertainty of β is determined by the linearity of the calibration curve, the number of calibration points and typical stability in the time period between calibrations, with an estimated value of 0.07 % (de Prez et al. 2016). Based on these calibrations, β and α are considered to be constant on the temperature range inside the water calorimeter.

1.3 Thermistor self-heat

Thermistor self-heat is caused by the power dissipated due to the current passing through it. As the thermistor's temperature is raised above that of its environment due to the dissipated power, heat transfer will take place. Due to the small temperature differences in the water calorimeter, radiative heat transfer effects can be neglected (Seuntjens and Duane 2009). Additionally, when thermistor power dissipation is below $\sim 120 \mu\text{W}$, convection is assumed to be negligible (Cen 2011). This leaves conduction as the primary method of heat transfer between the thermistor and its environment.

While the temperature of the thermistor is time-dependent for a brief period after a current is enabled to pass through it, a steady state temperature is eventually reached (typically taking five to ten minutes, see also ΔT_{sh} in Figure 2). By waiting long enough for the thermistor to reach its equilibrium temperature, the time-dependent behavior of the self-heat does not need to be taken into account. With that in mind, a thermistor's temperature, self-heat temperature and k_{sh} can be derived. To determine a thermistor's temperature change, a linear approximation of equation [7] is used:

$$\Delta T = \frac{1}{\alpha} \cdot \frac{\Delta R}{R} \quad [8]$$

where ΔT is the total temperature change of the thermistor (see equation [3]). The self-heat correction factor is used to isolate the water's temperature change from this result by determining the relationship between the change in water temperature and change in thermistor temperature (de Prez et al. 2016):

$$k_{\text{sh}} = \frac{dT_w}{dT} \quad [9]$$

Substituting equation [2] for T_w gives:

$$k_{\text{sh}} = 1 - \frac{d\Delta T_{\text{sh}}}{dT} \quad [10]$$

The change in thermistor self-heat is proportional to the power dissipated, which is proportional to the resistance of the thermistor (with constant source current), which in turn is a function of the temperature of the thermistor. Rewriting equation [10] in terms of these known relationships yields:

$$k_{\text{sh}} = 1 - \frac{d\Delta T_{\text{sh}}}{dP} \cdot \frac{dP}{dR} \cdot \frac{dR}{dT} \quad [11]$$

Equation [7] gives the relationship between resistance and temperature. As the current passing through the thermistor is constant when the system is in a steady state, $\frac{dP}{dR} = I^2$. $\frac{d\Delta T_{\text{sh}}}{dP}$ describes how the thermistor's self-heat changes as a function of power. Inserting the two known relationships while leaving $\frac{d\Delta T_{\text{sh}}}{dP}$ as it is, equation [11] becomes:

$$k_{\text{sh}} = 1 - \frac{d\Delta T_{\text{sh}}}{dP} \cdot I^2 \cdot R \cdot \alpha = 1 - \frac{d\Delta T_{\text{sh}}}{dP} \cdot P \cdot \alpha \quad [12]$$

$\frac{d\Delta T_{\text{sh}}}{dP} \cdot P$ is defined as the self-heat temperature ΔT_{sh} when convection is assumed to be negligible, which results in the following when substituted into equation [12]:

$$k_{\text{sh}} = 1 - \Delta T_{\text{sh}} \cdot \alpha \quad [13]$$

This is the self-heat correction factor, which is based on the self-heat temperature and the relative change in resistance per Kelvin of the thermistor. When convective heat transfer is assumed to be negligible, $\frac{d\Delta T_{\text{sh}}}{dP}$ is defined as the self-heat constant $C_{\text{sh},1}$ (in $\text{mK} \cdot \mu\text{W}^{-1}$) i.e. $\Delta T_{\text{sh}} = C_{\text{sh},1} \cdot P$. The "1" in the subscript of $C_{\text{sh},1}$ indicates that it refers to the self-heat parameter determined under the assumption that convection is negligible, as this is a 1st order approach to determining self-heat.

On the self-heat effects of thermistors

Page 13 of 74

However, this assumption is based on the results of computer simulations as described by Cen (2011). To investigate the magnitude of non-linear effects (such as convection cooling the thermistors) in the water calorimeter, a 2nd order approach is used for data analysis. A previous study (Mostert 2014) describes a method used to determine the self-heat temperature of thermistors where the influence of non-linear effects such as convection are included. This method involves measuring the thermistor's temperature at various known levels of power dissipation. Mostert (2014) derives an equation that relates the self-heat to power dissipation in cases where 2nd order effects are included:

$$\Delta T_{sh} = C_{sh,2} \cdot P + B \cdot P^2 \quad [14]$$

where B (in $mK \cdot \mu W^{-2}$) is the non-linearity parameter of the thermistor's self-heat and $C_{sh,2}$ is the self-heat parameter when 2nd order effects are included. Non-linear behavior of self-heat is assumed to be caused by convection cooling the thermistor. The advantage of including convective effects in the calculation is increased accuracy at higher levels of power dissipation, provided that $C_{sh,2}$ and B can be determined in a reliable manner with comparable accuracy to $C_{sh,1}$. The values of B and $C_{sh,2}$ are given by the coefficients of a 2nd order polynomial fit when plotting thermistor temperature as a function of dissipated power and compensating for background temperature drift (explained in section 2.5).

If convection is truly negligible, this will be reflected by the value of B ; the closer B is to zero, the smaller the influence of non-linear effects on thermistor self-heat. The assumption that convective cooling has a negligible influence on thermistor self-heat in the water calorimeter will be tested using the determined non-linearity parameter. For the assumption to hold true, a criterion is set:

$$|B \cdot P| \ll C_{sh,2} \quad [15]$$

For the above equation to be considered true, $|B \cdot P|$ should be at most 1 % of $C_{sh,2}$. If that is the case, then the influence of non-linear effects on the self-heat temperature is considered negligible; the self-heat is then calculated using $\Delta T_{sh} = C_{sh,2} \cdot P$.

Both the linear and 2nd order method for determining self-heat will be studied and the results compared. The uncertainty of each method is determined and the influence on the accuracy of k_{sh} is calculated. Before explaining how this is accomplished, a key piece of equipment is described in more detail.

1.4 Agilent 3458A digital multimeter

VSL's water calorimeter setup includes two Agilent 3458A opt002, 8½ digit digital multimeters for measuring the resistance of the thermistors. This model has been selected primarily because of its excellent linearity on the 1 volt scale, which is used internally to measure on the 10 kΩ range (where the thermistor's nominal resistance lies). The option 002 model of the 3458A DMM decreases the voltage reference's drift to 4 parts-per-million (ppm) per year, ensuring high accuracy in the time period between calibrations. Linearity is particularly important when performing water calorimetry, which is based on resistance *change* measurements rather than an absolute measurement. On the 1 volt scale, the 3458A opt002 DMM shows a linearity that is better than 40 nV/V (van den Brom et al. 2007). When read out through a GPIB (General Purpose Interface Bus) connection, the DMM provides two additional digits for its measurement. The value of these digits is based on analysis of the last digit on the display. The result is a better measurement resolution than the specifications suggest when a GPIB connection is used, due to the large number of samples used in the analysis.

An additional advantage of using this method of determining the thermistor's resistance is flexibility for on-site measurements. An alternative method used for determining the resistance of a thermistor inside a water calorimeter is a Wheatstone bridge, which experiences a decrease in sensitivity when lead resistances increase (Domen 1994). Some on-site applications of the calorimeter require the use of leads longer than 15 meters, which may be troublesome when using a Wheatstone bridge circuit. Direct measurements of the thermistor's resistance with a DMM are not affected by these lead resistances (explained in more detail in the next chapter), making this method better suited for such on-site applications.

On the self-heat effects of thermistors

Offset-compensation (OCOMP) and auto-zeroing (AZERO) are enabled on the DMM for enhanced accuracy when measuring resistance changes during water calorimetry. When offset-compensation is enabled, the DMM makes an additional voltage measurement without any source current applied. The total offset voltage in the circuit is measured in this manner and subtracted from the measurement samples. With auto-zeroing, the DMM measures its internal offset voltage and removes this from its measurement samples as well. Figure 3 shows the measurement cycle of the DMM with these settings activated.

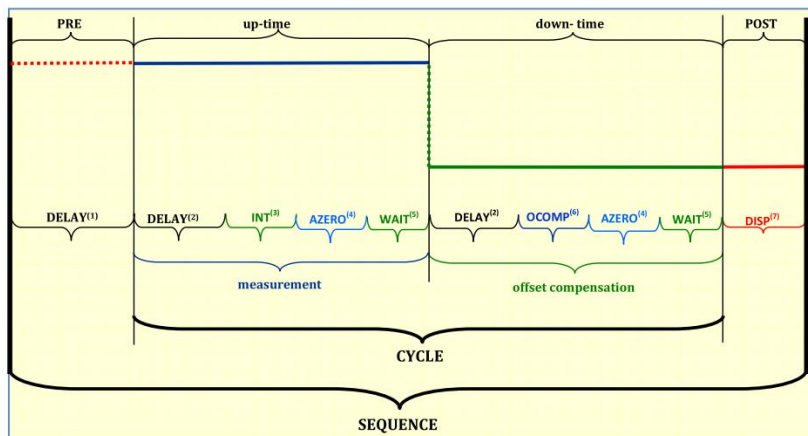


Figure 3: DMM measurement sequence with OCOMP and AZERO enabled (taken from Hamoen 2013).

The integration time of each measurement is set to 10 power line cycles (200 ms for the 50 Hz network frequency used in The Netherlands) to reduce the influence of noise introduced by the power network. Each measurement therefore takes 200 ms and 4 measurements are needed per cycle (measurement, AZERO, OCOMP, AZERO), so each measurement cycle takes 800 ms. Because of the length of time needed for a single cycle, a 1 Hz external trigger source is used (Gabotronic XProtolab) to provide a constant measurement frequency. This also ensures that both DMMs will sample at the same time.

These settings are used primarily to enhance the accuracy of absorbed dose measurements, where resistance changes of $\sim 0.2 \Omega$ are measured, which is equivalent to an absorbed dose of 2 Gray. For measuring the self-heat (where resistance changes on the order of 10-100 Ω occur), this level of accuracy is not strictly necessary. However, the OCOMP setting inserts a period where no source current is active into the measurement cycle. In the time where the current is not flowing, the thermistor will cool down (Mostert 2014).

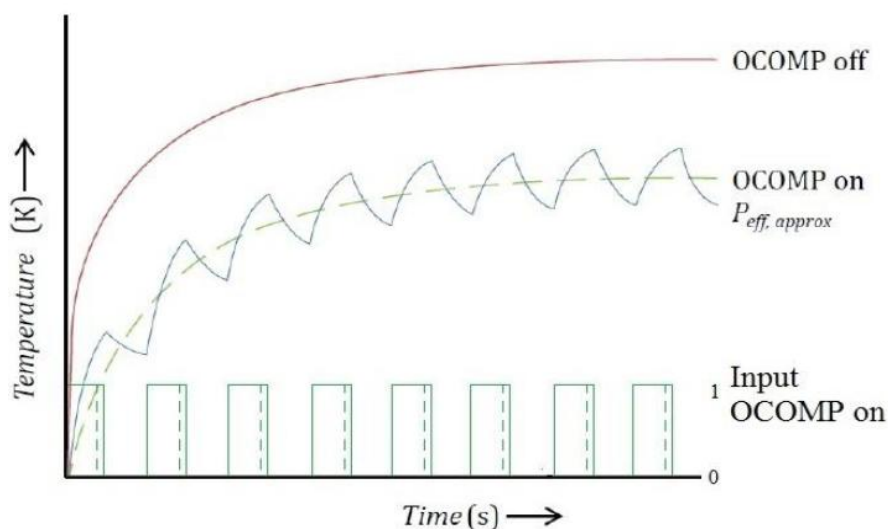


Figure 4: Qualitative representation of influence of OCOMP setting on thermistor self-heat over time (taken from Mostert 2014).

On the self-heat effects of thermistors

Page 15 of 74

As the thermistor's temperature is fluctuating over time, the self-heat temperature needs to be determined at the time when the DMM makes its measurement sample. The approximate time where sampling occurs is indicated by the area to the right of the dotted line on the input current blocks in Figure 4. By using the same DMM settings for both self-heat measurements and water calorimetry, use of the determined self-heat parameter is most likely to yield an accurate representation of the thermistor's self-heat temperature at the time when the sample is made.

1.5 Evaluation of measurement uncertainties

Knowing the uncertainty of a measurement is as important as the measurement itself. For that reason, the uncertainties evaluated in this report follow the *Guide to the expression of uncertainty in measurement* (JCGM 2008). Uncertainties are rounded to 2 significant figures.

The combined standard uncertainty of a function f with parameters x_1 through x_N is given by:

$$u_f = \sqrt{\sum_{i=1}^N (s_{x_i} \cdot u_{x_i})^2} \quad [16]$$

where u_{x_i} is the standard uncertainty of variable x_i and s_{x_i} is its sensitivity coefficient. These coefficients describe how the output of the function varies with a change in the corresponding input parameter. They are determined by taking the absolute value of the partial derivative of the function with respect to the corresponding variable:

$$s_{x_i} = \left| \frac{\partial f}{\partial x_i} \right| \quad [17]$$

The uncertainty of a variable can be divided into two categories: Type A and Type B. Type A uncertainties are derived from statistical analysis of a series of observations, while all other types of uncertainties are categorized as Type B. An example of a Type B uncertainty is the resolution of a measurement instrument. Both types are based on probability distributions however, and are quantified in the same manner.

A coverage factor k may be given alongside a standard uncertainty, e.g. $k = 1$. The coverage factor is used as a multiplier of the standard uncertainty. For a Gaussian probability distribution, $k = 1$ means the uncertainty covers an interval of one standard deviation on either side of the mean value and corresponds with a confidence level of 68 %. In this report, unless stated otherwise, the coverage factor $k = 1$ is used.

In chapter 4, the process of constructing an uncertainty budget for the experiments in this report is explained further. A detailed example is presented, describing step-by-step how the uncertainty in the thermistor's resistance is calculated using measurement data, instrument specifications etc. First, however, the measurement method is explained in more detail.

2 Materials and methods

Building on the knowledge summarized in the previous chapter, a measurement setup is constructed and a method developed in this study to accurately determine the self-heat parameter of NTC thermistors. This chapter describes the chosen setup and method, discusses how they are validated, and explains how the self-heat parameter is determined from the measured data.

2.1 Measurement method

In the introduction, it is mentioned that a thermistor's self-heat parameter can be determined based on temperature measurements at varying levels of power dissipation. To vary the thermistor's power dissipation, a resistor is used in parallel to divert a portion of the DMM's source current from the thermistor as shown in Figure 5.

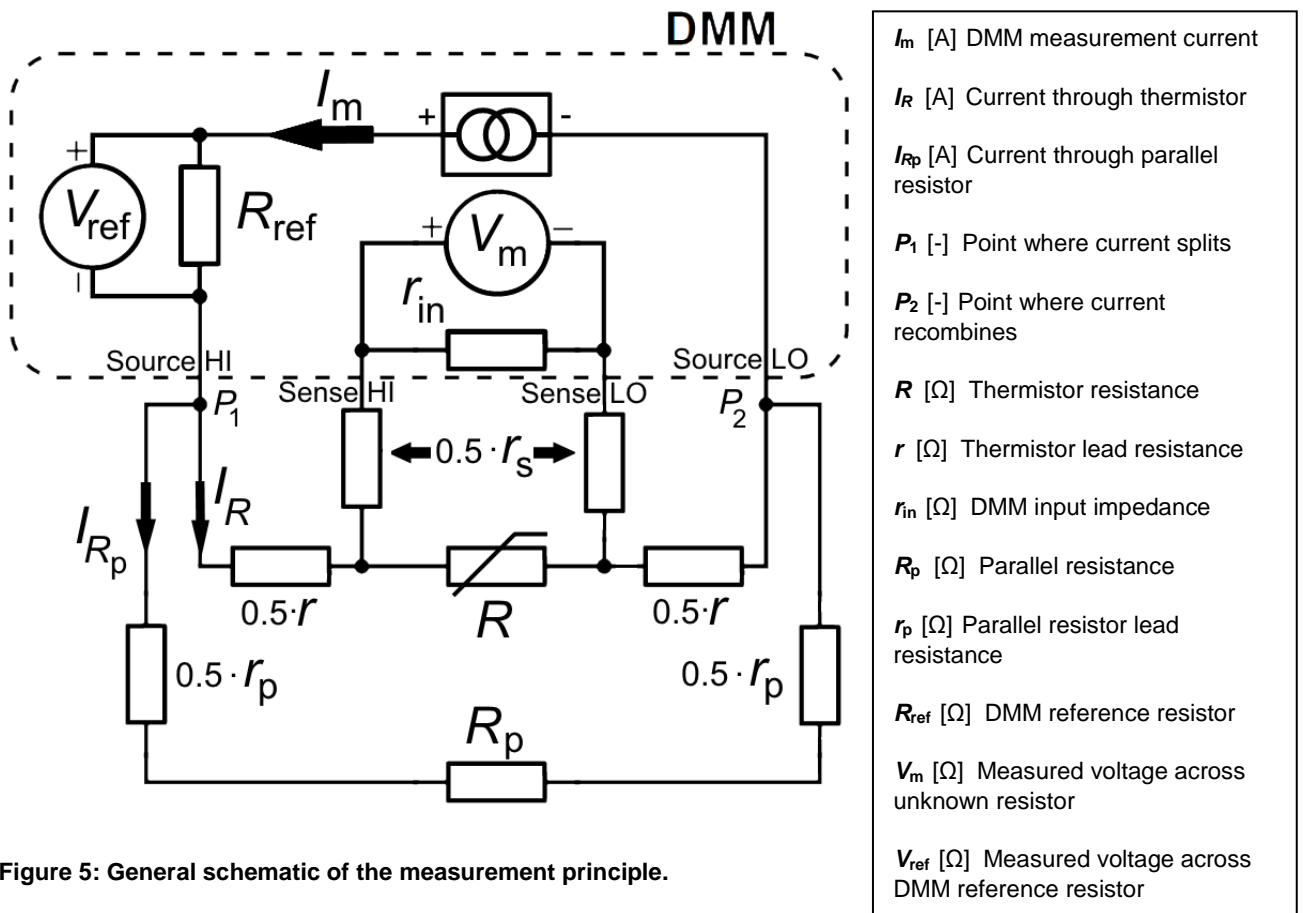


Figure 5: General schematic of the measurement principle.

The setup shown in Figure 5 can be used to measure the resistance of the circuit with two methods, referred to as 2-wire resistance measurements and 4-wire resistance measurements. For both methods, the DMM generates a constant measurement current I_m . The current passes through the reference resistor R_{ref} and the voltage drop across the reference resistor (V_{ref}) is measured by a voltmeter. At this point, the 2 and 4-wire methods diverge.

On the self-heat effects of thermistors

Page 17 of 74

In 4-wire resistance measurement mode, the voltage measured over the sense leads (V_m) is compared to the voltage over the reference resistor (Keithley 2004):

$$R_m = R_{ref} \cdot \frac{V_m}{V_{ref}} \quad [18]$$

where R_m is the (unknown) resistance being measured by the DMM. For the measurement setup shown in Figure 5, the thermistor is the unknown resistor. For 2-wire measurements, V_m is the voltage measured between the DMM's Source HI and LO inputs, including any lead resistances that are present. Therefore 4-wire measurements are more accurate than 2-wire measurements for this application, as the DMM will measure the thermistor's resistance without including lead resistances. In short, the 2-wire mode of the DMM is used to measure the resistance of a complete circuit including lead resistances. 4-wire mode is for measuring the resistance of specific components without the influence of lead resistances.

Including a parallel resistor as shown in Figure 5 influences 4-wire resistance measurements, however. When placing a resistor parallel to the thermistor, a portion of the measurement current is diverted. Equation [18] will only give the thermistor's resistance when the current passing through R_{ref} and the thermistor is the same. The point where the current is split is indicated by P_1 , with recombination of the two currents taking place at point P_2 . With less current passing through the thermistor, the voltage measured across it is also lower. As a result, the resistance shown on the DMM's display is the total resistance between P_1 and P_2 , not that of the thermistor. It is possible to calculate the thermistor's resistance based on the resistance measured by the DMM and the known value of the parallel resistance. First, the influence of the DMM's sense circuit on resistance measurements is investigated. Outside of the DMM, there are three significant resistors (the magnitude of the lead resistances is much smaller, so they are not considered for now): the thermistor (R), the parallel resistor (R_p) and the DMM's input impedance (r_{in}). Both R and R_p have a resistance on the order of 10 k Ω , while r_{in} is greater than 10 G Ω (Agilent Technologies 2011). As such, r_{in} 's influence on the total resistance of the circuit is negligible as demonstrated below:

$$\frac{1}{R_{total}} = \frac{1}{R} + \frac{1}{R_p} + \frac{1}{r_{in}} = \frac{1}{10^4} + \frac{1}{10^4} + \frac{1}{10^{10}} \quad [19]$$

$$\approx \frac{2}{10^4}$$

The error made when not including r_{in} 's contribution to the total resistance of the circuit is -2.5 m Ω . For measurements on the 10 k Ω scale of the DMM, this represents an uncertainty of at most 3 ppm. Compared to the other uncertainty contributions for measurements with the DMM, this is insignificant (see section 4.1). Therefore the influence of r_{in} is considered to be negligible, meaning that no current is considered to be passing through r_{in} and the sense circuit's leads. Thus, the sense circuit's lead resistance (r_s) has no influence on the measurements. This leaves R and R_p with their corresponding lead resistances to determine the thermistor's resistance.

Using Ohm's law, V_m and V_{ref} can be written in terms of current and resistance. Doing this in equation [18] gives the resistance measured by the DMM's sense circuit in terms of the current passing through the thermistor (I_R), DMM measurement current (I_m) and thermistor resistance (R):

$$R_m = R_{ref} \cdot \frac{I_R \cdot R}{I_m \cdot R_{ref}} = \frac{I_R \cdot R}{I_m} \quad [20]$$

When calculating the division of current between the thermistor and parallel resistor in this setup, it is necessary to take the total lead resistance that exists between points P_1 and P_2 (from Figure 5) into account. The current passing through the thermistor is then given by:

$$I_R = I_m \cdot \frac{R_p + r_p}{R_p + R + r + r_p} \quad [21]$$

Combining equation [21] and equation [20] yields:

$$R_m = \frac{R \cdot (R_p + r_p)}{R_p + R + r + r_p} \quad [22]$$

On the self-heat effects of thermistors

Page 18 of 74

It can be seen that if r and r_p are 0, equation [22] gives the well-known formula for the total resistance for a circuit with two parallel resistors. This equation can be rewritten to give the thermistor's resistance based on the measured, parallel and lead resistances:

$$R = \frac{R_m \cdot (R_p + r_p + r)}{R_p - R_m + r_p} \quad [23]$$

Both r and r_p represent the total lead resistance from point P_1 to point P_2 for their respective resistors R and R_p , which will be elaborated on in section 2.3. Equations [21] and [23] can also be combined to give the power dissipated by the thermistor:

$$P = I_R^2 \cdot R = \left(\frac{I_m \cdot (R_p + r_p)}{R_p + R + r + r_p} \right)^2 \cdot \frac{R_m \cdot (R_p + r_p + r)}{R_p - R_m + r_p} \quad [24]$$

Altering the power dissipated by the thermistor can be done by varying ($R_p + r_p$). To highlight the need to take lead resistances into account, an example calculation is presented.

Let $R = 10 \text{ k}\Omega$, $R_p = 1 \text{ k}\Omega$, $r_p = r = 0.001 \text{ k}\Omega$. With equation [22], R_m is calculated to be $0.9098 \text{ k}\Omega$. Using this value of R_m to re-calculate the value of R with equation [23] without including lead resistances (i.e. $r_p = r = 0$) results in a calculated thermistor resistance (R_{calc}) of $10.09 \text{ k}\Omega$. This is a difference of $90 \text{ }\Omega$ when compared to the original thermistor resistance of $10 \text{ k}\Omega$. Not including lead resistances in the calculation causes an error of nearly 1 % in the calculated thermistor resistance with the example values presented at the start of the paragraph. Despite the small magnitude of r and r_p , it is worthwhile to accurately measure these resistances and include them in the calculations.

2.2 Equipment

To implement the system shown in Figure 5, a number of instruments already present in the water calorimeter's mobile setup are used. A new piece of equipment (equipment interface box) is specifically designed and constructed in this study to allow for remote activation of parallel resistors using a switch system. Additionally, it provides physical connections for all leads and connectors in the setup. The setup contains 2 identical circuits dubbed "circuit 1" and "circuit 2", each of which consists of one DMM, one thermistor, 5 parallel resistors and the required leads to connect them. The two circuits share the switch system and interface box, but are kept isolated from each other. When referring to a specific component on a circuit e.g. $r_{i, x}$, x represents the circuit's number, so $r_{1, 2}$ is the thermistor lead resistance for circuit 2. For resistors, a subscript i is used, so $r_{\text{sc}, R3}$ refers to the switch system's internal resistance for resistor 3's channel.

A detailed schematic of the setup is shown in Figure 6. For a legend of the various resistances displayed, refer to the list below:

r_c	Flat cable resistance
$r_{dx, 1}$	DMM lead resistance
$r_{dx, 2}$	Interface box internal resistance
$r_{i, x}$	Lead resistance for connection to DMM I+ for circuit x
$r_{l, x}$	Lead resistance for thermistor extension lead on circuit x
$r_{\text{sc}, \text{in } x}$	Switch system input resistance for circuit x
$r_{\text{sc}, Ri}$	Switch system resistance for channel belonging to resistor i
$r_{\text{sc}, \text{Th}x}$	Switch system resistance for channel belonging to thermistor on circuit x
$r_{w, \text{Th}x} / r_{w, i}$	Interface box lead resistance for thermistor x / resistor i

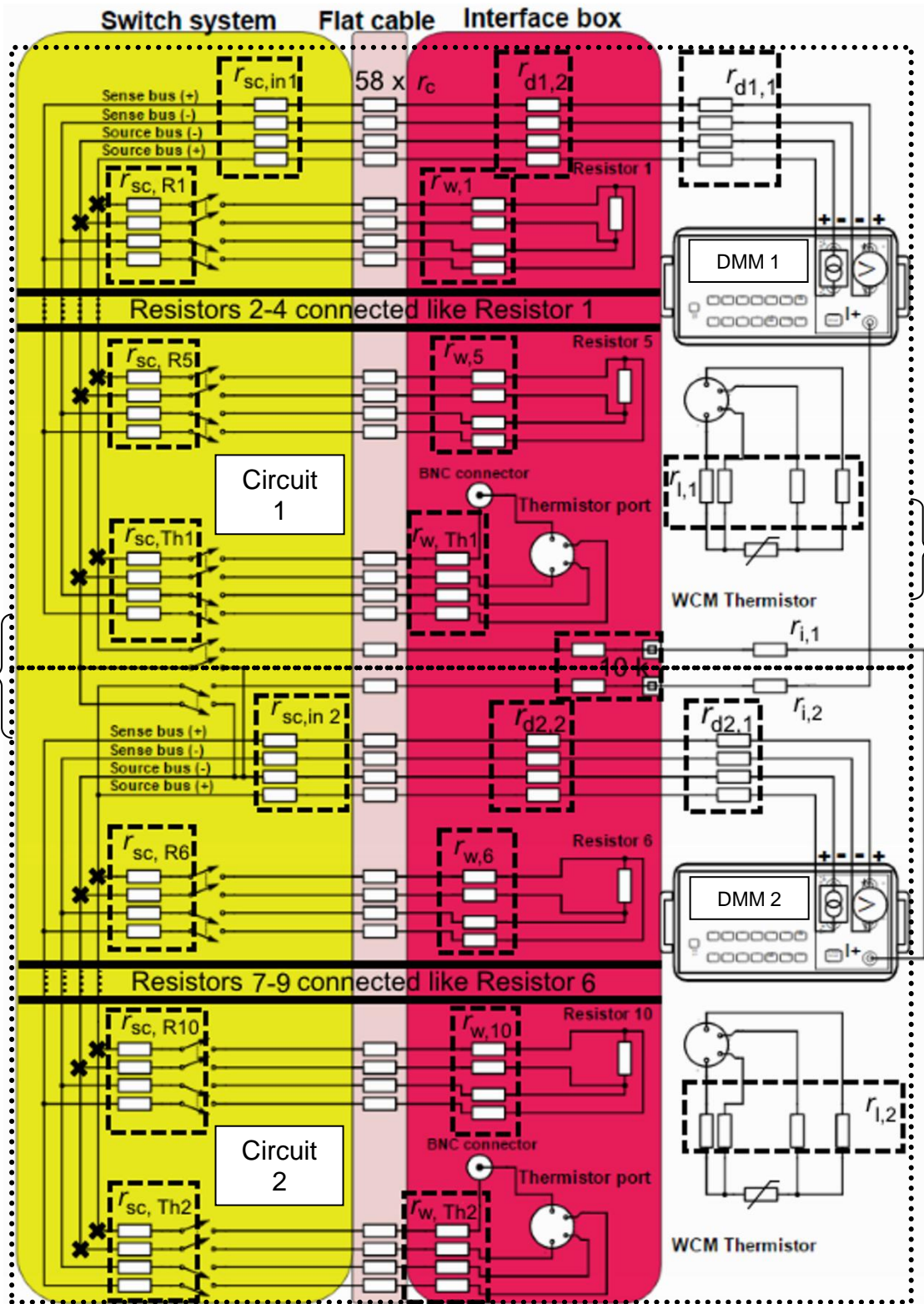


Figure 8

Figure 7

Figure 6: Detailed schematic of internal resistances and equipment interfacing, as developed and constructed for this study. The x's show points P_1 and P_2 from Figure 5 for each resistor. Certain parts of the schematic are examined in more detail in the figures listed above.

On the self-heat effects of thermistors

Page 20 of 74

The core of the setup is comprised of two Agilent 3458A opt002 digital multimeters (serial numbers US28029739 & US28029799, henceforth DMM 1 and DMM 2, respectively), a custom-made equipment interface box (ML1603003), a Keithley 7001 Switch System (serial number 0554743) containing 2 Keithley 7011-C relay cards, and two of VSL's NTC thermistors (VSL13T025 and VSL13T033).

The DMMs and switch system are connected to a General Purpose Interface Bus. The bus is connected to a laptop using a GPIB-to-USB converter. Software developed as a part of this study handles data acquisition and ensures that the DMMs and switch system are correctly configured for the requested measurement procedure.

In the next few sections, the functionality of the components of the measurement setup is described in more detail.

2.2.1 Equipment interfacing box

To handle the various in-and-outputs of the devices used in the measurement setup, a custom interfacing box is designed and built as part of this study. DMMs are connected to the box using coaxial cables with a BNC connector (one cable for source HI/LO and one for sense HI/LO) while the switch system is connected using a 96 core ribbon flat cable. The thermistors are connected with 4-pole electrical leads terminated with a LEMO (PCA-0S) connector. Additional features include a connector for the current input of the DMMs as well as a (usually short-circuited) BNC connector to measure the current flowing through the thermistors. The box fits on the 19" mobile rack which contains the other equipment belonging to the calorimeter's measurement setup (see section 8.9 of the appendix for a picture).

The interface box contains two sets of identical resistors (Neohm Type YR8B, (Tyco Electronics 2005)) with nominal resistances of 1 k Ω , 5 k Ω , 10 k Ω , 20.5 k Ω and 50 k Ω , as well as two ports that a thermistor (with or without extension cable) can be plugged into. The parallel resistors are selected primarily based on their nominal resistance and low temperature coefficient (15 ppm K⁻¹). The interface box is connected to the switch system with the flat cable shown in Figure 6. The switch system allows for remote activation of thermistors and/or parallel resistances by closing or opening the switches that link the resistors to the source and sense buses (see Figure 6). Using a bus-type connection, any number of resistors (up to 5 + 1 thermistor) can be added to the circuit in parallel. Measurements can be performed in 2 or 4-wire mode (explained in section 2.1). Most measurements will be performed using 4-wire mode, as it is the most accurate, but the 2-wire measurement mode is useful when measuring the lead and internal resistances as described in section 2.3.

The resistors in the interface box are calibrated using the DMMs and the software program. One at a time, the individual resistors are connected to the source and sense buses and a number of 4-wire measurements (specified by the user) are made. The average of the measurements gives the resistance of that specific resistor. This is useful for tracking the stability of the parallel resistors over long periods of time.

The interface box allows for additional functionality in the form of current measurements. When the correct channels are activated (see Figure 6 and section 8.2 of the appendix), one of the DMMs can measure the current produced by the other. This is used for calibration of the DMM's current source. Figure 7 shows a zoomed in schematic (from Figure 6) of the connection between the two circuits.

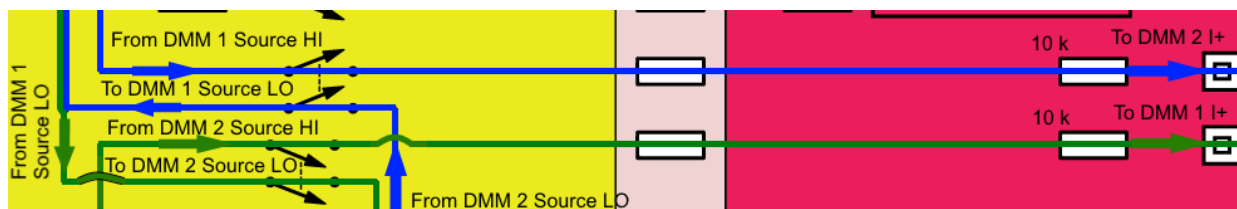


Figure 7: Connection between circuit 1 and circuit 2 for current measurements (see also Figure 6).

The measurement current of interest is the one produced by the DMM when performing resistance measurements on the 10 k Ω scale, which is the nominal resistance of the thermistors at 4 $^{\circ}$ C. To measure this current, one DMM is set to 4-wire resistance measurement mode with its range at 10 k Ω while the other is set to the 100 μ A range. A 10 k Ω resistor is placed before the exit lead to the DMMs' respective I+ sockets to ensure that the DMM providing the current does so using the correct resistance range. This prevents the DMM from generating too much current should the user forget to manually set the range (the DMM provides more current at lower resistance ranges).

On the self-heat effects of thermistors

Page 21 of 74

Between the thermistor port's connection with the DMMs Source + bus there is a BNC connector. Normally this connection is short circuited, but it can be used to directly measure the current flowing through the thermistor by connecting a lead to the 2nd DMM (or an additional DMM). When using DMM 1 to measure the current flowing through thermistor 2, manual adjustments to the leads going into DMM 1's rear terminal must be made (see Figure 8).

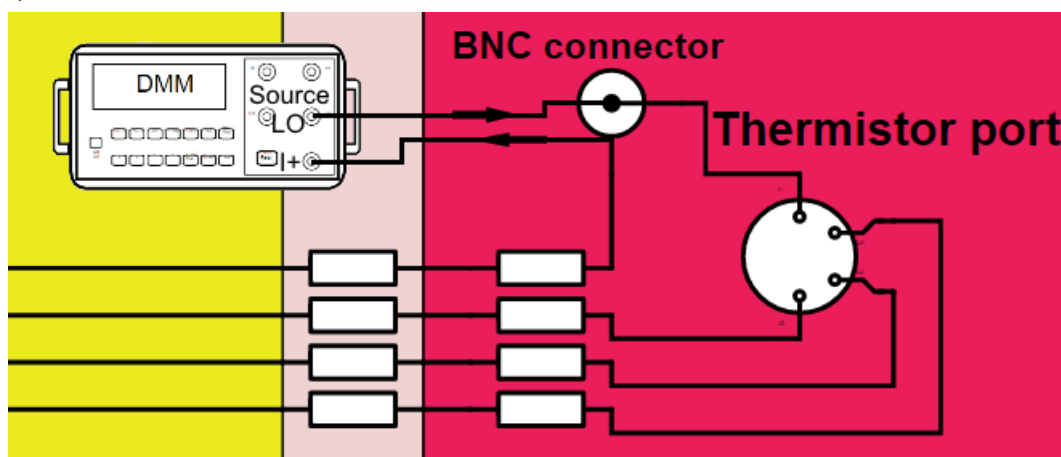


Figure 8: Schematic of current measurement through thermistor using 2nd DMM.

A detailed design schematic of the circuit board and an overview of the connections made inside can be found in the appendix (section 8.1).

2.2.2 Keithley 7001 Switch system

To facilitate automated measurements, a Keithley 7001 Switch equipped with two 7011-C multiplexer cards system is used to close or open the desired electrical connections. A 7011-C multiplexer card has 40 available channels (with two poles each), allowing for a maximum of 20 resistors to be connected in 4-wire mode. In the current setup, only 12 resistors are used. To connect a particular component to the desired bus (an electrical connection that is shared by all components), the corresponding channels must be closed. An overview of channel assignments for the measurement setup is given in Table 21 in the appendix (section 8.2).

2.2.3 Custom measurement program

To allow for automated control of the measurement setup, a computer program is written in the Delphi programming language. Delphi is an object-oriented programming language based on Pascal with its own integrated development environment (IDE). This allows for rapid program development. The primary functions of the program are to perform measurement procedures in an automated fashion and to save and display the results. The main interface of the program is shown in Figure 9.

On the self-heat effects of thermistors

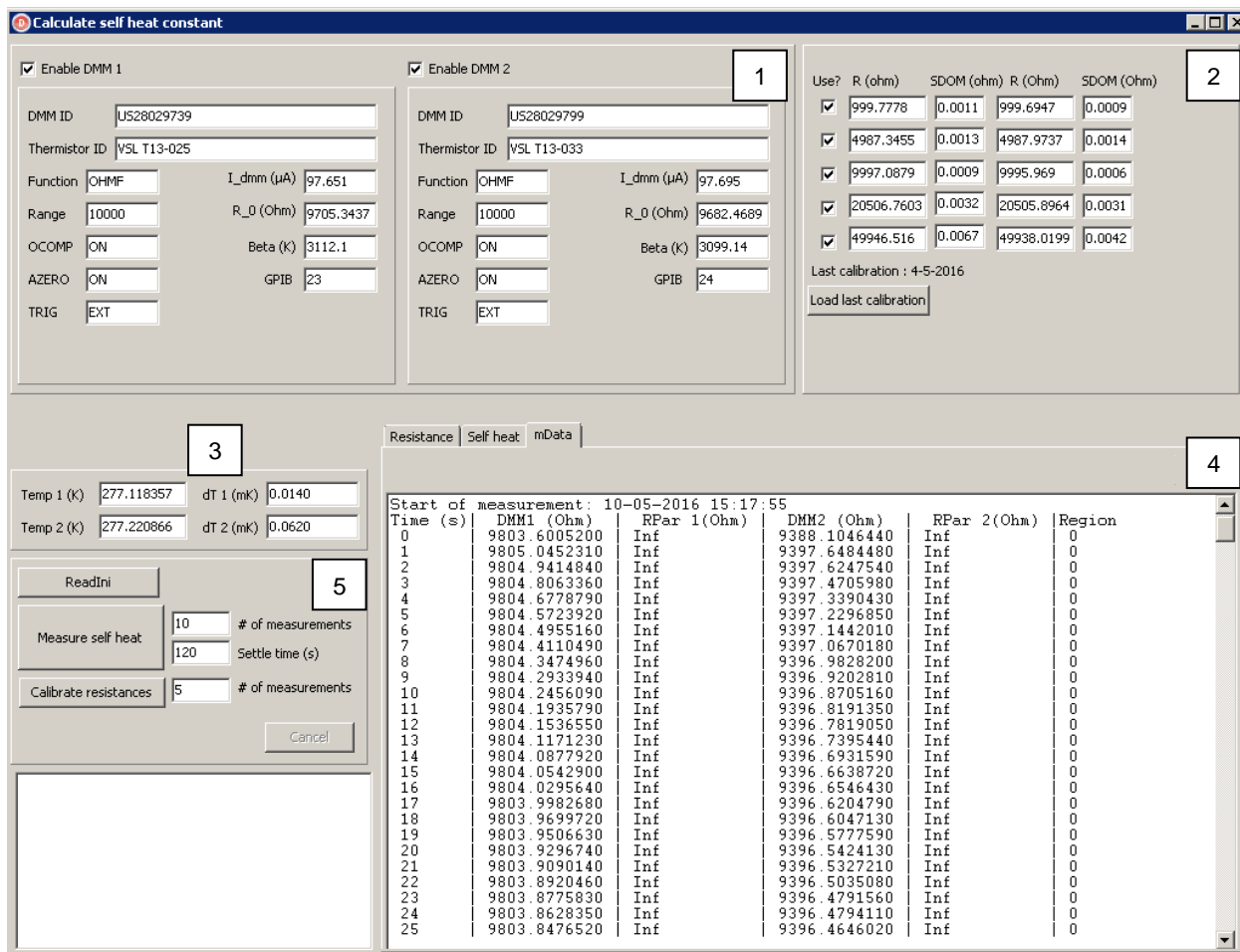


Figure 9: User interface of the self-heat parameter measurement program.

The interface has various components that either display information to the user or allow various actions to be performed. Below is a brief description of some important elements:

DMM info panels (1 in Figure 9): Here, the current settings of the DMM are displayed, as well as some important properties of the thermistor connected to the circuit. These properties are loaded from a text file at the user's request. One of the DMMs can also be disabled if the user wishes to measure with a single DMM instead.

Parallel resistor calibration information for circuit 1 (left) and circuit 2 (right) (2 in Figure 9): The result of the last resistance calibration performed is displayed here. A previous calibration can also be loaded from a text file. The checkboxes on the left side of the panel allow the user to exclude one or several parallel resistances from being used during a self-heat measurement procedure.

Thermistor temperature information (3 in Figure 9): During a measurement, the current temperature of the thermistor is displayed in addition to the change in temperature since the previous measurement.

Data display panels (4 in Figure 9): These three tabs show the user a variety of measurement information. The mData tab (visible in Figure 9) displays a log of the measurements made so far, along with the used parallel resistor (if any). The resistance tab shows a graph of the measured resistance over the course of the procedure. The self-heat tab shows a thermistor temperature vs. power graph at the conclusion of a measurement series.

Program functions (5 in Figure 9): These buttons allow the user to execute various procedures. "ReadIni" loads relevant program data from a text file, such as the DMM's GPIB addresses. "Measure self heat" initiates the self-heat measurement procedure with the selected parallel resistances. The user can input the amount of time that the system is allowed to settle after a change in setup (i.e. activating or deactivating a parallel resistor) and the number

On the self-heat effects of thermistors

of measurements made once that time has elapsed. "Calibrate resistances" initiates a calibration routine for the parallel resistors. The number of measurements made for each resistor can also be specified by the user. More details about the self-heat measurement and parallel resistance calibration procedures are given in section 2.4.3.

Before using the program to perform experiments, however, a number of steps must be taken to validate the equipment, measurement setup, and method.

2.3 Measurement of lead and internal resistances

Based on the model of the setup described in section 2.1, the lead and internal resistances of various components influence the accuracy of the calculated thermistor resistance. The next two sections describe the components that these internal resistances are comprised of and how they are calculated. The results of these measurements (which are made by hand) are then used to enhance the accuracy of the thermistor resistance calculation. Measurement of parallel resistor lead resistances

In Figure 6, various internal and lead resistances are shown. To accurately calculate the resistance of an unknown resistor for this system using equation [23], it is necessary to measure and include some of these values in the calculation. A resistance measurement of a single resistor in 4-wire mode is not affected by lead resistance; however, when a parallel resistor is included, lead resistances between points P_1 and P_2 (as shown in Figure 5) affect the division of current between the two. The current passing through the resistor that is being measured determines the voltage measured by the DMM (equation [20]). Additionally, when the parallel resistors are calibrated, it is done in 4-wire mode. The value of the total parallel resistance includes any lead or internal resistances between points P_1 and P_2 in Figure 5, which is not measured during the calibration.

First, the total resistance of a full path including lead resistances (see Figure 10) is determined by measuring each resistor in the equipment interface box separately using the 3458A's 2-wire mode. Then, each resistor is measured again in 4-wire mode. The difference between the two measurements for each resistor is the total internal resistance of each circuit.

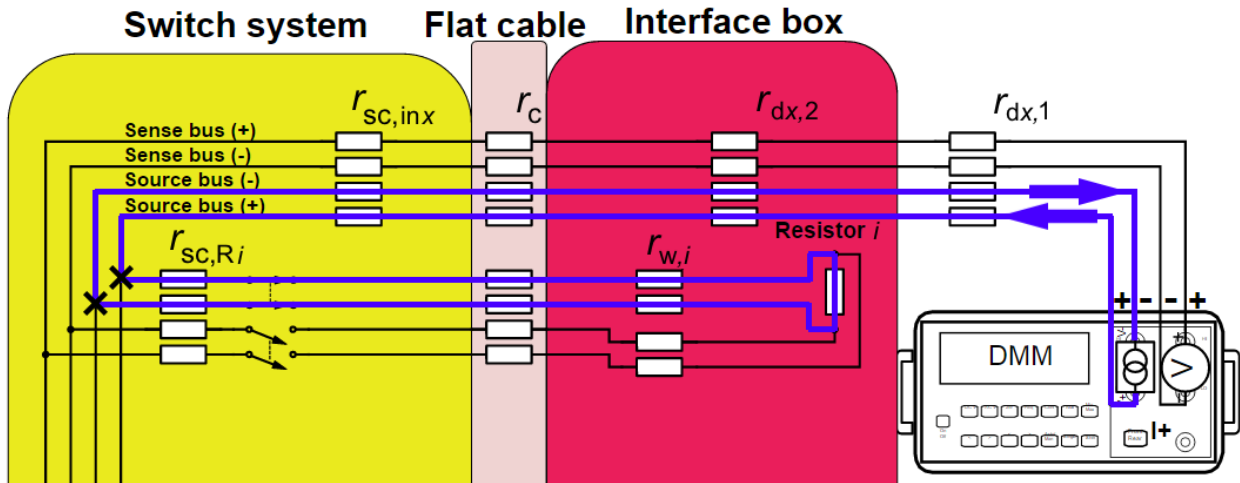


Figure 10: Path measured during 2-wire resistance measurement of single resistor.

In Figure 10, the components that make up the total lead resistance of a full path through resistor i on circuit x are shown:

$$r_{lead,i,x} = 4 \cdot r_c + 2 \cdot (r_{dx,1} + r_{dx,2} + r_{sc,in x} + r_{sc,Ri} + r_{w,i}) \quad [25]$$

On the self-heat effects of thermistors

Page 24 of 74

This is assuming that the paired resistances are equal to each other i.e. $r_{c,1} = r_{c,2} = r_{c,i}$. Points P_1 and P_2 from Figure 5 are represented by the crosses in Figure 10, indicating where the current splits off from the bus for the resistor.

To measure the resistance of individual components (those on the right hand side of equation [25]), an Agilent 34420A micro-ohmmeter (serial number US36003197) is used with offset-compensation turned on. This DMM has an estimated uncertainty of 500 ppm (see section 8.6 of the appendix for more details). Using Kelvin clips, 4-wire resistance measurements are performed on each component for each resistor on both circuits.

The flat cable's resistance is measured by probing the same pin on the connectors on either end of the cable. Each of the 96 cores is measured in this manner. The average resistance of these 96 measurements is used as the flat cable's resistance wherever needed, with the uncertainty determined by the DMM's specifications and the standard deviation of the 96 measurements. The other leads are also measured end-to-end, with an uncertainty based on the specifications of the DMM.

For the switch system's internal resistance, a slightly different measurement method is used. By inserting the flat cable into the multiplexer card and measuring the resistance between the corresponding HI or LO pins for each channel (as shown in Figure 11), the total internal resistance of the switch system is determined. This is done because it is not feasible to measure the two resistance components inside the switch system separately.

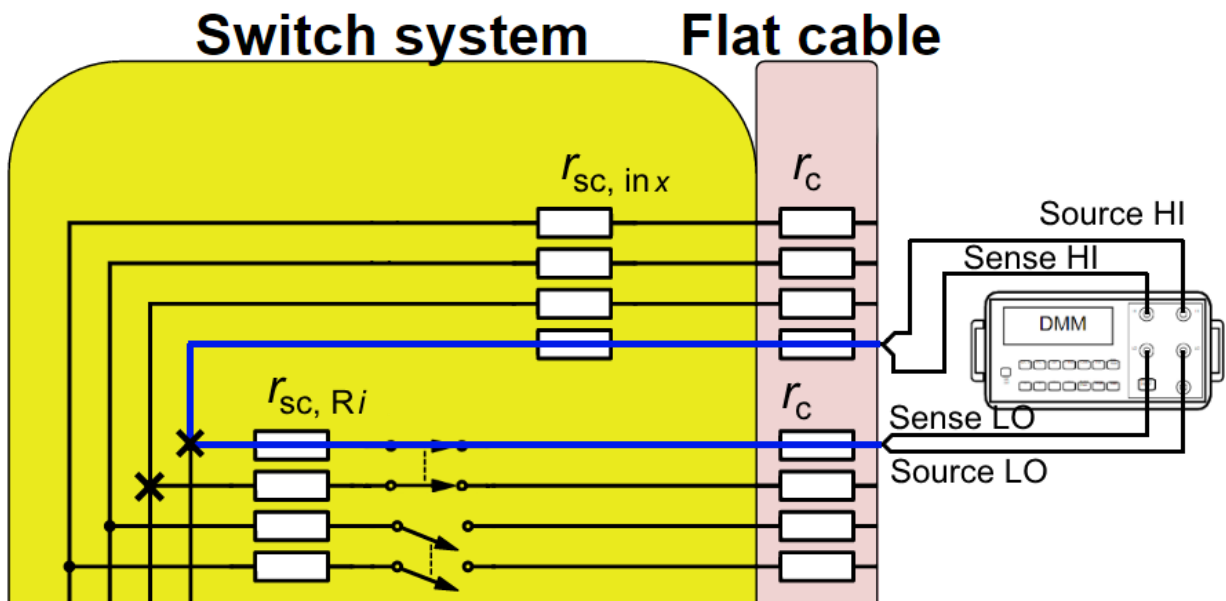


Figure 11: Schematic of switch system internal resistance measurement on a channel's HI side.

A measurement like the one shown above is performed for each channel's HI and LO side. Subtracting the resistance of the flat cable from the measured resistance gives the internal resistance of the switch channel's HI or LO side. Adding the resulting resistances for the HI and LO side gives the total internal resistance of that channel in the switch system, i.e. $r_{sc,total,i} = R_{measured,HI} + R_{measured,LO} - 4 \cdot r_c$.

An additional challenge is correctly splitting the total resistance between $r_{sc,in x}$ and $r_{sc,Rx}$. As measuring these resistances separately is impractical if not impossible, an estimate is made based on measurement results. The majority of the internal resistance is expected to be caused by the relays that contain the switches. Each channel has one relay that it uses exclusively and another that is shared by all resistors on a circuit. As each relay is of the same type, it is expected that they will all have approximately the same resistance. $2 \cdot r_{sc,in x}$ will be given a value equal to the average measured resistance of all channels on the circuit. This value is subtracted from the total resistance measured for each channel to give the value of $r_{sc,Ri}$ i.e. $2 \cdot r_{sc,Ri} = r_{sc,total,i} - 2 \cdot r_{sc,in x}$.

For example, if 5 channels on circuit 1 are measured and the average resistance of these channels is 1Ω , then $2 \cdot r_{sc,in x} = 0.5 \Omega$. This value is chosen because it is expected that the resistance of each channel is caused by the

On the self-heat effects of thermistors

two relays, one of which all channels have in common. As the value of $r_{sc,inx}$ doesn't change depending on which channel is activated, its value is based on the average of the measurement results. If channel 1's total resistance was 1.2Ω , then $2 \cdot r_{sc,R1} = 1.2 \Omega - 0.5 \Omega = 0.7 \Omega$. This approach is expected to resemble the actual situation the most, as $r_{sc,inx}$ is the same for all channels on a circuit. Differences in the measured resistances of the channels are therefore caused by small deviations in the placement and quality of the individual channel relays. This method is a best-guess, however, so an uncertainty of 20 % is assigned to the values of $r_{sc,Ri}$ to encompass possible deviations from this estimate.

When measuring the resistance of the paths inside the interface box, one Kelvin clip is always placed on the corresponding pin on the box's 96-pin connector. The other is placed at the end of the path that is being measured as shown in Figure 12

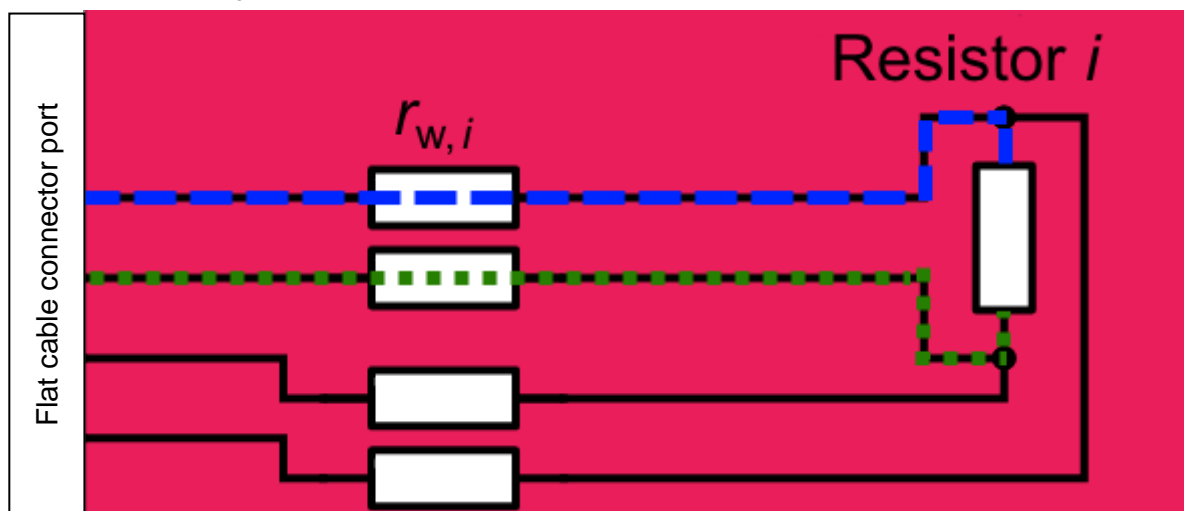


Figure 12: Schematic of path resistance measurement inside interface box.

The dashed line in Figure 12 shows the path that is measured from the HI-pin corresponding to the resistor to the resistor itself. The dotted line shows the return path going from the resistor to the LO-pin on the connector. The sum of the two is the total lead resistance for this resistor. Both resistors are assigned a value equal to half of their sum, rather than applying each value individually. For example, if the path resistance through resistor R1 is measured to be 1Ω , with 0.4Ω measured on one side of the resistor and 0.6Ω on the other, both resistances are treated as though they are 0.5Ω . These resistances are connected in series, so no error is made in this way.

As validation, the result of using equation [25] to calculate the total resistance should equal the resistance determined with the "whole circuit" method (within their uncertainty), which was measured using the 2-wire method described earlier in this chapter. If that is the case, then the measurement results of the individual components can be used to determine a value for $r_{p,Ri}$ for each resistor (R_i):

$$r_{p,Ri} = 2 \cdot (r_c + r_{w,Ri} + r_{sc,Ri}) \quad [26]$$

These components are found between the crosses in Figure 10, which indicate the points where the current splits and recombines. The value of r_p for each individual parallel resistor will be used in later experiments to determine the thermistor's resistance based on measurement results using equation [23]. Next, the lead resistances on the thermistor's connection are investigated.

On the self-heat effects of thermistors

Page 26 of 74

2.3.1 Measurement of thermistor lead resistances

The thermistors are connected to the interface box with extension leads. While both the thermistor and resistors share some internal resistance components ($r_{sc,in}$ and r_c), some additional measurements must be made to determine the lead resistance for the thermistor (r). Using an extension lead and connectors on the interface box, the thermistor is connected to the circuit inside. The path from DMM through thermistor and back is illustrated in Figure 13.

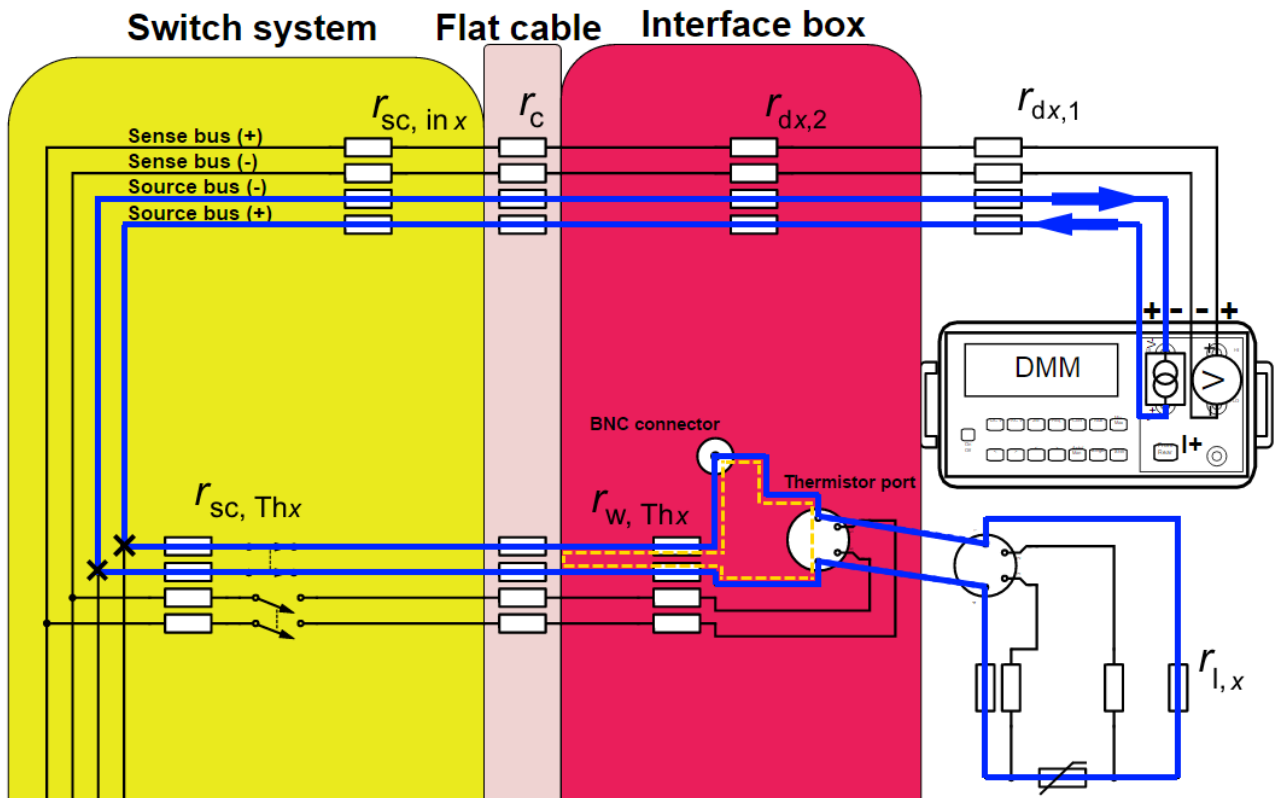


Figure 13: Path from DMM to thermistor and back (solid line).

Two additional components are measured: the resistance from the input to the output pin corresponding to the thermistor port on the flat cable connector ($2 \cdot r_{w, Thx}$) and the loop resistance of the thermistor extension lead ($2 \cdot r_{l,x}$). These resistances are measured using the same Agilent 34420A DMM as before.

By short-circuiting the thermistor port using a small piece of tinned copper wire (resistance ~ 0.1 m Ω), the resistance of a full loop from the HI-side connection pin to the corresponding LO-side pin is measured (indicated by the dashed line in Figure 13). The thermistor extension leads' resistances are also measured ten times. $r_{l,x}$ is based on the average value of these ten measurements. The results of this experiment and the one described in the previous section are used to determine a value for the thermistor's lead resistance in circuit x :

$$r_x = 2 \cdot (r_c + r_{l,x} + r_{sc,Thx} + r_{w,Thx}) \quad [27]$$

This is the total lead resistance in the circuit between points P_1 and P_2 from Figure 5 (shown as crosses in Figure 13) for the thermistor. Once all the lead resistances have been determined, validation of the measurement method and setup can take place.

2.4 Validation of measurement method and setup

To verify that the measurement method is valid and that the setup is functioning within the boundaries determined by uncertainty analysis, a number of validation experiments are performed manually. In each case, a known, stable resistor is used as a substitute thermistor. By placing resistors parallel to this “proxy thermistor”, the measurement displayed by the DMM can be converted to give the proxy’s resistance with equation [23]. Comparing the result of this calculation (referred to as R_{calc} henceforth) to the measured resistance provides an indication of the accuracy of the method. Additionally, comparing values of R_{calc} with and without lead resistance compensation highlights the accuracy of the applied correction. It is expected that neglecting to include lead resistances will result in a significant error, as highlighted by the example in section 2.1.

2.4.1 Method validation experiments

In the first validation experiment, the 10 kΩ resistors in the interface box are used as thermistor proxies. The resistors are measured in 4-wire mode, whilst the other resistors are placed parallel to this resistor (see Figure 14) as shown in Figure 5. Measurements are made manually by writing down the value shown on the DMMs’ displays.

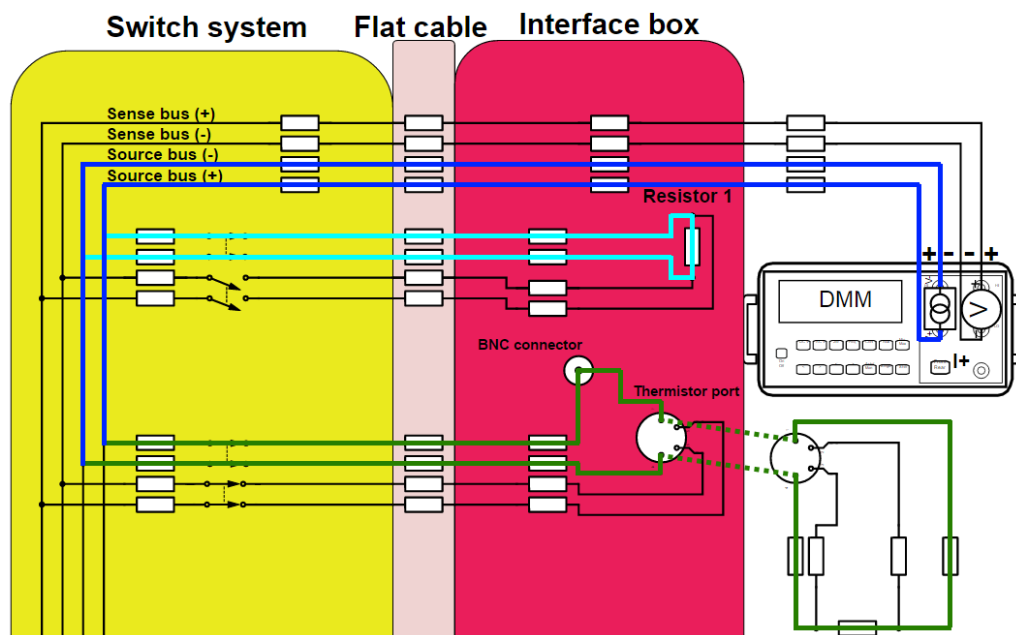


Figure 14: Single circuit configuration with thermistor proxy tor in 4-wire mode and resistor 1 in 2-wire mode.

Five measurements are made of each configuration, including a set of measurements without any parallel resistors activated to determine the value of the proxy thermistor. The validation procedure is repeated with a stable, known resistor (Welwyn type RC55YB, nominal resistance 10 kΩ at room temperature with 0.5 ppm stability) placed directly in the thermistor port of the interface box. A final validation is performed using the same proxy thermistor with additional thermistor extension cables. The cable is plugged into the interface box and the known resistor is placed at the cable’s other end. For a successful validation, the results of each experiment should show that the calculated value of the proxy thermistor (R_{calc}) matches the directly measured value of proxy thermistor within the determined uncertainty.

2.4.2 Measurement of thermistor settling time

The time needed for the thermistors to reach a steady state temperature is determined experimentally. The thermistors are left unused for several hours to ensure they are at the temperature of the water calorimeter. Then, the thermistors are measured in 4-wire mode with no parallel resistances connected. The resistance of the

On the self-heat effects of thermistors

Page 28 of 74

thermistors is sampled once per second for thirty minutes using the computer program. While not fully validated yet, it is straightforward to check whether the program is working correctly in this case; a comparison reveals that the values on the DMMs' displays match those recorded by the program. By analyzing the change in resistance over time, it can be determined when the thermistors have "settled" into a steady state.

2.4.3 Validation of automated data acquisition

To validate the data acquisition module of the program, a self-heat measurement is performed manually using the measurement setup. Initially, the parallel resistances are measured individually in 4-wire mode with OCOMP ON and AZERO ON to calibrate them. Five measurements are made of each resistor and averaged to give the value of the parallel resistance. Next, the DMM is set to measure on the 10 k Ω scale and the thermistors (VSL13T025 and VSL13T033) are connected to their respective DMMs with no parallel resistance active. After waiting for more than the determined minimum settling time to allow the thermistor to reach a steady state, the measurement shown on the DMM's display is written down. Ten measurements are made for each DMM in alternating fashion, taking approximately two minutes in total. Then, a parallel resistor is added to each circuit and another waiting period is applied. After this waiting period, measurements are made in the same manner as before. The parallel resistor is then removed from the circuit and the procedure is repeated until each parallel resistance has been added to the circuit once, resulting in ten sets of ten measurement samples (five sets with $R_p = \infty$, one set with $R_p = R_1$ etc.). The measured resistance is then translated to the thermistor's resistance using equation [23] and plotted as a function of thermistor power to determine its self-heat parameter. The procedure is repeated using the computer program. The program saves the measured resistances in a text file, which can be analyzed in the same manner as the manual measurement series. The determined resistances should be the same in both measurement series (within uncertainty margins). Upon successful validation of the data acquisition module, self-heat parameter measurements can be made in an automated fashion.

2.5 Self-heat parameter measurements

Self-heat parameter measurements are performed using the computer program's validated data acquisition functionality. The procedure is performed as described in the previous section, with measurements being made both with and without parallel resistances in an alternating fashion. The values of $C_{sh, 1}$, $C_{sh, 2}$, and B are based on analysis of this data.

In each self-heat parameter measurement there is the potential for temperature drift. This can be compensated for using the measurements with no parallel resistance active. As the current passing through the thermistor at these points is equal, the self-heat ΔT_{sh} should be the same each time. Any difference noted can be attributed to temperature drift. A trend line of the measured temperature at these points over time provides a measure of the change in temperature per unit of time. Most often, a linear trend line is expected to be a good match for the data, but in some cases a polynomial fit may be used. This is evaluated on a case-by-case basis. The determined rate of temperature drift is used to adjust all measurements so that they are compensated for the drift that has occurred since the start of the measurement series. As the temperature drift is less than $1 \mu\text{K} \cdot \text{s}^{-1}$ for VSL's water calorimeter (de Prez et al. 2016), it is not expected that significant drift will be noted in measurement series lasting two hours or less as self-heat temperatures are typically between 50 mK and 200 mK.

Using the computer program, a number of self-heat measurements are made. Using the same settling time, the self-heat and non-linearity parameters are determined fifty times with the automated routine. After plotting the thermistor temperature as a function of power dissipation, both a linear and a 2nd order polynomial fit are applied to each measurement series. The fits should pass by the data points within their respective uncertainties, as determined in section 8.5.4 of the appendix. Analysis of the fit residuals will provide a point of comparison for both fit methods, with the best fit method expected to have the smallest overall deviation from the measured data. Using the data, an average value is calculated for the self-heat ($C_{sh, 1}$ and $C_{sh, 2}$) and non-linearity (B) parameters.

The type A uncertainty in these parameters is based on the standard deviations of their measurement data. This is chosen primarily for on-site applications; there may only be time to perform one measurement series to determine the self-heat and non-linearity parameters. Therefore the uncertainty margin should reflect the confidence level that this single measurement is going to fall within them.

3 Results

In this chapter, the results of the experiments described in sections 2.3 through 2.5 are summarized. First, various lead and internal resistances are measured. This is followed by a validation of the measurement setup and method. Finally, self-heat measurements are performed with two thermistors.

3.1 Lead resistance measurement results

The lead resistances play a small but influential role in the division of the DMMs source current between the thermistor and any active parallel resistors, as described in section 2.1. It is worth quantifying these internal resistances accurately to compensate for this influence. The measurements are performed as described in section 2.3.

3.1.1 Parallel resistor lead resistances, r_p

The results of both experiments performed to determine the lead and internal resistances relevant to the parallel resistors are summarized in Table 1. A comprehensive overview of the measurement results is found in the appendix (section 8.3). Uncertainty budgets for both sets of measurements can be found in section 8.5.1.

The table shows that the sum of the internal and lead resistances is between 2.0465 Ω and 2.4968 Ω for each resistor. This is closely mirrored by the results of the other experiment, where the total lead resistance is measured. The largest contributor is the switch system's internal resistance which is approximately 50 % of the total lead resistance. The average resistance of the channels in the switch system is 1 Ω for both circuits. As described in section 2.3, this means a value of 0.5 Ω is assigned to $2 \cdot r_{sc, in}$ for both circuits. An uncertainty of 0.05 Ω (20 %) is attributed to this variable to take possible deviations from this value into account.

The difference between the two methods of measuring the total lead resistance has a minimum value of -0.0668 Ω with an average difference of -0.0386 Ω . Each result falls outside of the determined standard uncertainty (see Table 28 in section 8.5.1 of the appendix for a full uncertainty budget). In each case, the sum of the individual component resistances is larger than the result from the other method. The likely cause of this discrepancy is the difficulty in measuring the resistance of some of the components. It was sometimes difficult to make solid contact with the component using the Kelvin clips. When the circuit is fully connected, the contact between components is better, resulting in a slightly lower resistance. Therefore the listed uncertainty is likely underestimating the actual uncertainty of the measurements. It is difficult to quantify what the impact is of making less-than-ideal contact when measuring a component's resistance. However, the scope of this error is expected to be limited when compared to the uncertainty of the lead resistance compensations r and r_p , as determined in section 8.5.2 of the appendix.

On the self-heat effects of thermistors

Table 1: Comparison of results from two experiments to determine the total lead resistance of the circuit.

Resistor	$r_{\text{lead,total}}$ (From summation of individual component resistances) [Ω]	Δr (From total lead resistance measurement) [Ω]	$\Delta r - r_{\text{lead,total}}$ [Ω]	Standard uncertainty of ($\Delta r - r_{\text{lead,total}}$) [Ω]
R1	2.197 9	2.170	-0.027 9	0.008 9
R2	2.046 5	2.023	-0.023 5	0.008 9
R3	2.144 7	2.110	-0.034 7	0.008 9
R4	2.234 6	2.200	-0.034 6	0.008 9
R5	2.154 1	2.150	-0.004 1	0.008 9
R6	2.385 7	2.338	-0.047 3	0.008 9
R7	2.105 0	2.069	-0.036 0	0.008 9
R8	2.360 5	2.314	-0.046 5	0.008 9
R9	2.496 8	2.430	-0.066 8	0.008 9
R10	2.254 3	2.190	-0.064 3	0.008 9

Despite not falling within the uncertainty margins, the results indicate that the two methods are in agreement within 36.6 m Ω on average. This is expected to be sufficient when incorporating the results into the other experiments. Therefore, the resistances of the individual components are used to determine the lead resistances for the parallel resistors, as given by r_p (see equation [26]).

3.1.2 Thermistor lead resistances, r

The resistance of the thermistor's path through the interface box and LEMO connector is measured as described in section 2.3. The results of this measurement show that the values of $2 \cdot R_{w, \text{Thx}}$ are $0.184341 \Omega \pm 9.2 \cdot 10^{-5} \Omega$ and $0.191340 \Omega \pm 9.6 \cdot 10^{-5} \Omega$ for thermistor ports 1 and 2, respectively. Repeat measurements of the extension leads' resistance results in an average of $3.792 \Omega \pm 0.012 \Omega$ for thermistor 025's lead and $3.6013 \Omega \pm 0.0033 \Omega$ for thermistor 033's lead. The uncertainty is determined by quadratic summation of the standard deviations and DMM uncertainty as explained in section 1.5 (in this example, the sensitivity coefficient equals 1 for both variables). The full data from this experiment is located in Table 23 in section 8.3 of the appendix. The results from measurement of the components that make up the parallel lead resistance and thermistor lead resistance (as shown in this section and the one preceding it) are used to determine the values of r and r_p , which is used to include the influence of lead resistances on the calculated thermistor resistance as given by equation [23].

3.1.3 Determination of total lead resistance in parallel resistor and thermistor circuits

Using equations [26] and [27], values are determined for the thermistor and parallel resistor lead resistances based on the results from the previous experiments. The results are summarized in Table 2 at the end of this section.

On the self-heat effects of thermistors

Page 31 of 74

For the parallel resistors, compensation between 0.73 Ω and 1.12 Ω should be added to incorporate lead resistances, depending on the resistor. Due to the long extension cables, the thermistor's lead resistance compensation is significantly higher at 8.41 Ω and 8.81 Ω . Both compensations have an uncertainty of 0.10 Ω , which is calculated using the method demonstrated in chapter 4. Uncertainty budgets for r and r_p can be found in Table 29 of section 8.5.2 of the appendix.

Table 2: Total lead resistance of each channel for both circuits.

	Flat cable r_c [Ω]	Interface box internal leads r_w [Ω]	Switch system internal resistance $r_{sc, Ri}$ [Ω]	Thermistor lead resistance $r_{l, x}$ [Ω]	Sum of lead resistance components [Ω]	Standard uncertainty [Ω]
Th1	0.35	0.18	0.69	7.58	8.81	0.10
R1	0.35	0.11	0.51	-	0.97	0.10
R2	0.35	0.12	0.36	-	0.82	0.10
R3	0.35	0.12	0.45	-	0.92	0.10
R4	0.35	0.12	0.53	-	1.01	0.10
R5	0.35	0.12	0.45	-	0.93	0.10
Th2	0.35	0.19	0.67	7.20	8.41	0.10
R6	0.35	0.12	0.54	-	1.01	0.10
R7	0.35	0.11	0.26	-	0.73	0.10
R8	0.35	0.10	0.53	-	0.98	0.10
R9	0.35	0.12	0.65	-	1.12	0.10
R10	0.35	0.12	0.40	-	0.87	0.10

3.2 Results from validation of measurement method and setup

In section 2.4, a description is given of five experiments performed to validate that the measurement setup and method are functioning within the determined uncertainty margins. Three of these experiments use a known, stable resistor as a thermistor proxy. Two additional experiments are performed: one to determine the minimum time needed for the thermistors to settle to a steady state temperature and another to validate the data acquisition module of the software. The results of the validations are described in this section, beginning with the validation using a resistor inside the interface box.

3.2.1 Validation of setup and method using internal resistor

Using the 10 k Ω resistor in each circuit as a thermistor proxy, measurements are made with the other resistors in parallel (one at a time). Based on the measured resistance (R_m), the value of the thermistor proxy is calculated (R_{calc}). If R_{calc} is equal to the resistance of the thermistor proxy within two standard uncertainties, the setup and method are successfully validated.

Having made five measurements in each configuration (one set without R_p , one set with $R_p = 1$ k Ω etc.), an average value is determined for each set of measurements. The average of measurements without an active parallel resistor is the measured value of the thermistor proxy R_{proxy} . The average measured resistance (R_m) with $R_p = 1$ k Ω is then used to determine the calculated value of the thermistor proxy's resistance (R_{calc}). First, equation [23] is used with $r = 0$ and $r_p = 0$, so no compensation is applied for internal resistances. The difference between R_{proxy} and R_{calc} is shown in the ΔR column of Table 3. R'_{calc} is then determined by using equation [23] and values for r and r_p as determined by the experiments described in section 3.1. $\Delta R'$ is the difference between R_{proxy} and R'_{calc} .

In this section, the results of measurements with $R_p = 1$ k Ω for both circuits are investigated in more detail. The full results from this validation experiment can be found in Table 25 in section 8.4 of the appendix.

On the self-heat effects of thermistors

Page 32 of 74

Table 3 shows that if no lead resistance compensation is applied, R_{calc} differs nearly 100 Ω from R_{proxy} for both circuits. In other words, an error of 100 Ω is introduced for R_{calc} . This difference is much larger than the standard uncertainty of 28 Ω . Using the values of r and r_p to correct for internal resistances, this difference is reduced to 4 Ω and 2 Ω for circuits 1 and 2, respectively. For the other resistors both R_{calc} and R'_{calc} fall within the two standard uncertainties.

Table 3: Validation experiment results with $R_p = 1 \text{ k}\Omega$.

Measured			No lead resistance compensation		With lead resistance compensation		Standard uncertainty of R_{calc} & R'_{calc}
Circuit	R_{proxy}	R_m	R_{calc}	ΔR	R'_{calc}	$\Delta R'$	
-	[k Ω]	[k Ω]	[k Ω]	[k Ω]	[k Ω]	[k Ω]	[k Ω]
1	9.997	0.910	10.092	0.095	10.001	0.004	0.028
2	9.996	0.910	10.095	0.099	9.998	0.002	0.028

Having applied lead resistance compensation, each of the determined values of R'_{calc} falls within two standard uncertainties. This validation is considered a success as a result.

3.2.2 Validation of setup and method with proxy thermistor

Instead of using one of the resistors inside the interface equipment box, a different known resistor is used as thermistor proxy. This proxy is placed in the port that the thermistors' extension leads usually connect to. The validation procedure is then carried out in the same manner as the previous validation. This section investigates the results of measurements with $R_p = 1 \text{ k}\Omega$. For the results with the remaining parallel resistors, see Table 26 in section 8.4 of the appendix.

The data in Table 4 is similar to that from the previous validation. With no lead resistance compensation applied, ΔR falls far outside the standard uncertainty margin; this difference is 85 Ω and 90 Ω for circuits 1 and 2, respectively. With lead resistance compensation, $\Delta R'$ is 5 Ω for both circuits. For the other parallel resistors, applying lead resistance compensation has little impact, with all results falling within the expanded uncertainty margin ($k = 2$) both with and without compensation for lead resistances.

Table 4: Validation experiment with thermistor proxy results, with $R_p = 1 \text{ k}\Omega$.

Measured			No lead resistance compensation		With lead resistance compensation		Standard uncertainty of R_{calc} & R'_{calc}
Circuit	R_{proxy}	R_m	R_{calc}	ΔR	R'_{calc}	$\Delta R'$	
-	[k Ω]	[k Ω]	[k Ω]	[k Ω]	[k Ω]	[k Ω]	[k Ω]
1	9.999	0.910	10.084	0.085	9.994	-0.005	0.028
2	9.999	0.910	10.089	0.090	9.994	-0.005	0.028

With all results falling within the expanded uncertainty margin ($k = 2$) after lead resistance compensation, this validation is also considered a success.

3.2.3 Validation of setup and method with proxy thermistor and extension leads

For the final validation of the method, the proxy thermistors from the previous experiment are placed at the end of a thermistor extension lead (as described in section 2.4.1). The other end of the lead is connected to the thermistor port in the interface box. The resistance of both leads is measured using an Agilent 34420A DMM and is found to be approximately 1.25 Ω for one length. As the current must travel two lengths of the lead before arriving back at the interface box, the resistance of the lead is $\sim 2.50 \text{ }\Omega$. The remainder of the procedure is the same as the previous two validations. The results of measurements with $R_p = 1 \text{ k}\Omega$ are shown in Table 5 at the end of this section.

On the self-heat effects of thermistors

For this validation, all results fall outside of the expanded uncertainty margin ($k = 2$) when lead resistances are not incorporated in the calculations. Whereas before the error introduced by neglecting to include lead resistances in the calculation were noticeable only in measurements with the smallest parallel resistor, it is now seen in each measurement. Applying compensation for lead resistances significantly improves the accuracy of the results, with all measurements complying with the expanded uncertainty margin ($k = 2$).

Table 5: Validation experiment using extension leads and thermistor proxy, with $R_p = 1 \text{ k}\Omega$.

Measured			No lead resistance compensation		With lead resistance compensation		Standard uncertainty of R_{calc} & R'_{calc}
Circuit	R_{proxy}	R_m	R_{calc}	ΔR	R'_{calc}	$\Delta R'$	
-	[k Ω]	[k Ω]	[k Ω]	[k Ω]	[k Ω]	[k Ω]	[k Ω]
1	9.998 95	0.909 39	10.057	0.058	9.993	-0.006	0.028
2	9.999 00	0.909 37	10.062	0.063	9.992	-0.007	0.028

With this validation and the preceding two all successful, the method and setup are used for further experiments.

3.2.4 Settling time determination

To know how long a thermistor should be allowed to settle before it has reached a steady state, the resistance of thermistors VSL13T025 and VSL13T033 is measured over a period of thirty minutes as described in section 2.4.2. The change in resistance over time is shown in Figure 15. Both data sets are normalized by subtracting the first measurement from all subsequent measurements. In doing so, the data can be plotted on the same graph for easier comparison.

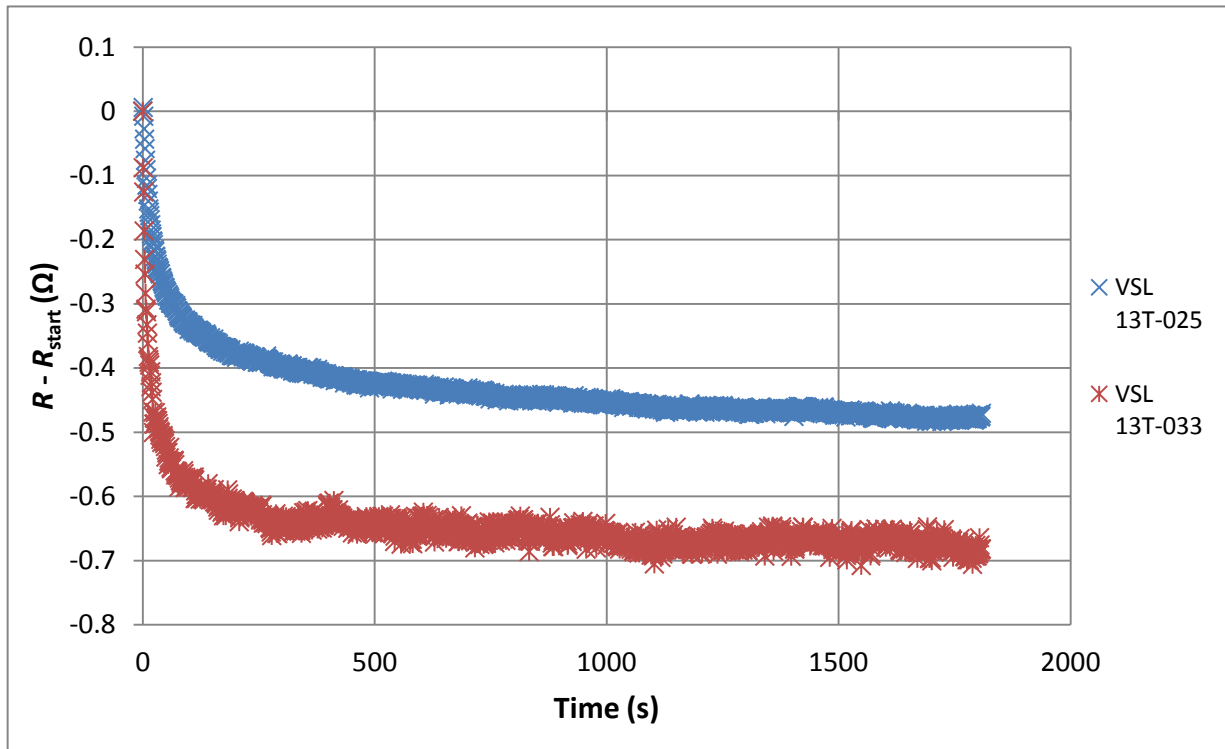


Figure 15: Thermistor resistance over time after enabling DMM measurement current.

On the self-heat effects of thermistors

As expected, the resistance of the thermistors decreases rapidly at first due to self-heating. The total change in resistance, however, is smaller than anticipated. When going from 0 μW power to $\sim 90 \mu\text{W}$, the expected resistance change is on the order of 100 Ω . However, most of this occurs in the first second, before any samples are made. By the time the system starts sampling, the thermistor has already heated up significantly. This makes it difficult to determine a settling time based on a time constant, but it can be seen in Figure 15 that the thermistor resistance change slows down after approximately 500 seconds. To look more closely at the change in resistance, the data is analyzed further. For every 10th sample, the total resistance change in the last minute is calculated i.e. $\Delta R[1] = R_{\text{sample}70} - R_{\text{sample}10}$, $\Delta R[2] = R_{\text{sample}80} - R_{\text{sample}20}$ etc. This data is shown in Figure 16.

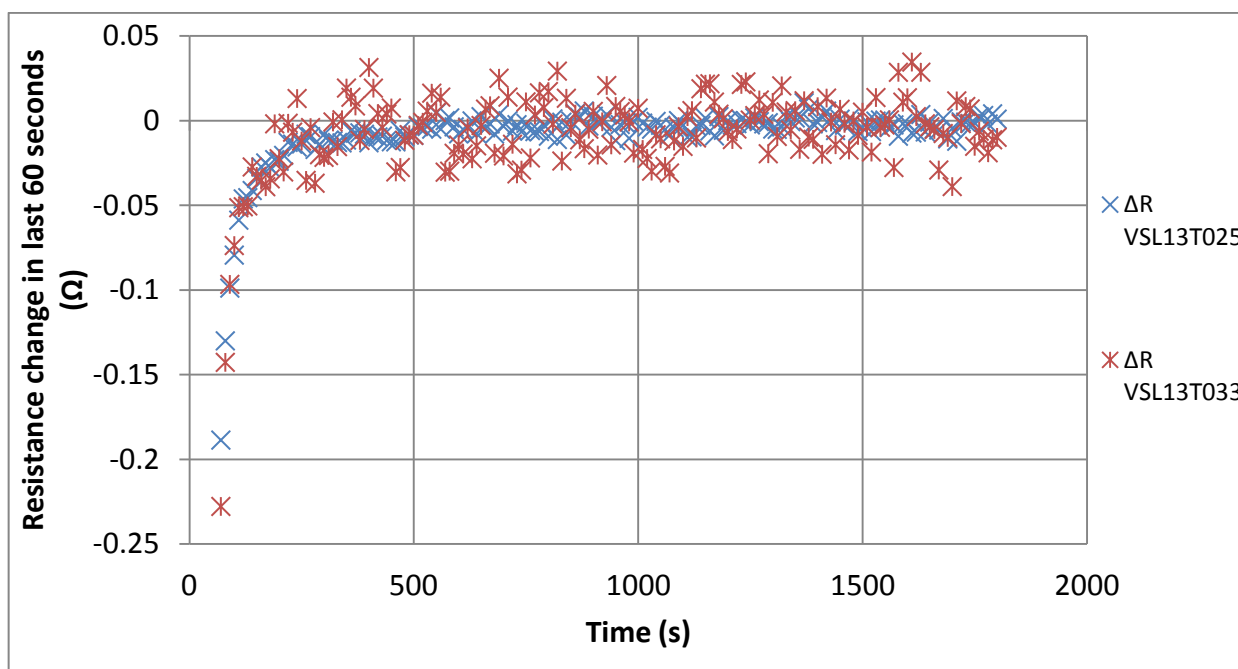


Figure 16: Resistance change of thermistor over one minute intervals after DMM measurement current is enabled.

It is noted that both thermistors appear to have settled somewhere between 400 and 500 seconds. Before then, their resistance is still decreasing at a rate less than -0.03Ω per minute, while almost never experiencing a positive resistance change. Post 500 seconds, both thermistors' rate of resistance change has slowed down. While Figure 15 shows that both thermistors continue to experience a decrease in resistance over the course of the entire measurement, this can be attributed to drift. Between the 500 second mark and the end of the measurement series, the resistance of the thermistors decreases by 0.05 Ω and 0.04 Ω for VSL13T025 and VSL13T033, respectively. Converted to a change in temperature (with equation [7]) and divided by the time between the two points, this is a rate of $0.1 \mu\text{K} \cdot \text{s}^{-1}$ and $0.08 \mu\text{K} \cdot \text{s}^{-1}$, well within the expected rate of temperature drift. A settling time of 10 minutes is expected to be sufficient to allow the thermistors to reach a steady state.

3.2.5 Validation of automated data acquisition program

To ensure that the automated data acquisition module is working as expected, a comparison is made between the results of a manual measurement series and the results of a measurement series performed by the program as described in section 2.4.3. First, each set of 10 samples is averaged to give an average resistance for that particular setting ($R_p = \infty$, $R_p = 1 \text{ k}\Omega$ etc). This resistance is then translated to a value for the thermistor's resistance using equation [23] and the results from the lead resistance experiments. Subsequently, the thermistor's resistance is

On the self-heat effects of thermistors

converted to a temperature reading with equation [5] and its corresponding parameters from the temperature calibration. The results are shown in Figure 17.

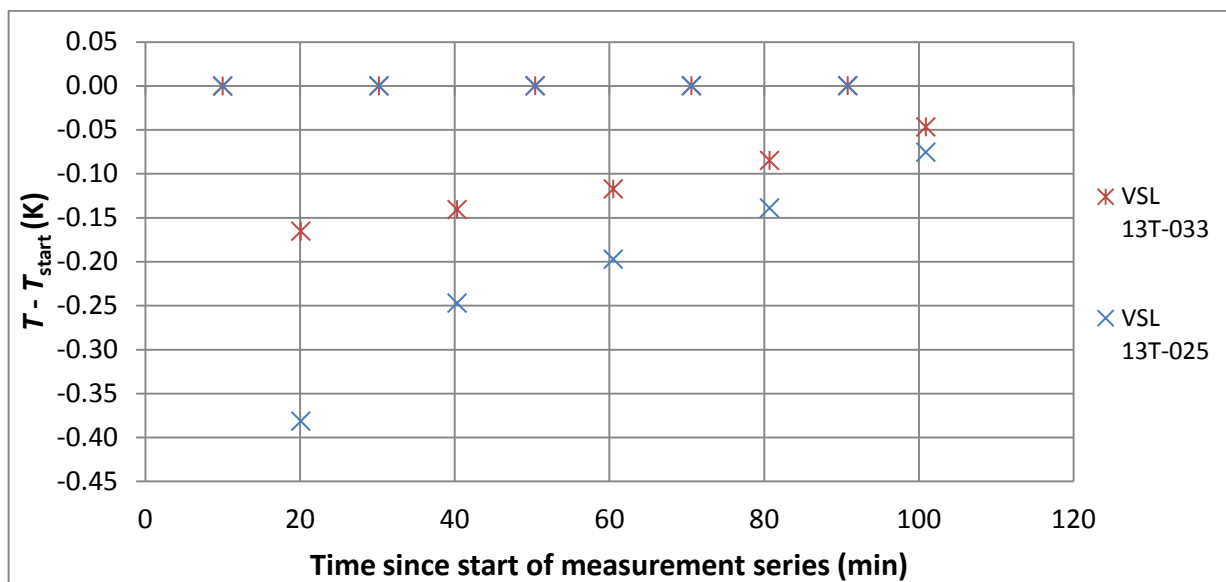


Figure 17: Thermistor temperature over time for the manual measurement series.

As expected, the thermistor's temperature is highest with maximum measurement current, so when no parallel resistances are active. As each parallel resistor is activated in turn, the temperature decreases. The standard deviation of each set of 10 samples is on the order of 0.001Ω , which is negligible when compared to the type B uncertainties of the thermistor resistance R (see Table 31 in section 8.5.3 of the appendix). A slight temperature drift is observed in the measurements with no active parallel resistors. This is shown in Figure 18.

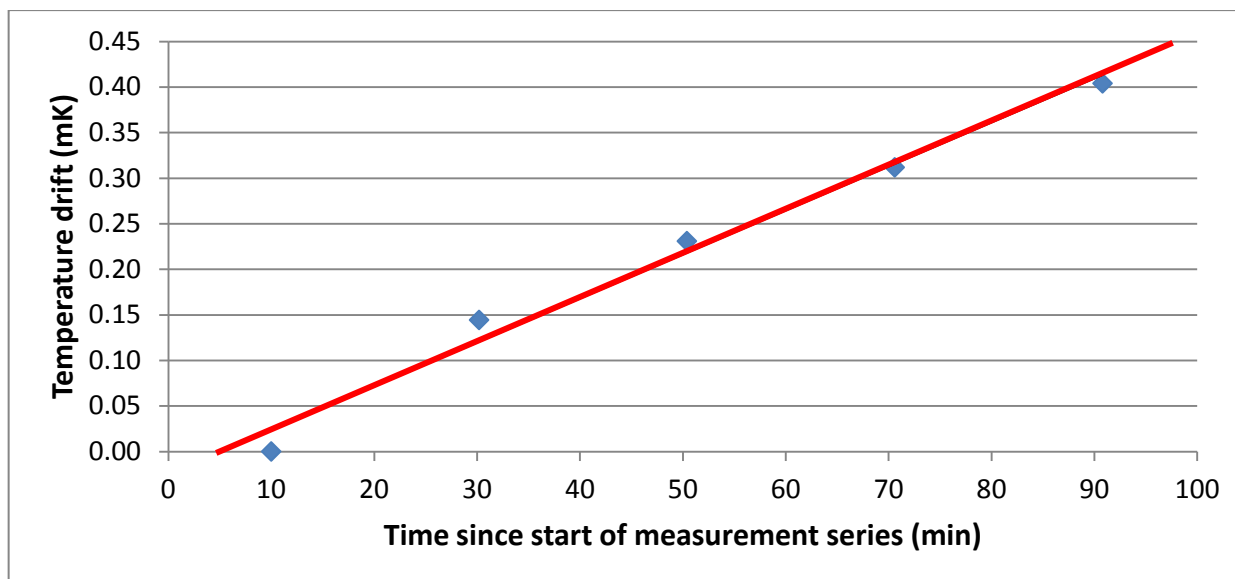


Figure 18: Temperature drift from $t = 10$ minutes with linear fit of the data points.

Linear regression shows an average temperature drift of $\sim 4.8 \mu\text{K} \cdot \text{min}^{-1}$. Based on this rate, the measured temperatures are adjusted. Using the y-intercept value of the fit, the thermistor's temperature at $t = 0$ minutes is

On the self-heat effects of thermistors

determined. Measurements made later in the run are adjusted more significantly, but in each case this correction is less than 0.5 mK. With the drift correction applied to the measurements, the measured temperatures are then normalized by subtracting the thermistor's temperature at $t = 0$ minutes. This provides a better indication of the self-heat of the thermistors. The results of these adjustments are shown in Figure 19.

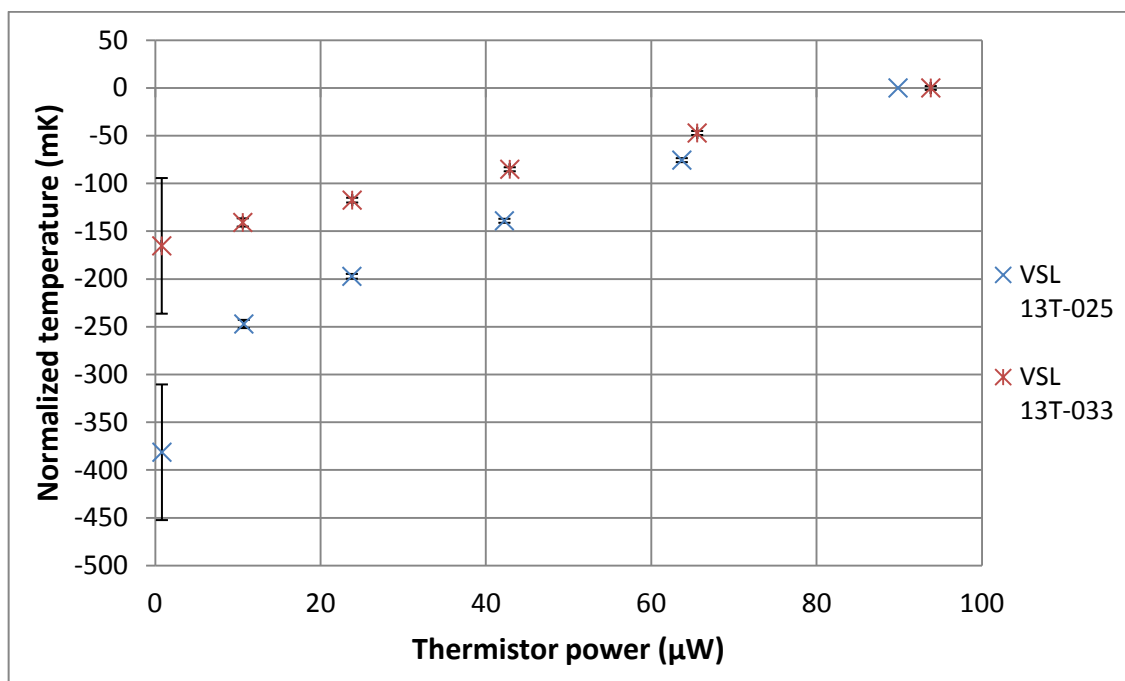


Figure 19: Normalized thermistor temperatures against power dissipated with drift compensation applied. Each point has error bars corresponding to their standard uncertainty, though they are less noticeable for some points.

Normalizing the thermistor temperatures shows that at full power, the temperature is approximately 170 mK above the water's temperature for thermistor 033 and almost 400 mK for thermistor 025. Whereas thermistor 033's temperature appears to increase linearly with an increase in power, a clear jump can be seen in thermistor 025's temperature when going from 1 μW to 10 μW . This is likely the result of an error in r_p , which is most noticeable with the smallest parallel resistors (as indicated by the sensitivity coefficients in section 4.1). Based on linear regression of the other measurements for thermistor VSLT13025, the error in its leftmost data point in Figure 19 is estimated to be 40 Ω . This result is still within the expanded uncertainty ($k = 2$) as shown in section 4.1.

While including this data point would cause an error in a trend line applied to this data, it is a good point of comparison for the automated measurement. With the same compensation added, the automated measurement data should also show this error. A comparison between the data from the automated and manual measurement series is shown in Figure 20.

On the self-heat effects of thermistors

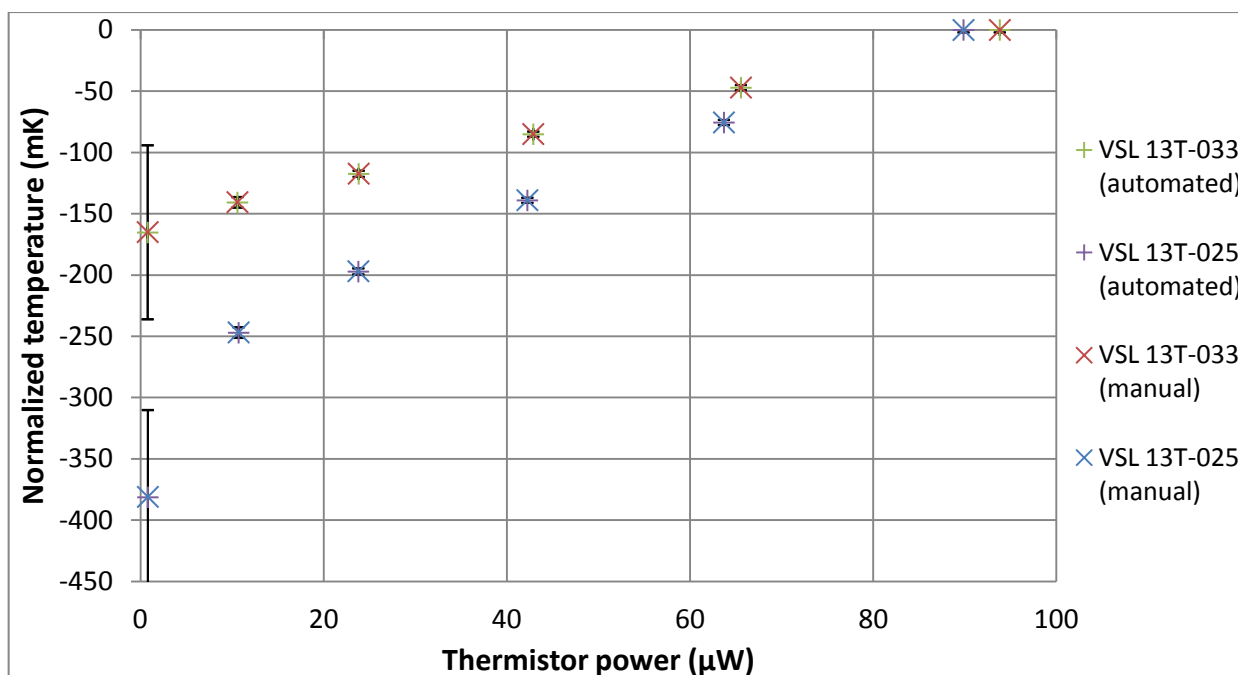


Figure 20: Comparison of data from manual and automated measurement series.

The data from both measurement series is coherent. The determined temperatures, including thermistor 025's large jump between 1 μW and 10 μW , are in alignment. For both thermistors, the difference in the determined temperatures for each data point is less than 0.5 mK, with an average deviation of 0.3 mK. This means that the automated measurement procedure is successfully validated and can be used for self-heat parameter measurement procedures. However, the large uncertainty in the measurement at the lowest power level is likely to influence the determined trend lines. As such, data measured with $R_p = 1 \text{ k}\Omega$ is excluded from further analysis.

3.3 Results from self-heat parameter measurements

Having successfully validated the data acquisition of the measurement program, the software program is used to perform fifty self-heat measurement routines, which are described in section 2.5. Using statistical analysis of the coefficients from both a linear and 2nd order polynomial fit of the data, the type A uncertainty is determined for the parameters described in section 1.3: $C_{\text{sh}, 1}$, $C_{\text{sh}, 2}$ and B .

To determine the self-heat and non-linearity parameters ($C_{\text{sh}, 1}$, $C_{\text{sh}, 2}$ and B) for thermistors VSL13T025 and VSL13T033, the automated measurement procedure is used. The data from this procedure is analyzed as described in section 3.2.5. Once the thermistor temperatures have been determined and normalized, $C_{\text{sh}, 1}$, $C_{\text{sh}, 2}$ and B can be determined. Using one measurement series as an example, the data analysis is explained further.

This measurement series was performed using a settling time of 600 seconds with ten samples made once the settling time has elapsed. The thermistor temperatures are calculated with equation [5], drift compensation is applied and the data is normalized using the determined thermistor temperature at $t = 0$ minutes. The result is shown in Figure 21 with error bars corresponding to the standard uncertainty.

On the self-heat effects of thermistors

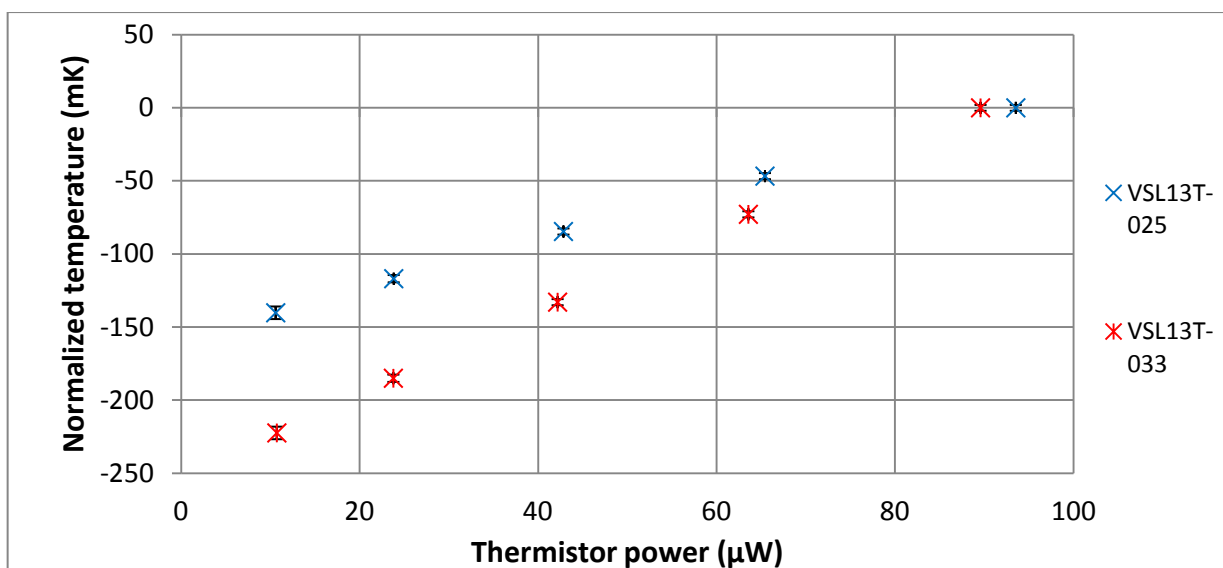


Figure 21: Normalized thermistor temperature at various levels of power dissipation, with error bars indicating the standard uncertainty for each point.

To determine the self-heat temperature of the thermistors, both a linear fit and a 2nd order polynomial fit are applied to this data. Both trend lines for thermistor 13T025 are shown in Figure 22.

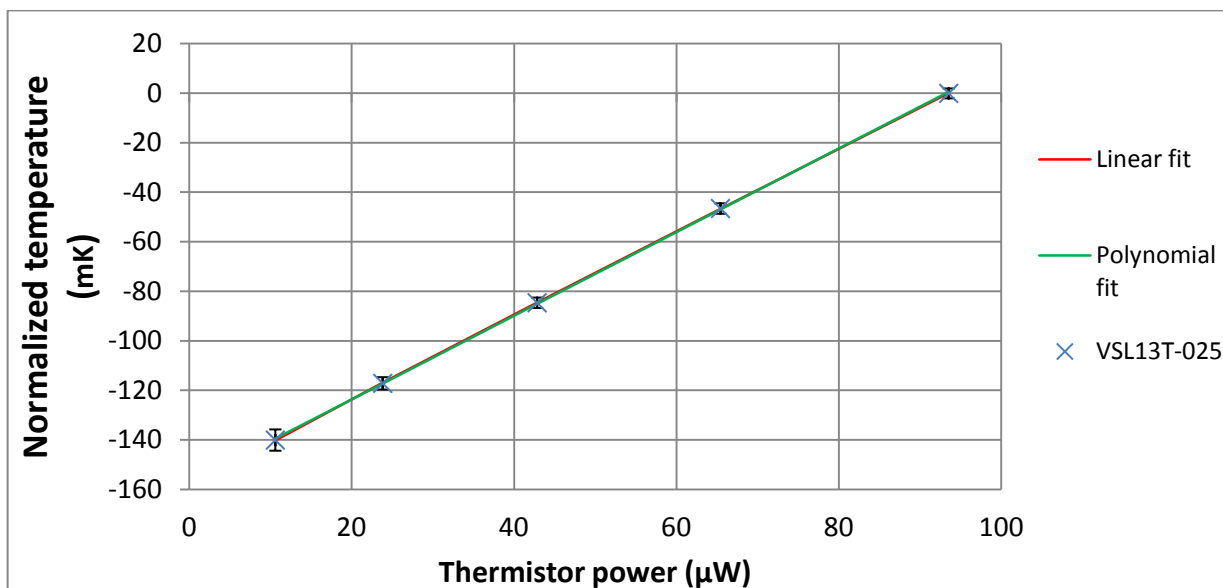


Figure 22: Example using normalized temperature of VSL13T025 with linear and polynomial fits of the data.

Both trend lines pass each data point within the uncertainty margin. For this measurement, the linear fit indicates a value of $C_{sh, 1}$ equal to $1.687 \text{ mK} \cdot \mu\text{W}^{-1}$ with a “0 power” temperature of -157 mK ; that is, the temperature with no current through the thermistor is 157 mK lower than its temperature at full power. The polynomial fit gives values of $1.752 \text{ mK} \cdot \mu\text{W}^{-1}$ and -158 mK for $C_{sh, 2}$ and the y-intercept, respectively, along with a non-linearity parameter B of $-0.00061 \text{ mK} \cdot \mu\text{W}^{-2}$. As described in section 1.3, this parameter indicates the magnitude of 2nd order effects on the thermistor’s temperature, which are assumed to be caused by convection. To determine which fit method is most accurate for the data, the residuals of both fit methods are calculated. The result is shown in Figure 23.

On the self-heat effects of thermistors

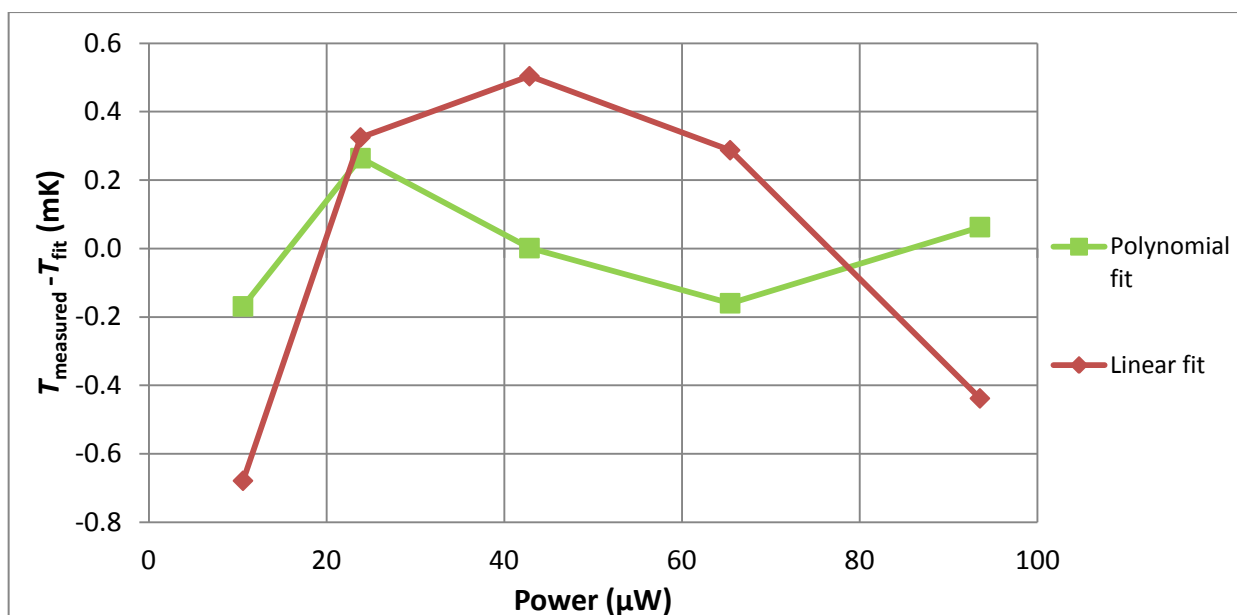


Figure 23: Fit residuals for VSL13T025 for both fit methods applied to the data.

While both fits match the data within the uncertainty margin, the polynomial fit is a slightly better match. The linear fit has negative residuals at both the low and high-power ends of the graph, with positive ones in between. This suggests that there is a higher order effect that has not been accounted for. The polynomial fit’s residuals are evenly distributed around $T_{\text{measured}} - T_{\text{fit}} = 0$ mK on the temperature axis and are also smaller in magnitude. The standard deviation of the linear fit’s residuals is larger than the polynomial fit’s standard deviation (0.51 mK vs. 0.19 mK in this example). Analysis of the residuals indicates that a polynomial fit is a better match for the measurements, meaning that non-linear effects such as convection may be influencing measurements.

Forty-nine additional measurements series are performed with the same settling time and number of samples. The average values of C_{sh} (for both 1st and 2nd order methods) and B for these fifty measurement series are shown in Table 6 along with their respective standard uncertainties.

Table 6: Results and standard uncertainties from self-heat experiments with settling time = 600 s.

Thermistor ID	$C_{\text{sh},1}$ [mK · μW ⁻¹]	Uncertainty, $C_{\text{sh},1}$ [mK · μW ⁻¹]	$C_{\text{sh},2}$ [mK · μW ⁻¹]	Uncertainty, $C_{\text{sh},2}$ [mK · μW ⁻¹]	B [mK · μW ⁻²]	Uncertainty, B [mK · μW ⁻²]
VSL13T025	1.687	0.050	1.752	0.050	$-6.1 \cdot 10^{-4}$	$5.3 \cdot 10^{-4}$
VSL13T033	2.819	0.050	2.865	0.050	$-4.5 \cdot 10^{-4}$	$5.3 \cdot 10^{-4}$

The results in Table 6 highlight a large difference compared to the self-heat parameters determined by Mostert (2014), who found them to be 1.2 ± 0.1 mK · μW⁻¹ and 1.7 ± 0.1 mK · μW⁻¹ for these thermistors. The thermistors have been used extensively for radiation measurements in the two years between Mostert’s study and this one, so it is possible that the thermistors have changed.

The uncertainty in $C_{\text{sh},1}$ and $C_{\text{sh},2}$ is mostly caused by the uncertainty in the self-heat temperature (as explained in section 4.2). For smaller parallel resistances such as $R_p = 5$ kΩ, the uncertainty in the self-heat is caused predominantly by the uncertainty in the thermistor’s resistance.

On the self-heat effects of thermistors

Page 40 of 74

The non-linearity parameters are measured to be $(-6.1 \pm 5.3) \cdot 10^{-4} \text{ mK} \cdot \mu\text{W}^{-2}$ for thermistor 025 and $(-4.5 \pm 5.3) \cdot 10^{-4} \text{ mK} \cdot \mu\text{W}^{-2}$ for thermistor 033. At maximum power dissipation for each thermistor (94 μW and 90 μW , respectively), these B parameters mean that a 2nd order approach will determine a self-heat temperature that is 2.9 % and 1.2 % lower than a linear approach. This is determined by comparing the results of the two different equations used to determine the self-heat temperature: $\Delta T_{\text{sh}} = C_{\text{sh},1} \cdot P$ for a linear approach and $\Delta T_{\text{sh}} = C_{\text{sh},2} \cdot P + B \cdot P^2$ for a 2nd order method. This result backed up by the fit residuals in Figure 23, where a linear approach results in a higher temperature at maximum power dissipation compared to a 2nd order approach. The magnitude of the linear fit's residual is also ten times larger in this point when compared to the polynomial fit's (0.296 mK vs. 0.030 mK), which suggests that the polynomial fit is better at predicting the temperature at this power. The uncertainty in B is significant however, and is caused by the influence of type B uncertainties (see section 4.3 in the appendix).

While the polynomial fit suits the data better, the uncertainty in the non-linearity parameter B is the same magnitude as the value of the parameter. Until B can be determined with greater accuracy, it is preferable to apply the linear self-heat parameter instead. The uncertainty makes it difficult to establish whether convection cooling the thermistors is of significant influence at maximum measurement current. Using the determined values of B and applying it to the criterion mentioned in the introduction (convection is assumed to be negligible if $|B \cdot P| \ll C_{\text{sh},2}$) would lead to the conclusion that convection is not negligible. Using VSL13T025 with maximum measurement current passing through it as an example, $|B \cdot P|$ is $0.057 \text{ mK} \cdot \mu\text{W}^{-1}$ and $C_{\text{sh},2}$ is $1.752 \text{ mK} \cdot \mu\text{W}^{-1}$. In other words, $|B \cdot P|$ is 3 % of $C_{\text{sh},2}$, which is not small enough to consider the criterion set out in equation [15] true. As stated in the introduction, for $|B \cdot P| \ll C_{\text{sh},2}$ to be considered true the left-hand side of the equation should be at most 1 % of the right-hand side.

However, there are possible values of B within the uncertainty margin that would lead to the opposite conclusion. A value for B of $0 \text{ mK} \cdot \mu\text{W}^{-2}$ lies within the expanded uncertainty margin ($k = 2$) for both thermistors, for example. As there is not enough data of sufficient accuracy to determine whether the value of the non-linearity parameter is significant, the self-heat correction factor will be determined only using the results of the 1st order approach.

Based on a linear fit of the data, k_{sh} is determined using equation [13]. The result is 1.00638 ± 0.00018 for thermistor VSL13T025 and 1.01016 ± 0.00018 for thermistor VSL13T033. The relative standard uncertainty of this correction is 0.018 %, which represents an improvement over the previous relative standard uncertainty of 0.07 %.

4 Analysis of uncertainties in the results

In this chapter, the process of constructing an uncertainty budget is described using the calculated thermistor resistance and linear self-heat parameter $C_{sh, 1}$ as examples. The uncertainty of the 2nd order parameters ($C_{sh, 2}$ and B) is also calculated. At the end of this chapter, an overview is given of the contributors to the uncertainty for several important parameters. Where needed, more explanation is given. Finally, a summary is given of the variables whose uncertainty calculations can be found in the appendix.

The uncertainties described in this chapter are all standard uncertainties, so a coverage factor of $k = 1$ is used.

4.1 Uncertainty of thermistor resistance

As an example, the process of constructing an uncertainty budget for a thermistor resistance calculation using equation [23] is demonstrated. The uncertainties of the variables are determined based on instrument specifications, calibration result; type A uncertainties, and further uncertainty analysis of the variables themselves, if needed. Table 7 shows the uncertainty components of R_p and R_m .

Table 7: Uncertainty components of measured resistance R_m and parallel resistance R_p .

	Component	Value	Standard uncertainty	Unit	Probability distribution	Type	Uncertainty contribution
R_p	DMM calibration	-	0.13	Ω	Normal	B	0.13
	DMM resolution	-	0.000 29	Ω	Normal	B	0.000 29
	DMM stability	-	0.001 0	Ω	Normal	B	0.001 0
	DMM input impedance r_{in}		0.003 0	Ω	Normal	B	0.003 0
	Repeated measurements of R_p	-	0.002 0	Ω	Normal	A	0.002 0
	R_p	999.77	-	Ω	Normal	Total	0.13
R_m	DMM calibration	-	0.13	Ω	Normal	B	0.13
	DMM resolution	-	0.000 29	Ω	Normal	B	0.000 29
	DMM stability	-	0.001 0	Ω	Normal	B	0.001 0
	DMM input impedance r_{in}		0.003 0	Ω	Normal	B	0.003 0
	Repeated measurements of R_m	-	0.002 0	Ω	Normal	A	0.002 0
	R_m	907.21	-	Ω	Normal	Total	0.13

The calibration uncertainty is based on the results of a calibration performed by VSL (certificate numbers 3352534 and 3352535 for DMM 1 and DMM 2, respectively. Found in section 8.8 of the appendix). The DMM's resolution is based on the number of digits displayed on the instrument. The DMM has a higher resolution when reading out values over GPIB, but in both cases the contribution from the DMM's resolution is negligible compared to the other sources of uncertainty. For this reason, the uncertainty contribution of the DMM's resolution is calculated based on the lower of the two resolutions. To translate the rectangular probability distribution of this uncertainty to a normal probability distribution, the standard uncertainty is divided by $2 \cdot \sqrt{3}$. Taking the quadratic sum of the uncertainty components as explained in section 1.5 yields a standard uncertainty for R_p and R_m equal to 0.13 Ω , which is entirely the result of the DMM's calibration uncertainty.

r and r_p are based on the sum of various lead and internal resistances, as described in equations [26] and [27] and shown in section 2.3. The sensitivity coefficient for all variables in these equations is 2, as both equations are sums of the different variables multiplied by two. For each partial derivative, only a single constant term remains. Therefore the uncertainty of each component contributes equally to the uncertainty of r and r_p . As shown in Table 8, the uncertainties of r and r_p are almost entirely determined by the uncertainty in the switch system's internal resistance ($r_{sc, R1}$ in this example). A broad estimate for this value was used due to the inability to accurately measure this resistance on its own, as explained in section 3.1.

On the self-heat effects of thermistors

Table 8: Uncertainty components of lead resistances in parallel resistor (r_p) and thermistor (r) circuits.

	Component	Value	Standard uncertainty	Unit	Probability distribution	Sensitivity coefficient	Type	Uncertainty contribution
r_p	r_c	0.176 1	$2.0 \cdot 10^{-3}$	Ω	Normal	2	A	$4.0 \cdot 10^{-3}$
	$r_{w,1}$	0.050 404	$4.5 \cdot 10^{-5}$	Ω	Normal	2	B	$9.0 \cdot 10^{-5}$
	$r_{sc,R1}$	0.255	$5.0 \cdot 10^{-2}$	Ω	Normal	2	B	$1.0 \cdot 10^{-1}$
	r_p	0.96	-	Ω	Normal	-	Total	0.10
r	r_c	0.176 1	$2.0 \cdot 10^{-3}$	Ω	Normal	2	A	$4.0 \cdot 10^{-3}$
	$\eta_{1,1}$	3.792	$1.2 \cdot 10^{-2}$	Ω	Normal	2	A	$2.4 \cdot 10^{-2}$
	$r_{sc,Th1}$	0.347	$5.0 \cdot 10^{-2}$	Ω	Normal	2	B	$1.0 \cdot 10^{-1}$
	$r_{w,Th1}$	0.092 171	$1.3 \cdot 10^{-5}$	Ω	Normal	2	B	$2.6 \cdot 10^{-5}$
	r	8.81	-	Ω	Normal	-	Total	0.10

Next, the sensitivity coefficients are calculated with partial derivatives:

Table 9: Sensitivity coefficients for calculated thermistor resistance from equation [23].

Sensitivity coefficient	Partial derivative	Equation
S_{R_p}	$\left \frac{\partial R}{\partial R_p} \right $	$\frac{R_m \cdot (R_m + r)}{(R_p - R_m + r_p)^2}$
S_{R_m}	$\left \frac{\partial R}{\partial R_m} \right $	$\frac{(R_p + r_p) \cdot (R_p + r + r_p)}{(R_p - R_m + r_p)^2}$
S_{r_p}	$\left \frac{\partial R}{\partial r_p} \right $	$\frac{R_m \cdot (R_m + r)}{(R_p - R_m + r_p)^2}$
S_r	$\left \frac{\partial R}{\partial r} \right $	$\frac{R_m}{(R_p - R_m + r_p)}$

The sensitivity coefficients show that with parallel resistances of less than 1 k Ω , the sensitivity of R_p , R_m , and r_p will increase rapidly. As R_p approaches 0 Ω , R_m will approach R_p . Therefore, the denominator of the sensitivity coefficients will become smaller and smaller as R_p approaches 0 Ω , increasing the value of the coefficient as a whole. For R_p , R_m , and r_p , the denominator is squared, which further increases the rate at which the sensitivity coefficient escalates with decreasing values of R_p . This is verified by the results of the validation experiments, where not including a lead resistance on the order of 1 Ω resulted in a deviation of 100 Ω from the actual value.

With the determined uncertainties and sensitivities of each variable in equation [23], the standard uncertainty of thermistor resistance R can be determined. This is shown in Table 10.

Table 10: Uncertainty budget for thermistor resistance calculated with equation [23].

Name	Component	Value	Standard uncertainty	Unit	Probability distribution	Sensitivity coefficient*	Type	Uncertainty contribution
Thermistor resistance (R)	R_p	999.78	0.13	Ω	Normal	96.5	B	12
	R_m	907.86	0.13	Ω	Normal	117	B	15
	r_p	0.96	0.10	Ω	Normal	193	B	19
	r	8.81	0.10	Ω	Normal	19.6	B	2.0
	R	9869	-	Ω	Normal	-	Total	27

* See Table 9 for the equations of the sensitivity coefficients.

On the self-heat effects of thermistors

Page 43 of 74

With these values, the result of this calculation is a thermistor resistance of $9869 \Omega \pm 27 \Omega$. This is mostly due to the uncertainty in the value of r_p . With $R_p = 1000 \Omega$, any uncertainty in r_p is multiplied by a sensitivity coefficient of 193, which results in a large contribution to the uncertainty of R . The sensitivity of R_p and R_m is also large, resulting in an uncertainty of 27Ω .

4.2 Uncertainty of linear self-heat parameter $C_{sh,1}$

The uncertainty budget for the self-heat constant $C_{sh,1}$ is constructed as previously demonstrated. Type A and B uncertainties for each variable are determined and the sensitivity coefficients are calculated. For the linear self-heat parameter (given by $C_{sh,1} = \frac{\Delta T_{sh}}{P}$), the uncertainty in ΔT_{sh} and P needs to be determined first.

Equation [24] describes the power dissipated by the thermistor in terms of current passing through it and resistance of the thermistor. With the latter having been determined in the previous section, the uncertainty in the current is determined by analyzing equation [21].

Table 11: Example uncertainty budget for current passing through thermistor with $R_p = 5 \text{ k}\Omega$.

Name	Component	Value	Standard uncertainty	Unit	Probability distribution	Sensitivity coefficient	Type	Uncertainty contribution
Current through thermistor (I_R)	I_m	$9.65186 \cdot 10^{-5}$	$6.0 \cdot 10^{-9}$	A	Normal	0.336	B	$2.0 \cdot 10^{-9}$
	R_p	4 987.33	0.13	Ω	Normal	$4.31 \cdot 10^{-9}$	B	$5.4 \cdot 10^{-10}$
	R	9 856.9	1.5	Ω	Normal	$2.18 \cdot 10^{-9}$	B	$3.3 \cdot 10^{-9}$
	r_p	0.96	0.10	Ω	Normal	$8.63 \cdot 10^{-9}$	B	$8.7 \cdot 10^{-10}$
	r	8.81	0.10	Ω	Normal	$4.36 \cdot 10^{-9}$	B	$4.4 \cdot 10^{-10}$
	I_R	$3.24068 \cdot 10^{-9}$	-	A	-	-	Total	$4.0 \cdot 10^{-9}$

With a parallel resistance of $\sim 5 \text{ k}\Omega$, the uncertainty in the current passing through the thermistor is 4 nA, primarily caused by the uncertainty in the thermistor's resistance. In relative terms, the uncertainty is 123 ppm. With the uncertainty of both variables that make up P known, the uncertainty in P can be calculated. How these uncertainties propagate is determined by analyzing the equation $P = I_R^2 \cdot R$. The result is shown in Table 12.

Table 12: Example uncertainty budget for power dissipated by thermistor with $R_p = 5 \text{ k}\Omega$.

Name	Component	Value	Standard uncertainty	Unit	Probability distribution	Sensitivity coefficient	Type	Uncertainty contribution
Power dissipated by thermistor (P)	I_R	$3.24068 \cdot 10^{-5}$	$4.0 \cdot 10^{-9}$	A	Normal	0.639	B	$1.6 \cdot 10^{-9}$
	R	9 856.88	1.5	Ω	Normal	$1.05 \cdot 10^{-9}$	B	$2.6 \cdot 10^{-9}$
	P	$1.03517 \cdot 10^{-5}$	-	W	-	-	Total	$3.0 \cdot 10^{-9}$

The uncertainty in the power dissipated by the thermistor is primarily caused by the uncertainty in the thermistor's resistance. For a power dissipation level of $\sim 10 \mu\text{W}$, the uncertainty is 3 nW. This represents a relative uncertainty of 290 ppm.

On the self-heat effects of thermistors

Next, the uncertainty in ΔT_{sh} is determined by analyzing the combination of equations [7] and [8], the result of which is:

$$\Delta T_{sh} = -\frac{T^2}{\beta} \cdot \frac{R_2 - R_1}{\bar{R}} \tag{28}$$

where R_1 is the resistance at maximum power dissipation, R_2 is the resistance of the thermistor with a parallel resistor ($R_p = 5 \text{ k}\Omega$ in this example) and \bar{R} is the average of these two resistances. The change in temperature determined based on these two resistances is caused by a change in self-heat when using this method. Analyzing the equation yields the uncertainty budget shown in Table 13.

Table 13: Example uncertainty budget for self-heat of thermistor VSL13T025 with $R_p = 5 \text{ k}\Omega$.

Name	Component	Value	Standard uncertainty	Unit	Probability distribution	Sensitivity coefficient	Type	Uncertainty contribution
Thermistor self-heat (ΔT_{sh})	T	276.983	0.002 0	K	Normal	$1.01 \cdot 10^{-3}$	B	$2.0 \cdot 10^{-6}$
	β	3 104.7	2.2	K	Normal	$4.51 \cdot 10^{-3}$	B	$9.8 \cdot 10^{-5}$
	R_1	9 801.7	0.13	Ω	Normal	$2.49 \cdot 10^{-3}$	B	$3.1 \cdot 10^{-4}$
	R_2	9 857.5	1.5	Ω	Normal	$2.51 \cdot 10^{-3}$	B	$3.8 \cdot 10^{-3}$
	ΔT_{sh}	$4.13 \cdot 10^{-2}$	-	K	-	-	Total	$3.8 \cdot 10^{-3}$

The determined uncertainty for the self-heat temperature of the thermistor with $R_p = 5 \text{ k}\Omega$ is 3.8 mK on a self-heat of 41.3 mK, a relative uncertainty of 9.2 %. This is primarily caused by the uncertainty in the thermistor's resistance.

How the uncertainties of ΔT_{sh} and P influence the uncertainty of $C_{sh, 1}$ is explained next. $C_{sh, 1}$ is based on a trend line when plotting ΔT_{sh} as a function of P . The influence of type B uncertainties on this trend line is estimated using the uncertainty of ΔT_{sh} , which is the dependent variable in this case. Additionally, the relative uncertainty of ΔT_{sh} is approximately 300 times larger than that of P , so it is expected to have much more influence on the accuracy of $C_{sh, 1}$. Further explanation of the estimate for the type B uncertainties in $C_{sh, 1}$ is based on Figure 24 .

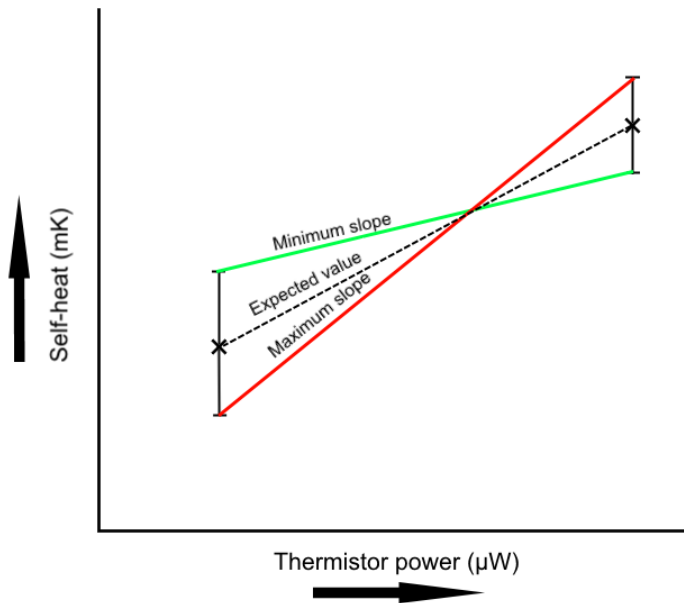


Figure 24: Qualitative illustration of minimum and maximum slopes within which all possible values of $C_{sh, 1}$ are found.

On the self-heat effects of thermistors

The two lines in Figure 24 start out separated based on the uncertainty in self-heat temperature when using the smallest parallel resistor (5 kΩ in this case). The uncertainty in the self-heat temperature at maximum power dissipation determines the end point for both lines, with the minimum slope ending at the low end of the uncertainty margin and the maximum slope at the high end. Each straight line that passes by both points within the uncertainty indicated by the error bars will have a slope that is between the minimum and maximum values illustrated in Figure 24. The type B uncertainty in $C_{sh,1}$ is estimated to be half of the difference between the minimum and maximum slope:

$$u_{C_{sh,1},type\ B} = \frac{1}{2} \cdot (\text{slope}_{\text{max}} - \text{slope}_{\text{min}}) \quad [29]$$

Half of the difference between the slopes is used to reflect that this uncertainty represents an area above and below the expected value. For the example described in this section, the resulting type B uncertainty is $0.050 \text{ mK} \cdot \mu\text{W}^{-1}$ (3.0 %). Repeating this analysis on the results of other measurement series yields values between $0.040 \text{ mK} \cdot \mu\text{W}^{-1}$ and $0.050 \text{ mK} \cdot \mu\text{W}^{-1}$ for both thermistors. The estimate of the type B uncertainty is based on the largest of these values to ensure full coverage. Combining this uncertainty with the type A uncertainty from a repeated series of measurements results in the combined standard uncertainty shown in Table 14.

Table 14: Uncertainty budget for self-heat parameter (1st order) based on data from fifty measurement series.

Name	Component	Value	Unit	Probability distribution	Type	Uncertainty contribution
1 st order self-heat parameter ($C_{sh,1}$)	Repeated measurements	$1.3 \cdot 10^{-3}$	$\text{mK} \cdot \mu\text{W}^{-1}$	Normal	A	$1.3 \cdot 10^{-3}$
	Uncertainty from method and instruments	0.050	$\text{mK} \cdot \mu\text{W}^{-1}$	Normal	B	$5.0 \cdot 10^{-2}$
	$C_{sh,1}$	1.687	$\text{mK} \cdot \mu\text{W}^{-1}$	-	-	0.050

The determined 1st order self-heat parameter is $(1.687 \pm 0.050) \text{ mK} \cdot \mu\text{W}^{-1}$ for thermistor VSL13T025. Performing the same analysis for thermistor VSL13T033 results in 1st order self-heat parameter of $(2.819 \pm 0.050) \text{ mK} \cdot \mu\text{W}^{-1}$. The standard deviation of the measured $C_{sh,1}$ value is selected to represent the type A uncertainty. This is because, for on-site applications, there may only be time to perform a single self-heat measurement. The uncertainty should accurately reflect the confidence level that this single measurement will fall within the uncertainty margin. In this case, however, the type A uncertainty is negligible compared to type B. The estimated influence of the type B uncertainties is dominant in the self-heat parameter.

4.3 Uncertainty analysis of 2nd order self-heat parameter $C_{sh,2}$ and non-linearity parameter B

To determine the uncertainty of the 2nd order approach to measuring a thermistor's self-heat, as described by equation [14], an estimate is required for the type B uncertainty of $C_{sh,2}$. Basing the estimate on the minimum and maximum possible slopes within the uncertainty of the self-heat temperature (as shown in Figure 24) is more difficult as it concerns a 2nd order function. However, despite the noticeable difference between the 1st and 2nd order approaches to self-heat determination (highlighted in Figure 23), the magnitude of this difference is at most 3 % for these thermistors. The influence of type B uncertainties on the accuracy of $C_{sh,2}$ is therefore expected to be similar to $C_{sh,1}$. Therefore the type B relative uncertainty of $C_{sh,2}$ is estimated to be $0.050 \text{ mK} \cdot \mu\text{W}^{-1}$ as well. This is combined with the type A uncertainty, which is based on the standard deviation of the measurement data (as demonstrated in the previous section).

On the self-heat effects of thermistors

Page 46 of 74

The combined standard uncertainty of $C_{sh, 2}$ is shown in Table 15.

Table 15: Combined standard uncertainty of 2nd order self-heat parameter.

Name	Component	Value	Unit	Probability distribution	Type	Uncertainty contribution
2 nd order self-heat parameter ($C_{sh, 2}$)	Repeated measurements	$6.2 \cdot 10^{-3}$	$\text{mK} \cdot \mu\text{W}^{-1}$	Normal	A	$6.2 \cdot 10^{-3}$
	Uncertainty from method and instruments	0.050	$\text{mK} \cdot \mu\text{W}^{-1}$	Normal	B	$5.0 \cdot 10^{-2}$
	$C_{sh, 2}$	1.752	$\text{mK} \cdot \mu\text{W}^{-1}$	-	-	0.050

The result of this calculation for $C_{sh, 2}$ is $(1.752 \pm 0.050) \text{mK} \cdot \mu\text{W}^{-1}$ for thermistor 13T025 and $(2.862 \pm 0.050) \text{mK} \cdot \mu\text{W}^{-1}$ for 13T033. How this uncertainty propagates in the uncertainty of B is determined next. Equation [14] can be rewritten to give B in terms of $C_{sh,2}$, P and ΔT_{sh} :

$$B = \frac{\Delta T_{sh}}{P^2} - \frac{C_{sh,2}}{P} \quad [30]$$

The same uncertainties for P and ΔT_{sh} are used, though the sensitivity coefficients are different when using this method. With the estimated uncertainty of $C_{sh, 2}$, the type B uncertainty of B is shown in Table 16.

Table 16: Type B uncertainties for non-linearity parameter B .

Name	Component	Value	Standard uncertainty	Unit	Probability distribution	Sensitivity coefficient	Type	Uncertainty contribution
Non-linearity parameter (B)	$C_{sh, 2}$	1.752	0.050	$\text{mK} \cdot \mu\text{W}^{-1}$	Normal	$1.06 \cdot 10^{-2}$	B	$5.3 \cdot 10^{-4}$
	P	93.542 6	0.003 0	μW	Normal	$1.87 \cdot 10^{-4}$	B	$5.6 \cdot 10^{-7}$
	ΔT_{sh}	158.39	0.39	mK	Normal	$1.13 \cdot 10^{-4}$	B	$4.4 \cdot 10^{-5}$
	B	$-6.1 \cdot 10^{-4}$	-	$\text{mK} \cdot \mu\text{W}^{-2}$	-	-	Total	$5.3 \cdot 10^{-4}$

The relative type B uncertainty of B in this example is significant, with the uncertainty being nearly as large as the value of B . This is caused by the uncertainty in the self-heat parameter. The uncertainty in the power dissipated by the thermistor and self-heat temperature is negligible in comparison.

From the measurement data, it is seen that B also has a sizeable type A uncertainty based on the standard deviation.

Table 17: Combined standard uncertainty of non-linearity parameter B .

Name	Component	Value	Unit	Probability distribution	Type	Uncertainty contribution
Non-linearity parameter (B)	Repeated measurements	$4.7 \cdot 10^{-5}$	$\text{mK} \cdot \mu\text{W}^{-2}$	Normal	A	$4.7 \cdot 10^{-5}$
	Uncertainty from method and instruments	$5.3 \cdot 10^{-4}$	$\text{mK} \cdot \mu\text{W}^{-2}$	Normal	B	$5.3 \cdot 10^{-4}$
	B	$-6.1 \cdot 10^{-4}$	$\text{mK} \cdot \mu\text{W}^{-2}$	-	-	$5.3 \cdot 10^{-4}$

Based on the measurement results and subsequent uncertainty analysis, B is found to be $(-6.1 \pm 5.3) \cdot 10^{-4} \text{mK} \cdot \mu\text{W}^{-2}$ for VSL13T025 and $(-4.5 \pm 5.3) \cdot 10^{-4} \text{mK} \cdot \mu\text{W}^{-2}$ for VSL13T033.

On the self-heat effects of thermistors

Page 47 of 74

4.4 Overview of uncertainty contributions to self-heat correction factor

In this section, a compact version of the uncertainty budgets presented previously is given for the most impactful parameters for determining the uncertainty of the self-heat correction factor. Brief analysis of the contributions to the combined uncertainty of the variable highlights the most important contributors.

Table 18: Uncertainty contributions to calculated thermistor resistance with $R_p = 5 \text{ k}\Omega$.

Variable	Component	Type	Uncertainty contribution
	Parallel resistor R_p	B	0.49 Ω
	Measured resistance R_m	B	1.1 Ω
	Thermistor lead resistance r	B	0.40 Ω
	Parallel resistor lead resistance r_p	B	0.78 Ω
	Repeated measurements of R	A	0.00 Ω
Combined: thermistor resistance R	-	-	1.5 Ω

The uncertainty in the calculated thermistor resistance is caused predominantly by the measurement uncertainty of the DMM. However, the uncertainty in the thermistor lead resistance also plays a significant role. The uncertainties of the parallel resistor and its lead resistance also influence the combined uncertainty, but to a smaller degree. An expanded version of the uncertainty budget for the thermistor resistance R can be found in Table 10.

Table 19: Uncertainty contributions to thermistor self-heat with $R_p = 5 \text{ k}\Omega$.

Variable	Component	Type	Uncertainty contribution
	Thermistor parameter β	B	$9.8 \cdot 10^{-5} \text{ K}$
	Thermistor temperature T	B	$2.0 \cdot 10^{-6} \text{ K}$
	Resistance at maximum power dissipation R_1	B	$3.1 \cdot 10^{-4} \text{ K}$
	Resistance with $R_p = 5 \text{ k}\Omega$ R_2	B	$3.8 \cdot 10^{-3} \text{ K}$
	Repeated measurements of ΔT_{sh}	A	$1.0 \cdot 10^{-3} \text{ K}$
Combined: thermistor self-heat ΔT_{sh}	-	-	3.9 mK

For the thermistor's self-heat, the uncertainty in the calculated resistance of the thermistor with $R_p = 5 \text{ k}\Omega$ is dominant. This uncertainty budget is shown in expanded form in Table 13.

Table 20: Uncertainty contributions to self-heat correction factor.

Variable	Component	Type	Uncertainty contribution
	Self-heat parameter $C_{sh, 1}$	B	$1.8 \cdot 10^{-4}$
	Thermistor coefficient α	B	$7.1 \cdot 10^{-6}$
	Thermistor power P	B	$2.9 \cdot 10^{-6}$
	Repeated measurements of k_{sh}	A	$4.9 \cdot 10^{-6}$
Combined: self-heat correction factor k_{sh}	-	-	$1.8 \cdot 10^{-4}$

On the self-heat effects of thermistors

Page 48 of 74

The uncertainty in the self-heat correction factor is caused entirely by the uncertainty in the self-heat parameter $C_{sh,1}$. The expanded version of this table is found in Table 34 in section 8.5.5 of the appendix.

The most impactful uncertainty for all the variables shown above is the uncertainty in the calculated thermistor resistance R . It is the main contributor to the self-heat temperature's uncertainty, which is itself the dominant cause of uncertainty in $C_{sh,1}$ and $C_{sh,2}$ and ultimately k_{sh} . The components that R consists of all contribute to its uncertainty in a significant manner, with the most significant being the uncertainty in the DMM's measured resistance.

In the appendix, detailed uncertainty budgets can be found for several variables. The location of these budgets is summarized in the list below:

8.5.1 - Uncertainty budget for lead resistance experiment

8.5.2 - Uncertainty budget for lead resistances compensation

8.5.3 - Uncertainty budget for validation experiments with substitute thermistor

8.5.4 - Uncertainty budget for thermistor temperature

8.5.5 - Uncertainty analysis of self-heat correction factor k_{sh}

5 Discussion

In this study, a number of steps have been taken towards improving self-heat parameter measurements for the thermistors in VSL's water calorimeter. Using the information summarized in chapter 1, a method and equipment setup are designed and implemented to measure thermistor temperature as a function of dissipated power. This setup uses instruments in the water calorimeter's experimental setup, a newly designed piece of equipment (equipment interface box) and a custom software program to perform automated measurements of self-heat. The data gathered using the setup is analyzed in two ways. Both linear and 2nd order approaches are used to investigate the potential influence of non-linear effects on self-heat, for example due to convection cooling the thermistors. The end result of these measurements is the determination of a self-heat correction factor k_{sh} , which corrects for the thermistor under-reporting temperature changes when performing water calorimetry.

The lead resistances that affect the division of current between thermistor and parallel resistor have been measured for each channel used on the switch system. For the parallel resistors, lead resistances between $0.73 \Omega \pm 0.10 \Omega$ and $1.12 \Omega \pm 0.10 \Omega$ are measured. For the thermistors, lead resistance compensation is between $8.41 \pm 0.10 \Omega$ and $8.81 \pm 0.10 \Omega$. Errors in the parallel resistor lead resistances are most noticeable at low values for the parallel resistor, particularly for $R_p < 1000 \Omega$. This is illustrated in Figure 19, where the error bars for the measurement with $R_p = 1000 \Omega$ highlight how much larger the uncertainty is in this point compared to those where larger parallel resistors are used. The influence of the thermistor's extension leads is noticeable in the validation using where these leads are used. Neglecting to compensate for the lead resistance resulted in every measurement falling outside of the expanded uncertainty ($k = 2$). Incorporating the resistance of the extension leads in the calculations resulted in a successful validation. When taking lead resistances into account, each validation experiment is passed successfully.

Based on a linear fit of the data, the self-heat parameter $C_{sh, 1}$ is $1.687 \pm 0.050 \text{ mK} \cdot \mu\text{W}^{-1}$ for VSL13T025 and $2.819 \pm 0.050 \text{ mK} \cdot \mu\text{W}^{-1}$ for VSL13T033. While this is a large change from the values reported by Mostert (2014), it is likely that the thermistors have changed over the course of the two years between studies.

Based on a 2nd order polynomial fit of the data, the self-heat parameter is $1.752 \pm 0.050 \text{ mK} \cdot \mu\text{W}^{-1}$ for VSL13T025 and $2.865 \pm 0.050 \text{ mK} \cdot \mu\text{W}^{-1}$ for VSL13T033. B is determined to be $(-6.1 \pm 5.3) \cdot 10^{-4} \text{ mK} \cdot \mu\text{W}^{-2}$ and $(-4.5 \pm 5.3) \cdot 10^{-4} \text{ mK} \cdot \mu\text{W}^{-2}$ for the same thermistors, respectively. While the value of the non-linearity parameter suggests that non-linear effects that are assumed to be caused by convection reduce self-heat by as much as 3 % at maximum measurement current, the uncertainty in this parameter calls the significance of this result into question. Within the expanded uncertainty margin ($k = 2$), this result means that B could be zero for both thermistors. While analysis of the fit residuals of the measurement data indicates that a 2nd order fit matches the data well, the accuracy with which the fit coefficients can be determined is lacking. As it cannot be established with sufficient accuracy whether convection is a significant influence on self-heat in the water calorimeter, the linear self-heat parameter $C_{sh, 1}$ is used to determine the self-heat correction factor.

There are numerous improvements that could be made to improve the accuracy of k_{sh} . However, further improvements to the accuracy of k_{sh} may not be necessary. The relative standard uncertainty of k_{sh} as determined in this report is 0.018 %, an improvement over the relative standard uncertainty of k_{sh} is 0.07 % as reported by de Prez (2016). This improvement is realized largely by determining C_{sh} with better accuracy. As a result, the influence of k_{sh} 's uncertainty on the uncertainty of calorimetric measurements is diminished to the point of being negligible. As increasing the accuracy of k_{sh} is not going to increase the accuracy of absorbed-dose-to-water measurements in a noticeable way, it is better to focus on investigating other areas. To that end, a number of recommendations are made.

5.1 Recommendations

For continued use and development of the setup and method described in this report, a number of recommendations are made:

- The accuracy of the calculations for this method requires compensating for lead resistances. Therefore, when different extension leads are used for the thermistor, their resistance should be measured.
- Despite the large uncertainty of the non-linearity parameter, it seems worthwhile to further investigate potential convective effects inside the water calorimeter. This could be done via simulations or measurements with the setup.
- The thermistors have changed their self-heat parameters significantly in the past two years. Now that the setup is automated, it is worthwhile to measure these parameters a few times per year for each thermistor (or after using them for radiation measurements). This way changes in the self-heat parameters can be tracked.
- The switch system's internal resistance and how this resistance is divided amongst its components is a large source of uncertainty when calculating the thermistor's resistance. The uncertainty of the lead resistance compensation is currently entirely the result of having to estimate how much of the switch's resistance is found before the current splits and how much is found after. If a method could be devised to measure the resistance directly on the multiplexer card whilst it is in operation inside the switch system, this uncertainty could be reduced greatly. This, in turn, may make it possible for parallel resistances of less than 5 k Ω to be used in addition to increasing the accuracy of the setup.
- The non-linearity parameter may be better characterized if it were measured at different water temperatures. At 4 °C, it is expected that the least amount of non-linear behavior will occur. Reducing the water's density by raising the temperature should therefore result in larger negative values of B . This may be challenging due to the limited range on which the thermistor's temperature – resistance relationship is linear, but it is possible that even a small increase in water temperature results in noticeable changes in B . More knowledge of the non-linearity parameter may aid in reducing its uncertainty.
- The current passing through the thermistor can be measured using this setup. While reducing the number of active thermistors to a single one, the current measurement data can be compared to the resistance measurement data to check their coherence. The software currently does not have a procedure to perform this measurement however, so this will have to be written first. A measurement current calibration procedure may also be useful for tracking the long-term stability of the current source.

6 Conclusion

In this study, numerous improvements have been made to VSL's water calorimeter measurement setup. The equipment interface box along with the custom computer program allow for automated measurement of the data required to determine the self-heat parameter. Upon completion, minimal manual data analysis is required to calculate this parameter. This makes it possible to determine a self-heat correction factor on-site with minimal setup and human involvement required.

Lead resistances in the setup are measured and included when determining the thermistor's resistance. The method and equipment setup are validated successfully using stable, known resistors as a substitute for thermistors. The minimum settling time for the thermistors to reach a steady state temperature is found to be between 5 and 10 minutes after an applied step in power dissipation.

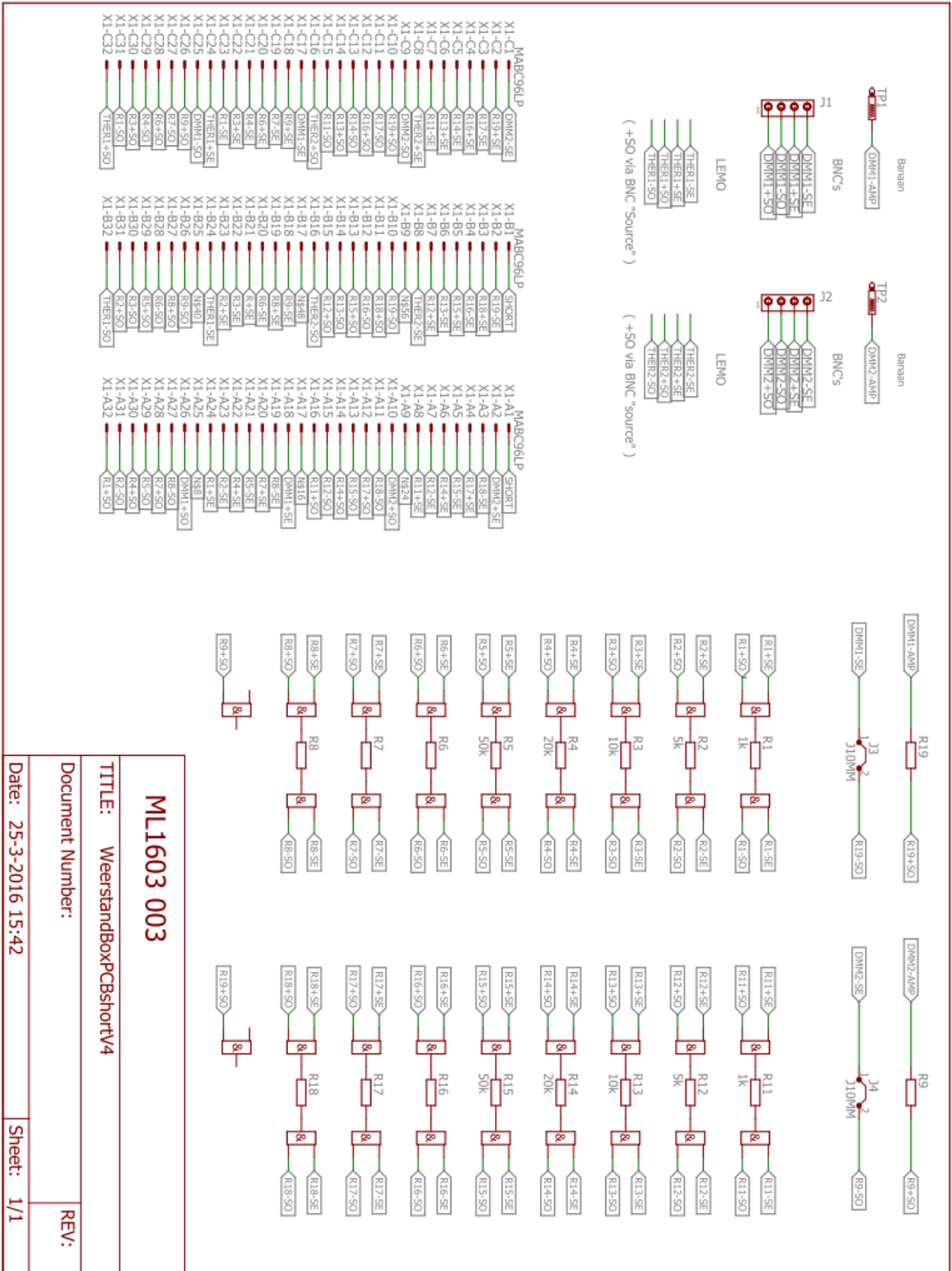
Fifty self-heat parameter measurements are performed and their data is analyzed. Based on these measurements, the self-heat correction factor is calculated for both thermistors along with their respective standard uncertainties. k_{sh} is determined to be 1.00638 ± 0.00018 for VSL13T025 and 1.01016 ± 0.00018 for VSL13T033. With a relative standard uncertainty of approximately 0.018 %, this method shows an improvement in the uncertainty of the self-heat correction factor; previously, this value was determined with a relative standard uncertainty of 0.07 %. This improvement in accuracy, alongside the automated measurement program, makes it possible to accurately determine a self-heat correction factor on-site with minimal setup and human input.

7 References

- Agilent Technologies. 2011. "Agilent 3458A Multimeter."
- Cen, J. 2011. "Report: Self-Heat Effect of Thermistors for Absorbed Dose Measurements," no. November.
- de Prez, Leon. 2008. "Report: De NMI Standaard Voor Geabsorbeerde Dosis in Water in Hoogenergetische Fotonenstraling" 2007.
- de Prez, Leon, and Jacco De Pooter. 2008. "The New NMI Orthovolt X-Rays Absorbed Dose to Water Primary Standard Based on Water Calorimetry." *Physics in Medicine and Biology* 53 (13): 3531–42. doi:10.1088/0031-9155/53/13/009.
- de Prez, Leon, Jacco De Pooter, B.J. Jansen, and A.H.L. Aalbers. 2016. "A Water Calorimeter for on-Site Absorbed Dose to Water Calibrations in 60Co and MV-Photon Beams Including MRI Incorporated Treatment Equipment," in preparation.
- Domen, S.R. 1982. "An Absorbed Dose Water Calorimeter: Theory, Design, and Performance." *Journal of Research of the National Bureau of Standards* 87 (3): 211–35. doi:10.6028/jres.087.016.
- . 1994. "A Sealed Water Calorimeter for Measuring Absorbed Dose." *Journal of Research of the National Institute of Standards and Technology* 99 (2): 121–41. doi:10.6028/jres.099.012.
- Epcos. 2009. "NTC Thermistors: General Technical Information," no. February: 1–16.
- Hamoen, V C S. 2013. "Characterization of the Self-Heat Effect of Thermistors in the VSL Water Calorimeter for Absorbed Dose."
- Joint Committee for Guides in Metrology (JCGM). 2008. "Evaluation of Measurement Data: Guide to the Expression of Uncertainty in Measurement," no. September: 120. doi:10.1373/clinchem.2003.030528.
- Keithley. 2004. "Low Level Measurements Handbook." Book, 239.
- Keysight. 2014. "Keysight 34420A NanoVolt / Micro-Ohm Meter," 1–6.
- Krauss, Achim. 2006. "The PTB Water Calorimeter for the Absolute Determination of Absorbed Dose to Water in 60 Co Radiation." *Metrologia* 43 (3): 259–72. doi:10.1088/0026-1394/43/3/008.
- Mostert, D. 2014. "Report: Self-Heat Effect of the Thermistors in the VSL Water Calorimeter," 1–49.
- Park, K, and D Y Bang. 2003. "Electrical Properties of Ni ± Mn ± Co ± (Fe) Oxide Thick- © Lm NTC Thermistors Prepared by Screen Printing." *Most* 4: 81–87.
- Rosenberg, I. 2008. "Radiation Oncology Physics: A Handbook for Teachers and Students." *British Journal of Cancer* 98: 1020. doi:10.1038/sj.bjc.6604224.
- Seuntjens, Jan, and Simon Duane. 2009. "Photon Absorbed Dose Standards." *Metrologia* 46 (2): S39–58. doi:10.1088/0026-1394/46/2/S04.
- Tyco Electronics. 2005. "Precision Metal Film Fixed Resistors."
- van den Brom, Helko E, Ernest Houtzager, Gert Rietveld, Roland van Bemmelen, and Oleg Chevtchenko. 2007. "Voltage Linearity Measurements Using a Binary Josephson System." *Measurement Science and Technology* 18 (11): 3316–20. doi:10.1088/0957-0233/18/11/008.
- World Health Organization. 2012. "Fact Sheet No 371"
[<http://www.who.int/mediacentre/factsheets/fs371/en/> - last accessed 10-03-2016]

8 Appendices

On the self-heat effects of thermistors



ML1603 003	
TITLE: WeerstandBoxPCBshortV4	
Document Number:	REV:
Date: 25-3-2016 15:42	Sheet: 1/1

Figure 26: Schematic of connections made inside equipment interfacing box.

8.2 Keithley 7001 switch system channel assignments

Table 21: Switch system channel connections for both circuits on the 2nd multiplexer card.

	Component	Nominal resistance	Connects to source bus with	Connects to sense bus with
Circuit 1	Thermistor	10 kΩ (at 4 °C)	Channel 1	Channel 11
	R1	1 kΩ	Channel 2	Channel 12
	R2	5 kΩ	Channel 3	Channel 13
	R3	10 kΩ	Channel 4	Channel 14
	R4	20.5 kΩ	Channel 5	Channel 15
	R5	50 kΩ	Channel 6	Channel 16
	Circuit 2	N/A	Channel 10	N/A
Circuit 2	Thermistor	10 kΩ (at 4 °C)	Channel 21	Channel 31
	R1	1 kΩ	Channel 22	Channel 32
	R2	5 kΩ	Channel 23	Channel 33
	R3	10 kΩ	Channel 24	Channel 34
	R4	20.5 kΩ	Channel 25	Channel 35
	R5	50 kΩ	Channel 26	Channel 36
	Circuit 1	N/A	Channel 30	N/A

As an example, measuring the thermistor on circuit 1 in 4-wire mode would require closing channels 1 and 11. Adding resistor R4 in parallel means channel 5 also needs to be closed. Measuring the current provided by DMM 1 with DMM 2 requires that all channels be open except for channel 10.

On the self-heat effects of thermistors

8.3 Data from lead and internal resistance measurements

Table 22: Difference between 2 and 4-wire resistance measurements of the resistors in the interface box.

	Resistor	2-wire r' (k Ω)	4-wire r (k Ω)	Δr (Ω)
Circuit 1	R1	1.001 940	0.999 770	2.170
	R2	4.989 329	4.987 306	2.023
	R3	9.999 075	9.996 965	2.110
	R4	20.50 866	20.506 46	2.200
	R5	49.94 672	49.944 57	2.150
Circuit 2	R6	1.002 023	0.9996 85	2.338
	R7	4.989 961	4.9878 92	2.069
	R8	9.998 109	9.9957 95	2.314
	R9	20.50 809	20.505 66	2.430
	R10	49.93 935	49.937 16	2.190

Table 23: Lead and internal resistance measurement results.

Resistor	r_c (Ω)	$r_{d,1}$ (Ω)	$r_{d,2}$ (Ω)	r_w (Ω)	$r_{sc,total}$ (Ω)	r_{extra} (Ω)	Total lead resistance (Ω)
R1	0.176 1	0.022 5	0.165 4	0.054 0	0.504 8	0.000 0	2.197 9
R2	0.176 1	0.022 5	0.165 4	0.059 7	0.423 5	0.000 0	2.046 5
R3	0.176 1	0.022 5	0.165 4	0.058 2	0.474 0	0.000 0	2.144 7
R4	0.176 1	0.022 5	0.165 4	0.060 4	0.516 8	0.000 0	2.234 6
R5	0.176 1	0.022 5	0.165 4	0.059 8	0.477 1	0.000 0	2.154 1
R6	0.176 1	0.021 6	0.215 6	0.058 4	0.518 6	0.026 6	2.385 7
R7	0.176 1	0.021 6	0.215 6	0.057 5	0.379 1	0.026 6	2.105 0
R8	0.176 1	0.021 6	0.215 6	0.051 6	0.512 7	0.026 6	2.360 5
R9	0.176 1	0.021 6	0.215 6	0.057 6	0.574 8	0.026 6	2.496 8
R10	0.176 1	0.021 6	0.215 6	0.060 1	0.451 0	0.026 6	2.254 3

On the self-heat effects of thermistors

Table 24: Thermistor extension lead resistance measurement results.

Calibration cable BLUE	Plus-side resistance (Ω)	Minus-side resistance (Ω)	Calibration cable RED	Plus-side resistance (Ω)	Minus-side resistance (Ω)
#1	7.599 78	7.585 97	#1	7.204 33	7.201 32
#2	7.596 12	7.578 44	#2	7.207 78	7.200 72
#3	7.597 61	7.576 31	#3	7.204 63	7.205 43
#4	7.588 51	7.581 35	#4	7.206 48	7.201 35
#5	7.581 62	7.583 14	#5	7.206 42	7.200 27
#6	7.587 50	7.581 37	#6	7.200 18	7.202 76
#7	7.577 40	7.578 72	#7	7.200 59	7.200 18
#8	7.583 02	7.579 83	#8	7.200 52	7.200 12
#9	7.581 63	7.584 19	#9	7.201 34	7.203 24
#10	7.582 34	7.578 09	#10	7.202 31	7.202 30
Average	7.587 55	7.580 74	Average	7.203 46	7.201 77
Standard deviation	0.012 07	0.003 03	Standard deviation	0.002 83	0.001 69

8.4 Data from validation procedures

Table 25: Results from first validation test of measurement setup.

Measured		No lead resistance compensation			With lead resistance compensation			Uncertainty of R_{calc}	
Circuit 1	R_{proxy}	R_m	R_{calc}	ΔR	$\Delta R/R$	R'_{calc}	$\Delta R'$	$\Delta R'/R$	Standard uncertainty
	[kΩ]	[kΩ]	[kΩ]	[kΩ]	[%]	[kΩ]	[kΩ]	[%]	[kΩ]
	9.996 87	0.909 65	10.092	0.095	0.95	10.001	0.004	0.044	0.028
	9.996 87	3.327 51	9.998 6	0.001 7	0.017	9.996 0	-0.000 9	-0.009	0.001 5
	9.996 87	9.996 87	9.996 869	-	-	9.996 87	-	-	-
	9.996 87	6.720 49	9.996 66	-0.000 2	-0.002	9.996 65	-0.000 2	-0.002	0.000 31
	9.996 87	8.329 50	9.996 72	-0.000 1	-0.001	9.996 77	-0.000 1	-0.001	0.000 22
Circuit 2	R_{proxy}	R_m	R_{calc}	ΔR	$\Delta R/R$	R'_{calc}	$\Delta R'$	$\Delta R'/R$	Standard uncertainty
	[kΩ]	[kΩ]	[kΩ]	[kΩ]	[%]	[kΩ]	[kΩ]	[%]	[kΩ]
	9.9962 2	0.909 64	10.096	0.099 6	0.987	9.998	0.002	0.024	0.028
	9.9962 2	3.327 79	9.997 4	0.001 2	0.012	9.994 9	-0.0013	-0.013	0.001 5
	9.9962 2	9.996 24	9.996 24	-	-	9.996 24	-	-	-
	9.9962 2	6.720 11	9.996 02	-0.000 2	-0.002	9.995 99	-0.0003	-0.003	0.0003 1
	9.9962 2	8.328 86	9.996 08	-0.000 2	-0.002	9.996 13	-0.0001	-0.001	0.0002 2

Table 26: Results from validation with resistor as thermistor proxy.

Measured		No lead resistance compensation			With lead resistance compensation			Uncertainty of R_{calc}	
Circuit 1	R_{proxy}	R_m	R_{calc}	ΔR	$\Delta R/R$	R'_{calc}	$\Delta R'$	$\Delta R'/R$	Standard uncertainty
	[kΩ]	[kΩ]	[kΩ]	[kΩ]	[%]	[kΩ]	[kΩ]	[%]	[kΩ]
	9.999 14	9.999 15	-	-	-	-	-	-	-
	9.999 14	0.909 61	10.083	0.084 7	0.840	9.994	-0.005	-0.049	0.028
	9.999 14	3.327 78	10.000 1	0.001 0	0.010	9.997 7	-0.001 4	-0.014	0.001 5
	9.999 14	4.999 04	9.998 88	-0.000 3	-0.003	9.998 54	-0.000 6	-0.006	0.000 59
	9.999 14	6.721 42	9.998 76	-0.000 4	-0.004	9.998 82	-0.000 3	-0.003	0.000 31
	9.999 14	8.331 03	9.998 92	-0.000 2	-0.002	9.999 00	-0.000 2	-0.002	0.000 22
Circuit 2	R_{proxy}	R_m	R_{calc}	ΔR	$\Delta R/R$	R'_{calc}	$\Delta R'$	$\Delta R'/R$	Standard uncertainty
	[kΩ]	[kΩ]	[kΩ]	[kΩ]	[%]	[kΩ]	[kΩ]	[%]	[kΩ]
	9.999 34	9.999 03	-	-	-	-	-	-	-
	9.999 34	0.909 59	10.089	0.090 3	0.895	9.993	-0.005	-0.054	0.028
	9.999 34	3.328 02	9.999 7	0.000 7	0.007	9.997 4	-0.001 6	-0.016	0.001 5
	9.999 34	4.998 75	9.998 83	-0.000 2	-0.002	9.998 44	-0.000 6	-0.006	0.000 59
	9.999 34	6.721 32	9.998 67	-0.000 3	-0.003	9.998 71	-0.000 3	-0.003	0.000 31
	9.999 34	8.330 75	9.998 80	-0.000 2	-0.002	9.998 88	-0.000 1	-0.001	0.000 22

On the self-heat effects of thermistors

Table 27: Results from validation with extension cable and known resistor.

Measured		No lead resistance compensation			With lead resistance compensation			Uncertainty of R_{calc}		
Circuit 1	R_{proxy}	R_m	R_{calc}	ΔR	$\Delta R/R$	R'_{calc}	$\Delta R'$	$\Delta R'/R$	Standard uncertainty	
	[kΩ]	[kΩ]	[kΩ]	[kΩ]	[%]	[kΩ]	[kΩ]	[%]	[kΩ]	
	9.998 95	9.999 15	-	-	-	-	-	-	-	
	9.998 95	0.909 60	10.057	0.058 1	0.578	9.992	-0.006	-0.060	0.028	
	9.998 95	3.327 77	9.994 3	-0.004 6	-0.046	9.997 0	-0.001 9	-0.019	0.001 5	
	9.998 95	4.999 04	9.995 93	-0.003 0	-0.030	9.998 11	-0.000 8	-0.008	0.000 59	
	9.998 95	6.721 41	9.997 44	-0.001 5	-0.015	9.998 72	-0.000 2	-0.002	0.000 31	
	9.998 95	8.331 02	9.998 27	-0.000 7	-0.007	9.998 85	-0.000 1	-0.001	0.000 22	
Circuit 2	R_{proxy}	R_m	R_{calc}	ΔR	$\Delta R/R$	R'_{calc}	$\Delta R'$	$\Delta R'/R$	Standard uncertainty	
	[kΩ]	[kΩ]	[kΩ]	[kΩ]	[%]	[kΩ]	[kΩ]	[%]	[kΩ]	
	9.999 14	9.998 99	-	-	-	-	-	-		
	9.999 14	0.909 36	10.061	0.062 9	0.625	9.991	-0.007	-0.074	0.028	
	9.999 14	3.327 39	9.993 9	-0.005 0	-0.050	9.996 7	-0.002 3	-0.023	0.001 5	
	9.999 14	4.998 05	9.996 03	-0.003 0	-0.030	9.998 15	-0.000 8	-0.008	0.000 59	
	9.999 14	6.720 78	9.997 47	-0.001 5	-0.015	9.998 73	-0.000 3	-0.003	0.000 31	
	9.999 14	8.330 40	9.998 29	-0.000 7	-0.007	9.998 87	-0.000 1	-0.001	0.000 22	

On the self-heat effects of thermistors

Page 61 of 74

8.5 Uncertainty budgets

8.5.1 Uncertainty budget for lead resistance experiment

The uncertainty in the lead and circuit resistance is determined by analyzing equation [25] as described in chapter 4.

Table 28: Uncertainty budget for lead resistance experiment, using R1.

Name	Component	Value	Standard uncertainty	Unit	Probability distribution	Sensitivity coefficient	Type	Uncertainty component
Lead resistance	r_c	0.176 1	0.002 0	Ω	Normal	4	A	0.008 0
	$r_{d1,1}$	0.022 507	$1.1 \cdot 10^{-5}$	Ω	Normal	2	B	$2.2 \cdot 10^{-5}$
	$r_{d1,2}$	0.165 395	$8.3 \cdot 10^{-5}$	Ω	Normal	2	B	$1.7 \cdot 10^{-4}$
	$r_{w,1}$	0.054 024	$2.7 \cdot 10^{-5}$	Ω	Normal	2	B	$5.4 \cdot 10^{-5}$
	r_{sc}	0.504 8	0.002 0	Ω	Normal	2	B	0.004 0
								Total
Circuit resistance	DMM linearity	-	$8.7 \cdot 10^{-8}$	Ω	Normal	1	B	$8.7 \cdot 10^{-8}$
	DMM resolution	-	$2.9 \cdot 10^{-4}$	Ω	Normal	1	B	$2.9 \cdot 10^{-4}$
							Total	$2.9 \cdot 10^{-4} \Omega$

Quadratic summation of these two uncertainties results in an uncertainty of 0.0089 Ω for the between the two methods.

8.5.2 Uncertainty budget for lead resistances compensation

To determine the uncertainty of the r and r_p , equations [26] and [27] are analyzed.

Table 29: Uncertainty budget for thermistor and parallel resistor lead resistances.

Name	Component	Value	Standard uncertainty	Unit	Probability distribution	Sensitivity coefficient	Type	Uncertainty component
r	r_c	0.176 1	0.002 0	Ω	Normal	2	A	0.004 0
	$r_{w,Th1}$	0.092 171	$4.6 \cdot 10^{-5}$	Ω	Normal	2	B	$1.9 \cdot 10^{-5}$
	$r_{l,1}$	3.792	0.012	Ω	Normal	2	B	0.024
	$r_{sc,Th1}$	0.299	0.050	Ω	Normal	2	B	0.10
								Total
r_p	r_c	0.176 1	0.002 0	Ω	Normal	2	A	0.004 0
	$r_{w,1}$	0.054 024	$2.7 \cdot 10^{-5}$	Ω	Normal	2	B	$5.4 \cdot 10^{-5}$
	$r_{sc,R1}$	0.252	0.050	Ω	Normal	2	B	0.10
								Total

On the self-heat effects of thermistors

8.5.3 Uncertainty budget for validation experiments with substitute thermistor

The uncertainty in the calculated resistance of the thermistor is determined by evaluating equation [23].

Table 30: Uncertainty analysis of calculated (proxy) thermistor resistance with $R_p = \sim 1 \text{ k}\Omega$.

Name	Component	Value	Standard uncertainty	Unit	Probability distribution	Sensitivity coefficient	Type	Uncertainty component
Thermistor resistance (R)	R_p	999.72	0.13	Ω	Normal	100	B	13
	R_m	909.61	0.13	Ω	Normal	121	B	15
	r	2.474	0.10	Ω	Normal	19.9	B	2
	r_p	0.972	0.10	Ω	Normal	200	B	20
							Total	28 Ω

This analysis is performed for each of the parallel resistors. The uncertainty of the thermistor resistance for each R_p is shown in Table 31.

Table 31: Summary of standard uncertainties with given parallel resistors.

Parallel resistance, nominal value ($\text{k}\Omega$)	Standard uncertainty of R (Ω)
1 $\text{k}\Omega$	28
5 $\text{k}\Omega$	1.5
10 $\text{k}\Omega$	0.59
20.5 $\text{k}\Omega$	0.31
50 $\text{k}\Omega$	0.22

On the self-heat effects of thermistors

Page 63 of 74

8.5.4 Uncertainty budget for thermistor temperature

The uncertainty in the thermistor's temperature measurements is determined by analyzing equation [5].

Table 32: Sensitivity coefficients for equation [5].

Sensitivity coefficient	Partial derivative	Equation
S_{β}	$\left \frac{\partial T}{\partial \beta} \right $	$\frac{T_0^2 \cdot \ln\left(\frac{R}{R_0}\right)}{\left(\beta + T_0 \cdot \ln\left(\frac{R}{R_0}\right)\right)^2}$
S_R	$\left \frac{\partial T}{\partial R} \right $	$\frac{\beta \cdot T_0^2}{R \cdot \left(\beta + T_0 \cdot \ln\left(\frac{R}{R_0}\right)\right)^2}$
S_{R0}	$\left \frac{\partial T}{\partial R_0} \right $	$\frac{\beta \cdot T_0^2}{R_0 \cdot \left(\beta + T_0 \cdot \ln\left(\frac{R}{R_0}\right)\right)^2}$
S_{T0}	$\left \frac{\partial T}{\partial T_0} \right $	$\frac{\beta^2}{\left(\beta + T_0 \cdot \ln\left(\frac{R}{R_0}\right)\right)^2}$

Table 33: Uncertainty budget for thermistor temperature measurement.

Name	Component	Value	Standard uncertainty	Unit	Probability distribution	Sensitivity coefficient	Type	Uncertainty component
Thermistor temperature	β	3 104	2.2	K	Normal	$2.35 \cdot 10^{-5}$	B	$5 \cdot 10^{-5}$
	R	9 870	28	Ω	Normal	0.003	B	0.07
	R_0	9 790.93	0.010	Ω	Normal	0.003	B	0.01
	T_0	277.150	0.002 0	K	Normal	0.999	B	$6 \cdot 10^{-6}$
								Total

On the self-heat effects of thermistors

8.5.5 Uncertainty analysis of self-heat correction factor k_{sh}

The standard uncertainty for the self-heat correction factor is calculated in Table 34.

Table 34: Uncertainty budget for self-heat correction factor k_{sh} for thermistor VSL13T033.

Name	Component	Value	Standard uncertainty	Unit	Probability distribution	Sensitivity coefficient	Type	Uncertainty contribution
Self-heat correction factor (k_{sh})	Self-heat constant $C_{sh,1}$	2.818	0.050	mK · μW^{-1}	Normal	$3.60 \cdot 10^{-3}$	B	$1.8 \cdot 10^{-4}$
	Thermistor coefficient α	$-4.0226 \cdot 10^{-5}$	$2.8 \cdot 10^{-8}$	mK ⁻¹	Normal	252	B	$7.1 \cdot 10^{-6}$
	Thermistor power P	89.591	0.026	μW	Normal	$1.13 \cdot 10^{-4}$	B	$2.9 \cdot 10^{-6}$
	Self-heat correction factor (k_{sh})	1.01016		-				$1.8 \cdot 10^{-4}$

8.6 Extrapolation of 34420A DMM uncertainty over time

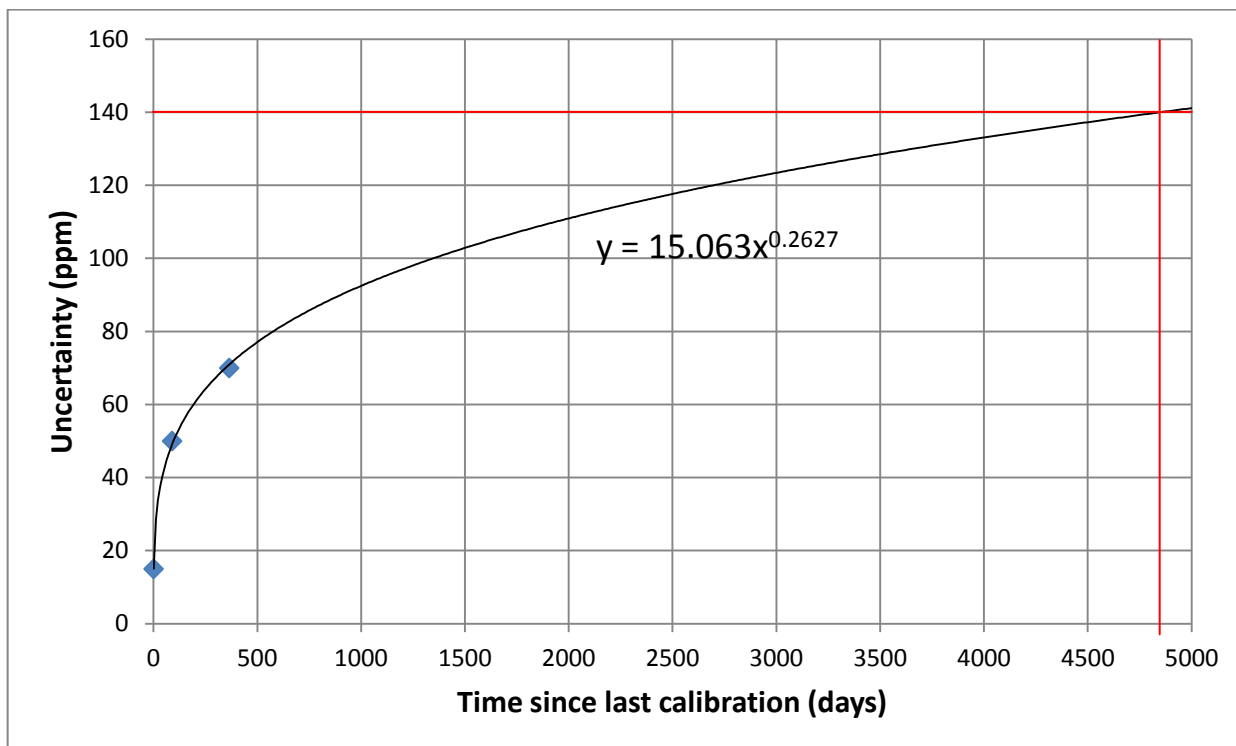


Figure 27: 34420A DMM’s measurement uncertainty based on manufacturer’s specifications, with extrapolation over the time period since last calibration.

Based on the 24 hour, 90 day and 1 year accuracy specifications of the DMM’s 1 Ω scale (Keysight 2014), a trend line based on a power function is extrapolated over the length of time since the last calibration of the DMM. Based on this extrapolation, its expected uncertainty is estimated to be 140 ppm. However, this estimate is purely a guess based on limited data. A power function is selected as trend line because it is the best fit for the data points, but this may not accurately reflect reality. Therefore an uncertainty of 500 ppm is assigned to the DMM. This value is expected to be large enough to adequately cover the uncertainty of the DMM’s measurements.

8.7 Original project description

Afstudeeropdracht

School: Haagse Hogeschool, Delft
Studie: Toegepaste Natuurkunde
Periode: 17 weken
Begeleider: Leon de Prez (algemeen); Bartel Jansen (software)
Project: VWS update calorimeter

Realisatie van een meetopstelling voor het automatisch meten van de thermistorself-heat in de VSL watercalorimeter (17 weken):

- kennisverwerving van bestaande meetmethoden en (meet)apparatuur; 2 w;
- kennisverwerving van de bij VSL gebruikte programmeertaal Delphi (= Object Pascal); 2 w;
- schrijven en testen van software(modules) voor data-acquisitie, opslag en verwerking (aansturen en uitlezen van apparatuur zoals bijv. digitale multimeters, stroombron, weerstandsdecade); 7 w;
- valideren van de meetopstelling (o.a. meten van de self-heatparameter, C_{sh} , van diverse thermistoren); 2 w;
- opstellen van een onzekerheidsbudget; 2 w;
- rapportage, bijvoorbeeld in het Engels; 2 w;

Eisen

Om in het stralingslaboratorium van VSL te kunnen werken wordt vereist dat de student de module 'stralingsveiligheid niveau 5' inclusief theorie-examen heeft afgerond.

Achtergrond

VSL is het Nationale Metrologie Instituut van Nederland en is internationaal een toonaangevend kennisinstituut op dit gebied. Naast het beheer en de ontwikkeling van de nationale primaire meetstandaarden, levert VSL diensten op maat en kalibraties van meetmiddelen in opdracht van klanten. VSL levert verschillende diensten voor ziekenhuizen, de medische industrie, producenten van bestralingsapparatuur en detectoren, dosimetriediensten en industrie die werkt met straling, zoals kerncentrales. Daarnaast werkt VSL in Europees verband aan verschillende onderzoeksprojecten.

Bij de behandeling van kankerpatiënten met ioniserende straling zijn nauwkeurige metingen van levensbelang. Bestralingen vinden plaats met behulp van externe stralingsbundels (tele-therapie) of bestraling met bronnen op korte afstand, soms zelfs in de patiënt (brachy-therapie). In de radiotherapie worden continu nieuwe geavanceerdere bestralingsmethoden en -apparatuur ontwikkeld, zoals lineaire versnellers gecombineerd met MRI-scanners of de toepassing van nieuwe stralingsmodaliteiten zoals bijvoorbeeld toegepast bij hadrontherapie. VSL ontwikkelt meetmethoden om de geabsorbeerde dosis (eenheid Gray) en de verdeling daarvan ook voor deze nieuwe behandelmethoden steeds nauwkeuriger te bepalen.

ZELFOPWARMING VAN THERMISTOREN IN DE VSL WATERCALORIMETER

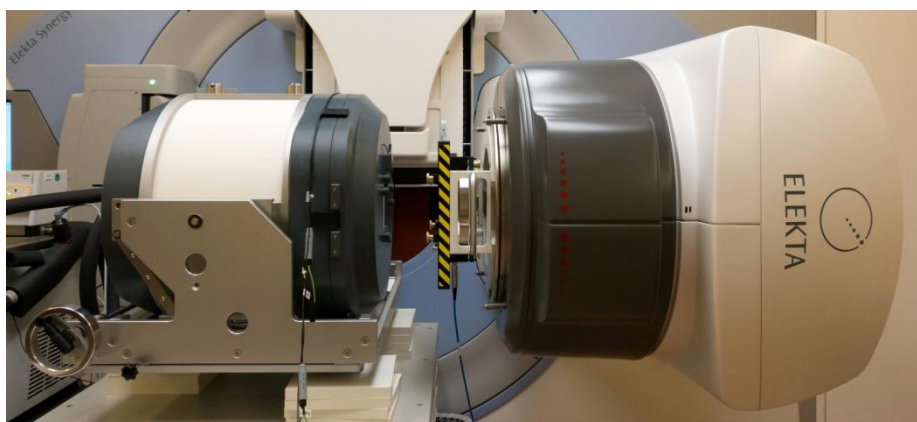
De Nederlandse primaire standaard voor geabsorbeerde-dosis-in-water, D_w , is een watercalorimeter (WCM). Deze bestaat uit een watervolume, een zogenaamd waterfantom van ca. $30 \times 30 \times 30 \text{ cm}^3$, dat zich op $4,0 \text{ °C}$ bevindt in een actief gekoelde thermostaatbehuizing. In de WCM wordt ten gevolge van bestraling met externe stralingsbundels (momenteel röntgen- of gammastraling) een temperatuursverandering van het water, ΔT_w in K, gemeten waarmee de eenheid Gray ($\text{Gy} = \text{J} \cdot \text{kg}^{-1}$) wordt gerealiseerd volgens:

$$D_w = C_{p,w} \cdot \Delta T_w \cdot \prod k \quad (1)$$

Hierin is $C_{p,w}$ de soortelijke warmte van water, $4207,5 \text{ J} \cdot \text{kg}^{-1} \cdot \text{K}^{-1}$. $\prod k$ is het product van dimensieloze factoren om te corrigeren naar de referentieomstandigheden. Een bestraling met bijvoorbeeld 1 Gy resulteert in een temperatuursverandering van circa $0,24 \text{ mK}$. Om deze verandering met een onzekerheid kleiner dan 1% te kunnen meten is zeer stabiele en lage achtergrondtemperatuurdrift vereist (zie Figuur 1).

On the self-heat effects of thermistors

Page 67 of 74



Figuur 1: De VSL watercalorimeter (links) in een klinische lineaire versnellerbundel (Elekta Versa HD) bij het AVL in Amsterdam.

De temperatuursverandering van het water, ΔT_w , wordt gemeten op basis van de weerstand en weerstandsverandering, respectievelijk R en ΔR in Ω , van NTC (negative temperature coefficient) thermische weerstanden. Deze zogenaamde thermistoren hebben een diameter van 0,35 mm en zijn gelijmd in uiteinden van glazen pipetjes met een binnen- en buitendiameter van respectievelijk circa 0,40 en 0,75 mm, de thermistor probes.

Elk van de thermistoren is aangesloten op een nauwkeurige en stabiele digitale multimeter (DMM). De temperatuursverandering van een thermistor, ΔT_{th} in K, wordt bepaald op basis van de via kalibratie verkregen thermistorcoefficient α (ca. $-0,043 \text{ K}^{-1}$):

$$\Delta T = \frac{1}{\alpha} \cdot \frac{\Delta R}{R} \quad (2)$$

De DMM bepaalt de weerstand(sverandering) van de thermistor door bij constante meetstroom, I (ca. $100 \mu\text{A}$), een spanning(sverandering) over de thermistor te meten. Als gevolg van de meetstroom in combinatie met de thermistorweerstand, R (ca. $10 \text{ k}\Omega$), wordt een vermogen gedissipeerd waardoor de temperatuur van de thermistor hoger is dan die van het waterfantom. Deze zogenaamde 'self-heat', δT_{sh} in mK, is in stationaire toestand en in het geval dat er in de calorimeter alleen thermische convectie plaatsvindt, evenredig met het gedissipeerde vermogen, P in μW :

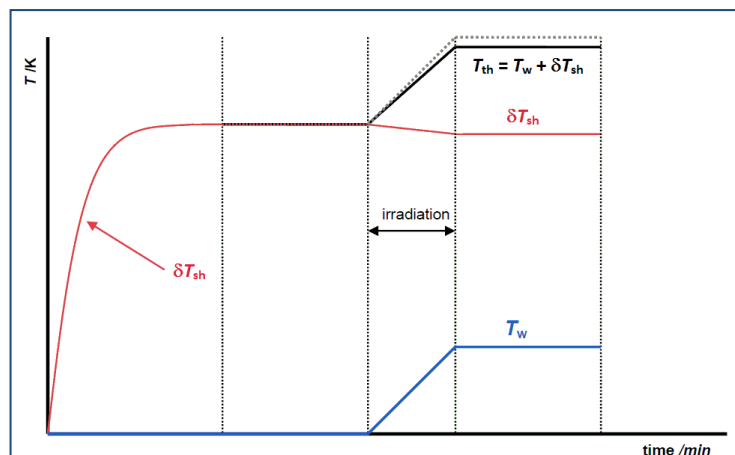
$$\delta T_{sh} = C_{sh} \cdot P \quad (3)$$

Hierin is C_{sh} , in $\text{mK} \cdot \mu\text{W}^{-1}$, de zogenaamde self-heatconstante.

Door de kleine afmetingen en de constructie van de thermistorprobes bedraagt de self-heatconstante, C_{sh} 1,5 tot $2,0 \text{ mK} \cdot \mu\text{W}^{-1}$. Dit resulteert, gecombineerd met de toegepaste DMMs, in een totale self-heat tussen 150 en 200 mK. Als gevolg van de toenemende watertemperatuur gedurende de bestraling (en dus toenemende thermistor temperatuur) vermindert de weerstand en daarmee de self-heat (geïllustreerd in Figuur 2). Het gevolg is dat de thermistor de temperatuursverandering van het water niet volledig volgt wat een schijnbare onderresponsie van de thermistor tot gevolg heeft in relatie tot de verandering van de watertemperatuur.

On the self-heat effects of thermistors

Page 68 of 74



Figuur 2: Verandering van de thermistorself-heat gedurende de bestraling, resulterend in een schijnbare verandering van de thermistorresponsie.

Het kan worden aangetoond dat, in afwezigheid van convectie, de relatie tussen de gemeten temperatuursverandering van de thermistor, ΔT_{th} , en de te bepalen temperatuursverandering van het water, ΔT_w , als volgt kan worden uitgedrukt:

$$\Delta T_w = \Delta T_{th} \cdot k_{sh} \quad (4)$$

waarbij de self-heatcorrectie, k_{sh} , kan worden uitgedrukt als:

$$k_{sh} = 1 - \delta T_{sh} \cdot \alpha \quad (5)$$

Bij een selfheat van tussen 150 en 200 mK bedraagt de selfheat-correctie 0,9935 tot 0,9914. Om de onzekerheid op deze correctie klein te houden dient de onzekerheid op zowel de thermistorcoefficient, α , als de self-heatconstante, C_{sh} , klein te zijn. De grootste uitdaging met betrekking tot de onzekerheid op de self-heatcorrectie, is hierbij de onzekerheid op de self-heatconstante.

On the self-heat effects of thermistors

Page 69 of 74

Uitgevoerd werk en huidige stand van zaken

Tussen 2001 en 2002 zijn self-heat metingen uitgevoerd met behulp van de AC-Wheatstone brug van de grafietermometer. Hierbij werd het gedissipeerde vermogen door de thermistoren gevarieerd door de AC-spanning te veranderen.

Tussen 2002 en 2006 zijn self-heat metingen uitgevoerd door het gedissipeerde vermogen door thermistoren te veranderen op basis van een variatie aan DMMs, DMM ranges én, waar mogelijk, verandering van de DMM power modes (alleen op de Agilent 34420A).

Tussen 2011 en 2014 hebben stage- en afstudeeronderzoeken plaatsgevonden naar het self-heat gedrag van thermistoren in combinatie met de DMM-methode in de VSL watercalorimeter.

De studie van Jiajun Cen (Cen 2011) beschrijft de differentiaalvergelijkingen m.b.t. de warmte-overdracht van de thermistoren naar hun omgeving. Gebruikmakend van Comsol Multiphysics zijn er warmtetransportmodellen opgesteld. Er is gekeken naar de invloed van de self-heat op convectie. Hieruit kon worden geconcludeerd dat indien het gedissipeerde vermogen voldoende groot is er kans bestaat op self-heat geïnduceerde convectie. Indien convectie verwaarloosbaar is, kan C_{sh} als constante verondersteld worden.

Omstreeks de studie van Jiajun Cen bleek dat de DMM instellingen (AZERO, OCOMP, OHMF, TRIG, etc.) invloed hebben op de tijd per sampleperiode waarop de meetstroom door de thermistor stroomt. Daarnaast bleek dat de thermistor temperatuur op het werkelijke DMM samplenmoment (i.e. het moment waarop daadwerkelijk de spanning over de thermistor wordt gemeten) niet persé representatief hoeft te zijn voor de gemiddelde temperatuur van de thermistor. Een analyse van gemiddelde self-heat op basis van gemiddeld gedissipeerd vermogen is niet vanzelfsprekend correct, de van belang zijnde self-heat is immers die op het samplenmoment. De vraag rees of het mogelijk zou zijn om een 'real-time' self-heat scan te maken van een thermistor op een DMM door de gelijktijdig de spanning over deze DMM met een andere stabiele en nauwkeurige DMM zeer snel te samplen.

De studie van Victor Hamoen (Hamoen 2013) beschrijft een poging om met een tweede DMM, parallel aangesloten op de 'meet-DMM' de spanning gelijktijdig te samplen. Dit bleek echter binnen de periode van de stage om technische redenen niet mogelijk. De oorzaken hiervan waren problemen met het snel aansturen en uitlezen van de tweede DMM via Delphi. Daarnaast bleek de toenemende onzekerheid van de tweede DMM als gevolg van de korte sampletijden het in kaart brengen van dit gedrag te bemoeilijken. Tevens rees vraag rees of de gepulste meetstroom van de DMM wellicht een vergrootte convectie tot gevolg kon hebben. De aanbevelingen van de studie van Victor Hamoen waren om de self-heat te verkleinen en een gepulste meetstroom te vermijden door te meten bij een kleinere continue meetstroom.

De studie van David Mostert (Mostert 2014) beschrijft twee methoden om de thermistor self-heat te bepalen:

- (1) metingen van de self-heat op basis van een continue stabiele en gekalibreerde meetstroom afkomstig van een stroombron. Het gedissipeerde vermogen wordt gevarieerd door de stroom te veranderen en de weerstand van de thermistor wordt bepaald op basis van de spanning gemeten over de thermistor;
- (2) variatie van het gedissipeerde vermogen door parallel aan de thermistor een stabiele en gekalibreerde vaste weerstand te plaatsen.

Methode (2) is uitgevoerd met zowel de DMM OCOMP instelling AAN als UIT waarbij met instelling UIT hetzelfde resultaat zou moeten worden verkregen als bij methode (1). Daarnaast is in onderzocht welke fit-methode het beste past bij bepaling van de self-heat met het oog op correctie van aanwezig temperatuurdriften op de achtergrond. De validatie van methode (2) met OCOMP UIT met methode (1) heeft niet helemaal kunnen plaatsvinden. De vergelijking met OCOMP UIT en AAN m.b.t. methode (2) heeft een waarde opgeleverd voor het effectieve vermogen gedissipeerd in de thermistor met de betreffende DMM instellingen. De metingen van David Mostert voldoen om de self-heat parameter C_{sh} nauwkeurig te bepalen. Deze zijn echter zeer tijdrovend. Een geautomatiseerd opstelling is nodig om deze metingen efficiënt uit te voeren voor de verschillende VSL thermistoren.

8.8 Calibration certificates of digital multimeters



Dutch
Metrology
Institute

KALIBRATIECERTIFICAAT

Nummer 3352534
Blad 1 van 4

Aanvrager	VSL B.V. Thijsseweg 11 2629 JA DELFT
Aangeboden	Een digitale multimeter Fabrikant : Agilent Type : 3458A Serienummer : US28029739
Wijze van onderzoek	Voor aanvang van de kalibratie is de functie "AUTOCAL ALL" gebruikt. Vervolgens is het 1 V gelijkspanningsbereik en de 4 draadweerstandsbereiken (10 k Ω en 100 k Ω) met behulp van een kalibrator onderzocht. De metingen zijn verricht bij een omgevingstemperatuur van (23,9 \pm 0,5) °C en een relatieve luchtvochtigheid van (40 \pm 5) %.
Datum van onderzoek	9 februari 2016 tot en met 10 februari 2016
Resultaat	De meetresultaten zijn weergegeven op blad 2 tot en met 4 van dit certificaat. De gerapporteerde meetonzekerheid is de standaardonzekerheid vermenigvuldigd met een dekkingsfactor $k = 2$, welke voor een normale verdeling overeenkomt met een dekkingswaarschijnlijkheid van ongeveer 95 %. De standaardonzekerheid is bepaald overeenkomstig de GUM 'Evaluation of measurement data - Guide to the expression of uncertainty in measurement'.
Herleidbaarheid	De resultaten van de uitgevoerde kalibraties zijn herleidbaar naar primaire en/of (inter)nationaal erkende meetstandaarden.
Opmerking	De digitale multimeter is gejusteerd. Het resultaat voor justeren is gegeven in de tabellen 3 en 4.



Dutch
Metrology
Institute

Delft, 1 maart 2016
VSL B.V.


R.P. van Bemmelen
Allround metroloog

Figure 28: Calibration certificate for DMM 1.



KALIBRATIECERTIFICAAT

Nummer 3352534
Blad 2 van 4

Tabel 1: Gelijkspanning (instelling: MATH NULL NPLC 20)

Bereik	Aangeboden waarde	Gemeten waarde	Onzekerheid in de gemeten waarde
V	V	V	$\mu\text{V/V}$
1	-1,000 000 0	-0,999 998 1	2,0
1	-0,800 000 0	-0,799 998 5	3,0
1	-0,600 000 0	-0,599 998 8	3,0
1	-0,400 000 0	-0,399 999 1	3,0
1	-0,200 000 0	-0,199 999 5	3,0
1	0,000 000 00	0,000 000 00	0.20 μV
1	0,200 000 0	0,200 000 4	3,0
1	0,400 000 0	0,400 000 6	3,0
1	0,600 000 0	0,600 000 8	3,0
1	0,800 000 0	0,800 001 0	3,0
1	1,000 000 0	1,000 001 1	2,0
1	0,950 000 0	0,950 001 1	2,0
1	0,960 000 0	0,960 001 2	2,0
1	0,970 000 0	0,970 001 1	2,0
1	0,980 000 0	0,980 001 0	2,0
1	0,990 000 0	0,990 001 1	2,0
1	1,000 000 0	1,000 001 1	2,0
1	1,010 000 0	1,010 001 1	2,0
1	1,020 000 0	1,020 001 2	2,0
1	1,030 000 0	1,030 001 1	2,0
1	1,040 000 0	1,040 001 1	2,0
1	1,050 000 0	1,050 001 2	2,0

Tabel 2: Vierdraadsweerstand (instelling: OCOMP ON NPLC 20)

Bereik	Aangeboden waarde	Gemeten waarde	Onzekerheid in de gemeten waarde
$\text{k}\Omega$	$\text{k}\Omega$	$\text{k}\Omega$	$\mu\Omega/\Omega$
10	1,900 00	1,900 00	100
10	10,000 00	10,000 01	25
100	19,000 0	19,000 0	30
100	100,000 0	99,999 9	10

Figure 29: Calibration results for DMM 1.



KALIBRATIECERTIFICAAT

Nummer 3352535
Blad 1 van 4

Aanvrager	VSL B.V. Thijsseweg 11 2629 JA DELFT
Aangeboden	Een digitale multimeter Fabrikant : Agilent Type : 3458A Serienummer : US28029799
Wijze van onderzoek	Voor aanvang van de kalibratie is de op de meter aanwezige functie "AUTOCAL ALL" gebruikt. Vervolgens is het 1 V gelijkspanningsbereik en de 4 draadsweerstandsbereiken (10 kΩ en 100 kΩ) met behulp van een kalibrator onderzocht. De metingen zijn verricht bij een omgevingstemperatuur van $(23,5 \pm 0,5)$ °C en een relatieve luchtvochtigheid van (41 ± 5) %.
Datum van onderzoek	9 februari 2016
Resultaat	De meetresultaten zijn weergegeven op blad 2 tot en met 4 van dit certificaat. De gerapporteerde meetonzekerheid is de standaardonzekerheid vermenigvuldigd met een dekkingsfactor $k = 2$, welke voor een normale verdeling overeenkomt met een dekkingswaarschijnlijkheid van ongeveer 95 %. De standaardonzekerheid is bepaald overeenkomstig de GUM 'Evaluation of measurement data - Guide to the expression of uncertainty in measurement'.
Herleidbaarheid	De resultaten van de uitgevoerde kalibraties zijn herleidbaar naar primaire en/of (inter)nationaal erkende meetstandaarden.
Opmerking	De digitale multimeter is gejusteerd. Het resultaat voor justeren is gegeven in de tabellen 3 en 4.

Delft, 1 maart 2016
VSL B.V.

R.P. van Bemmelen
Allround metroloog

VSL B.V.
Thijsseweg 11, 2629 JA Delft (NL)
Postbus 654, 2600 AR Delft (NL)
T 015 269 15 00
F 015 261 29 71
I www.vsl.nl

Dit certificaat wordt verstrekt onder het voorbehoud dat generlei aansprakelijkheid wordt aanvaard en dat aanvrager vrijwaring geeft voor elke aansprakelijkheid jegens derden.

Reproductie van het volledige certificaat is toegestaan. Gedeelten van dit certificaat mogen slechts worden gereproduceerd na verkregen schriftelijke toestemming.

Figure 30: Calibration certificate for DMM 2.



KALIBRATIECERTIFICAAT

Nummer 3352535
Blad 2 van 4

Tabel 1: Gelijkspanning (instelling: MATH NULL NPLC 20)

Bereik	Aangeboden waarde	Gemeten waarde	Onzekerheid in de gemeten waarde
V	V	V	$\mu\text{V/V}$
1	-1,000 000 0	-0,999 998 4	2,0
1	-0,800 000 0	-0,799 998 7	3,0
1	-0,600 000 0	-0,599 999 0	3,0
1	-0,400 000 0	-0,399 999 2	3,0
1	-0,200 000 0	-0,199 999 4	3,0
1	0,000 000 00	0,000 000 00	0.20 μV
1	0,200 000 0	0,199 999 9	3,0
1	0,400 000 0	0,399 999 7	3,0
1	0,600 000 0	0,599 999 5	3,0
1	0,800 000 0	0,799 999 4	3,0
1	1,000 000 0	0,999 999 1	2,0
1	0,950 000 0	0,949 999 1	2,0
1	0,960 000 0	0,959 999 1	2,0
1	0,970 000 0	0,969 999 1	2,0
1	0,980 000 0	0,979 999 1	2,0
1	0,990 000 0	0,989 999 0	2,0
1	1,000 000 0	0,999 999 0	2,0
1	1,010 000 0	1,009 999 0	2,0
1	1,020 000 0	1,019 999 0	2,0
1	1,030 000 0	1,029 999 0	2,0
1	1,040 000 0	1,039 999 0	2,0
1	1,050 000 0	1,049 998 9	2,0

Tabel 2: Vierdraadsweerstand (instelling: OCOMP ON NPLC 20)

Bereik	Aangeboden waarde	Gemeten waarde	Onzekerheid in de gemeten waarde
$\text{k}\Omega$	$\text{k}\Omega$	$\text{k}\Omega$	$\mu\Omega/\Omega$
10	1,900 00	1,900 00	100
10	10,000 00	10,000 00	25
100	19,000 0	19,000 0	30
100	100,000 0	99,999 8	10

Figure 31: Calibration results for DMM 2.

On the self-heat effects of thermistors

Page 74 of 74

8.9 Picture of 19" rack containing measurement instruments



Figure 32: 19" rack containing: switch system (top, left), Keithley 2001 DMM (top, right) and two Agilent 3458A opt 002 DMMs (center and bottom). In the background, the rear panel of the equipment interface box is also seen.